THEORETICAL RECONSTRUCTION OF THE STRUCTURE AND DYNAMICS OF POLYMER MELTS FROM THEIR COARSE-GRAINED DESCRIPTION

by

IVAN YURYEVICH LYUBIMOV

A DISSERTATION

Presented to the Department of Chemistry
and the Graduate School of the University of Oregon
in partial fulfillment of the requirements
for the degree of
Doctor of Philosophy

June 2012

DISSERTATION APPROVAL PAGE

Student: Ivan Yuryevich Lyubimov

Title: Theoretical Reconstruction of the Structure and Dynamics of Polymer Melts from Their Coarse-Grained Description

This dissertation has been accepted and approved in partial fulfillment of the requirements for the Doctor of Philosophy degree in the Department of Chemistry by:

Dr. Michael E. Kellman	Chair
Dr. Marina G. Guenza	Advisor
Dr. Andrew H. Marcus	Inside Member
Dr. John J. Toner	Outside Member

and

Kimberly Andrews Espy	Vice President for Research & Innovation/ Dean of the Graduate School

Original approval signatures are on file with the University of Oregon Graduate School.

Degree awarded June 2012

© 2012 Ivan Yuryevich Lyubimov

DISSERTATION ABSTRACT

Ivan Yuryevich Lyubimov

Doctor of Philosophy

Department of Chemistry

June 2012

Title: Theoretical Reconstruction of the Structure and Dynamics of Polymer Melts from Their Coarse-Grained Description

A theoretical formalism to reconstruct structural and dynamical properties of polymer liquids from their coarse-grained description is developed. This formalism relies on established earlier analytical coarse-graining of polymers derived from the first principles of liquid theory. The polymer chain is represented at a mesoscale level as a soft particle. Coarse-grained computer simulations provide input data to the reconstruction formalism and allow one to achieve the most gain in computational efficiency.

The structure of polymer systems is reconstructed by combining global information from mesoscale simulations and local information from small united-atom simulations. The obtained monomer total correlation function is tested for a number of systems including polyethylene melts of different degrees of polymerization as well as melts with different local chemical structure. The agreement with full united-atom simulations is quantitative, and the procedure remains advantageous in computational time.

The dynamics in mesoscale simulations is artificially accelerated due to the coarse-graining procedure and needs to be rescaled. The proposed formalism addresses two rescalings of the dynamics. First, the internal degrees of freedom averaged out during coarse-graining procedure are reintroduced in “a posteriori” manner, rescaling the simulation time. The second rescaling takes into account the change in friction when switching from a monomer level description to mesoscopic. Both friction coefficients for monomer and soft particle are calculated analytically and their ratio provides the rescaling factor for the diffusion coefficient. The formalism is extensively tested against the united-atom molecular dynamic simulations and experimental data. The reconstructed diffusive dynamics of the center-of-mass for polyethylene and polybutadiene melts of increasing degrees of polymerization show a quantitative agreement, supporting the foundation of the approach.

Finally, from the center-of-mass diffusion the monomer friction coefficient is obtained and used as an input into Cooperative Dynamics theory. The dynamics of polymer chains at any length scale of interest is described through a Langevin equation. In summary, the proposed formalism reconstructs the structure and dynamics of polymer melts enhancing computational efficiency of molecular dynamic simulations.

This dissertation includes previously published and unpublished co-authored material.

CURRICULUM VITAE

NAME OF AUTHOR: Ivan Yuryevich Lyubimov

GRADUATE AND UNDERGRADUATE SCHOOLS ATTENDED:
University of Oregon, Eugene, OR
Kazan Federal University, Kazan, Russia

DEGREES AWARDED:
Doctor of Philosophy in chemistry, 2012, University of Oregon
Master of Science in physics (with honors), 2006, Kazan Federal University
Bachelor of Science in physics (with honors), 2004, Kazan Federal University

AREAS OF SPECIAL INTEREST:
Soft Condensed Matter, Statistical Mechanics, Coarse-Graining Methods, Complex Fluids, Molecular Dynamics Simulations

PROFESSIONAL EXPERIENCE:

Research and Teaching Assistant, University of Oregon, 2006-2012

Research Assistant, Kazan Federal University, 2003-2006

Mentor and Tutor, Kazan Physics Olympiad Center at Kazan Federal University, 2000-2004

GRANTS, AWARDS AND HONORS:

1st degree award on Final Science Student Conference of Kazan Federal University for the best oral presentation, June 2006.

PUBLICATIONS:

I. Lyubimov and M. G. Guenza. First-principle approach to rescale the dynamics of simulated coarse-grained macromolecular liquids. *Phys. Rev. E*, **84**, 031801, (2011).

I. Y. Lyubimov, J. McCarty, A. Clark, and M. G. Guenza. Analytical rescaling of polymer dynamics from mesoscale simulations. *J. Chem. Phys.*, **132**, 224903, (2010).

J. McCarty, I. Y. Lyubimov, and M. G. Guenza. Effective soft-core potential and mesoscopic simulations of binary polymer mixtures. *Macromol.*, **43**, 3964, (2010).

J. McCarty, I. Y. Lyubimov, and M. G. Guenza. Multiscale modeling of coarse-grained macromolecular liquids. *J. Phys. Chem. B*, **113**, 11876, (2009).

I. Y. Lyubimov, N. F. Fatkullin, and R. Kimmich. Influence of the Local Displacements on Spin-Lattice Relaxation of the Twice-Renormalized Rouse Chain. *Proceedings of the XIII All-Russian Conference "Structure and Dynamics of Polymer Systems"*, **13**, part 1, p.491, Ufa, Russia (2006).

I. Y. Lyubimov, M. A. Krutyeva and N. F. Fatkullin. Influence of the Local Displacements on Spin-Lattice relaxation Rate in Polymer Melts. *Proceedings of the XI All-Russian Conference "Structure and Dynamics of Polymer Systems"*, **11**, part 2C, p.103, Kazan, Russia (2004).

ACKNOWLEDGEMENTS

I am heartily thankful to my research advisor, Prof. Marina Guenza. This dissertation would not have been possible without her supervision, encouragement and support during my entire doctoral program. I have been a part of research group with the highest ethical standards.

I would like to express my gratitude to my committee. The commitment of the chair, Prof. Michael Kellman, and of the external member, Prof. John Toner (physics) are greatly appreciated. I owe sincere and earnest thankfulness to Prof. Andrew Marcus.

I am grateful to my former and present officemates: Ed Sambriski who helped me at the beginning of my doctoral program and introduced me to the project I've been continuing, Pallavi Debnath, Anthony Clark, Jeremy Copperman, and James McCarty with whom I have being working the longest and maintaining intellectual comradeship.

Last, but surely not least, I would like to recognize the efforts of my undergraduate and masters research advisor, Prof. Nail Fatkullin. For the financial support, I am grateful to the National Science Foundation for the support of my research assistanship. I also thank the Department of Chemistry at the University of Oregon for providing me with GTF teaching assistant positions.

TABLE OF CONTENTS

Chapter Page

I. INTRODUCTION 1

I.1. Multiscale Approaches and Coarse-Grained Models 1

I.2. Computer Simulations of Macromolecular Systems 2

I.3. Organization of the Material 3

II. RECONSTRUCTION OF STRUCTURE OF MACROMOLECULAR LIQUIDS FROM MOLECULAR DYNAMICS SIMULATIONS 5

II.1. Introduction 5

II.2. Coarse-Graining of a Polymer at the Radius-of-Gyration Length Scale 10

II.3. Mesoscale Simulation 15

II.4. Building the Full Structural Description at the Monomer Scale Using a Multiscale Approach 17

II.5. Combining United Atoms and Coarse-Grained Simulations: The Crossover Length Scale 20

II.6. Conclusion 29

III. ANALYTICAL RESCALING OF POLYMER DYNAMICS FROM COARSE-GRAINED SIMULATIONS 33

III.1. Introduction 33

III.2. Coarse-Grain Model 36

III.3. Coarse-Grained Potential and Mesoscale Simulations 37

III.4. Mapping of the Atomistic Description onto a Freely-Rotating-Chain Model 38

III.5. Rescaling of the Friction Coefficient 39

III.6. Comparison of Predicted Diffusive Dynamics with Simulations and Experiments 41

III.7. Conclusion 43

Chapter Page

IV. THEORETICAL DEVELOPMENT OF FRAMEWORK FOR RECONSTRUCTION OF DYNAMICS OF COARSE-GRAINED MACROMOLECULAR LIQUIDS 45

IV.1. Introduction 45

IV.2. Coarse-Graining of Polymeric Liquids: Structural Properties 51

IV.3. Dynamical Coarse-Graining: From the Liouville to the Langevin Equations 53

IV.4. Monomer Level Representation of the Polymer Chain 56

IV.5. Solution of the Generalized Langevin Equation in the Monomer Representation 58

IV.6. Center-of-Mass Level Representation of the Polymer Chain 59

IV.7. Analytical Rescaling of the Coarse-Grained Dynamics due to Free Energy Change 61

IV.8. Theoretical Derivation for Monomer Friction Coefficient 62

IV.9. Friction Coefficient for a Liquid of Interacting Soft Colloidal Particles 67

V. APPLICATION OF THE RECONSTRUCTION PROCEDURE TO SIMULATED COARSE-GRAINED POLYMER MELTS 70

V.1. Coarse-Grained Interparticle Soft Potential and Accelerated Dynamics in Mesoscale Simulations 71

V.2. Calculations of the Monomer Friction Coefficient, ζ_m 74

V.3. Calculation of the Friction Coefficient of a Soft Colloid, ζ_{soft} 78

V.4. Results from the Rescaling Procedure: Comparison with Simulation and Experimental Data 79

V.5. Theoretical Predictions of Diffusion Coefficients for Polyethylene Samples 84

V.6. Conclusion 87

VI. RECONSTRUCTION OF GLOBAL AND LOCAL DYNAMICS FROM COARSE-GRAINED SIMULATIONS AND COOPERATIVE DYNAMICS THEORY 90

VI.1. Introduction 90

VI.2. Rescaling of the Free-Energy and Rescaling of the Friction 93

VI.3. Theoretical Predictions of Center-of-Mass Diffusion 99

VI.4. Internal Dynamics 103
VI.5. Theoretical Predictions Using the Freely Rotating Chain Model 110
VI.6. Conclusion 113

VII. CONCLUSION 116
VII.1. Summary 116
VII.2. Field Overview 117
VII.3. Future Research 118

APPENDICES

A. INTERNAL ENERGY CALCULATION FOR A FREELY-ROTATING-CHAIN MODEL 120

B. THE DYNAMIC MEMORY FUNCTION 122

C. EXTENSION OF RECONSTRUCTION METHOD TO THE MULTIBLOCK POLYMER CHAINS REPRESENTED AS THE CONNECTED SOFT SPHERES 123

REFERENCES CITED 126

LIST OF FIGURES

Figure Page

II.1. The total pair potential, which is input into MS-MD simulation 15

II.2. Plot of $h^{mm}(k)$ for different polymer melts 19

II.3. Plot of $h^{mm}(k)$ for different polymer melts 20

II.4. Fraction of intramolecular contacts, $f_s(r)$, for melts of polymers 21

II.5. Plot of the total correlation function for polymer melts 23

II.6. Plot of $h^{mm}(k)$ and $h^{mm}(r)$. Combining theory and UA simulation (iPP, PIB) . . . 24

II.7. Plot of $h^{mm}(k)$ and $h^{mm}(r)$ for polyethylene of different lengths (PE44, PE48) . . . 24

II.8. Plot of $h^{mm}(k)$ and $h^{mm}(r)$ for polyethylene of different lengths (PE66, PE96) . . . 25

II.9. Plot of the local peak for the total correlation function 26

II.10. Correlation coefficient for $h^{mm}(r)$ 27

III.1. Plot of diffusion coefficients as a function of degree of polymerization, N 43

III.2. Normalized rotational time decorrelation function for the end-to-end vector 44

IV.1. Illustration of monomer and overall coarse-graining of a homopolymer linear chain 52

IV.2. Cm mean-square displacement, for a polyethylene melt with $N = 44$ 54

V.1. Cm mean-square displacement. Cm velocity time correlation function 75

V.2. Plot of $D\beta\zeta_m$ as a function of hard core diameter d 77

V.3. Plot of mean-square displacement as a function of time for unentangled PE melts . . 82

V.4. Plot of diffusion coefficients as a function of degree of polymerization, N 85

VI.1. Dimensionless monomer friction coefficient as a function of hard sphere diameter . . 98

VI.2. The center of mass self-diffusion coefficient as a function of N 103

VI.3. Density as a function of degree of polymerization N 104

VI.4. End-to-end vector time decorrelation function for PB112 107

VI.5. The center of mass mean square displacement as a function of time 108

VI.6. Normalized dynamic structure factor for PB96 and q=0.04, 0.1, 0.2, 0.3Å^{-1} 109

VI.7. Normalized dynamic structure factor for PB400 and q=0.04, 0.1, 0.2, 0.3Å^{-1} 110

Figure Page

VI.8. The innermost chain segments msd as a function of time 111

VI.9. Density dependence of semiflexibility parameter g 112

VI.10. Radius of gyration squared over degree of polymerization R_g^2/N as a function of N 113

VI.11. Diffusion coefficient reconstructed from MS MD simulations with use of FRC model 114

LIST OF TABLES

Table Page

II.1. Simulation Parameters for Polyolefin Melts 16

II.2. Comparison of MS-MD Simulations with UA-MD Simulations 18

II.3. Correlation coefficient for polyolefin melts 27

II.4. Total Number of Sites (N_{sites}) and Number of Molecules (n) 28

III.1. MS-MD Parameters - UA-MD data 41

III.2. MS-MD Parameters - Experimental Data 42

V.1. Polyolefin melts UA MD simulation parameters 71

V.2. Monomer friction coefficient contributions with hard sphere potential for $d = 2.1$Å 78

V.3. Soft-colloids friction coefficient contributions 79

V.4. Diffusion coefficients in Å^2/ns from MS MD compared with UA MD simulation . . . 81

V.5. Theoretically calculated friction coefficient for monomer and soft colloid 84

V.6. Predicted diffusion coefficients in Å^2/ns from MS MD and experimental data 84

VI.1. Simulation parameters for 1,4-cis PB chains of increasing lengths. 100

VI.2. Diffusion coefficient reconstructed from MS MD simulation compared against UA MD simulations 102

CHAPTER I

INTRODUCTION

There is one general property among the whole variety of polymeric systems. All polymers constitute of a large number of building blocks called monomers. The number of different configurations of macromolecules can reach an astronomic value, which dictates the use of statistical mechanical methods to study polymers. Macromolecules can be characterized by different typology as well as by different chemical monomeric structure. In this work we focus on linear synthetic homopolymers, that is polymers composed of the same repeatedly connected monomers.

Synthetic linear polymers have a great importance in many areas from plastic production industries for everyday use to highly technological process of designing new materials. The theoretical and experimental study of polymers is a challenging task because the time and length scales where relevant physical phenomena take place encompass a very broad range. Furthermore, global properties of polymers strongly depend on local chemical structure, therefore the phenomena on the two scales can not be investigated separately. The polymers in their liquid phase represent the most interest for study since polymers are processed in their molten state. Theoretical approaches suffer from the fact that they are developed to describe a specific range of time and length scales, so that there is no formal consistency between numerous different theories currently existing for polymer dynamics.

Computational methods are useful because they can provide a microscopically detailed calculation of static and dynamic properties which are helpful in designing and testing new theoretical models. However, detailed atomistic simulations have intrinsic limitations by the computational power and simulation time which scales quadratically with the number of particles.

I.1. Multiscale Approaches and Coarse-Grained Models

A way to overcome this problem is to use coarse-graining techniques in the context of a multiscale modeling procedure. Recently, efforts to develop methods of a coarse-grained description of polymer systems have been undertaken to allow better understanding of the nature of phenomena that happen at a particular length scale. Coarse-graining at a particular length scale averages out the information at smaller length scales, and considerably speeds up the computational time, so that larger systems can be simulated and for longer times than in an all-atom simulation. However, the global properties of macromolecules strongly depend on local chemical structure, so the phenomena at different scales need to be formally correlated. After coarse-graining the system at several different levels, a multi-scale modeling scheme needs to be applied. The goal is to develop realistic and reliable theoretical procedures to coarse-grain the system at the different length scales of interest, and a sound theoretical procedure that reversibly relates the different length scales of interest.

Because of the abundant physics happening on very broad length and time scales, it is common to coarse-grain systems by eliminating not important features for the window we are interested in. Dividing the entire length and time scale into smaller windows helps to obtain the complete information in a given range of focus. The challenge of the multiscale procedures is to combine different pieces of information in a reliable rigorous way. It is important to connect hierarchical coarse-grained descriptions in a consistent way. There is a variety of multiscale methods to treat structural properties. However, the procedure of high-level coarse-graining always speeds up the simulation times. This gives an advantage of faster equilibration, however the dynamics becomes artificially accelerated. There are established numerical procedures to scale down dynamics which are based on calibration curves, or applicable only to the low degree of coarse-graining. Numerical schemes as a rule require performance of detailed simulations for obtaining the force field for coarse-grained units. The potentials obtained as the result of numerical procedures are state dependent. The necessity to run an atomistic simulation for each thermodynamic state diminishes the idea of coarse-graining as a way to increase efficiency and motivates us to develop totally analytical approaches. The method described in this dissertation represents an a posteriori reconstruction of dynamics of macromolecular liquids.

I.2. Computer Simulations of Macromolecular Systems

Molecular Dynamics computer simulations of polymer systems are governed by deterministic equations of motion. Having a trajectory of each molecule, one can obtain complete information of both structural and dynamical properties. In order to describe a real system the force field in the molecular dynamics simulations needs to be parametrized correctly and tested against well established experimental data.

There is a hierarchical family of computer molecular dynamics simulations for different levels of coarse-graining. In this dissertation we deal with primarily two levels of coarse-graining. The first level of coarse-graining provides the correct information at the monomer level. The polymer chain coarse-grained at the monomer level is constituted from so called united atoms. Each united atom represent several atoms which are lumped together into one effective particle interacting through a phenomenological Lennard-Jones potential. The simulations are called united atom simulations (UA MD).

The second type of coarse-grained system discussed here is another extreme level where the entire molecule is represented as a point particle interacting with an effecting pair soft potential. Soft potentials for this level of coarse-graining were developed before and are well tested in terms of reproducing the structure of homopolymer melts, polymer mixtures and diblock copolymers.

The central focus of this dissertation is on the reconstruction of the dynamics of the heavily coarse-grained macromolecular liquids.

I.3. Organization of the Material

In this dissertation the formalism for reconstructing both the structure and dynamics of polymer liquids from coarse-grained molecular dynamic simulations is presented.

The reconstruction of the structure of polymer systems from coarse-grained mesoscale simulations and local information provided by united-atom simulations is in-depth discussed in Chapter II. The global information from mesoscale simulations and local information from united-atom simulations are combined and the monomer total correlation function is reconstructed following the developed formalism. The approach is tested for several systems: polyethylene melts of different polymerization degree and polymer liquids with different chemical structure of the monomers. The materials presented in Chapter II have been published and collaboration with James McCarty is highly appreciated.

Chapter III gives a rather short description of the theoretical approach to scale the artificially fast dynamics of simulated coarse-grained polymer liquids. Two effects of high level of coarse-graining are discussed, namely elimination of internal degrees of freedom and change in friction. The corrections to these effects are made in an analytical way and transferability of the method is illustrated. The results of rescaling to polyethylene melts of increasing degree of polymerization is shown. The translational and rotational diffusion of unentangled and weakly entangles systems, predicted from mesoscale simulations, is compared against united-atom simulations and experimental data. This part has been published with co-authors James McCarty and Anthony Clark.

The theoretical foundations and detailed derivation of the framework for the reconstruction of dynamics for heavily coarse-grained polymer systems are given in Chapter IV. Two levels of coarse-graining are considered. The monomer level of coarse-graining is described as the "bead-and-spring" type model and the higher level of coarse-graining represents a polymer chain as a point particle interacting through an effective pair interaction potential. For both descriptions the Generalized Langevin equations are solved. The rescaling due to free energy change is discussed. Finally, the theoretical calculations of the friction coefficient of the monomer is mapped onto a hard-sphere potential and the friction coefficient for the soft colloid particles concludes Chapter IV.

In Chapter V the developed dynamics reconstruction method is applied to several set of polyethylene samples at different thermodynamic states. The results are compared against united-atom simulations and experiments. At the end of the chapter the theoretical predictions are made for unentangled and entangled polyethylene melts. The material from Chapters IV and V has been published with my advisor, Marina Guenza, as co-author.

Chapter VI extends the formalism to a polymer with different chemical structure of the monomer. The translational and rotational diffusion are reconstructed for polybutadiene melts of increasing degree of polymerization. In the second part of this chapter the predictions of cooperative dynamics theory are made for internal dynamical properties. The materials from Chapter VI will be published. Chapter VII concludes the dissertation.

CHAPTER II

RECONSTRUCTION OF STRUCTURE OF MACROMOLECULAR LIQUIDS FROM MOLECULAR DYNAMICS SIMULATIONS

In Chapter II a first-principle multiscale modeling approach is presented, which is derived from the solution of the Ornstein-Zernike equation for the coarse-grained representation of polymer liquids. The approach is analytical, and for this reason is transferable. It is here applied to determine the structure of several polymeric systems, which have different parameter values, such as molecular length, monomeric structure, local flexibility, and thermodynamic conditions. When the pair distribution function obtained from this procedure is compared with the results from a full atomistic simulation, it shows quantitative agreement. Moreover, the multiscale procedure accurately captures both large and local scale properties while remaining computationally advantageous. The material in Chapter II is a result of collaboration with James McCarty. My contribution to this chapter is in developing of the multiscaling scheme, performing simulations and running the analysis codes.

II.1. Introduction

Understanding the structure of complex fluids hinges on our ability of achieving a detailed picture of the system on an extended range of length scales. Many important phenomena, which are tightly dependent on the local chemical structure, occur on a large scale. Thermodynamic properties, which can be considered as characterized by a macroscopic (infinite) length scale change as the local, monomeric structure is modified. For example compressibility or phase diagrams of a macromolecular liquid depend on the type of polymer involved. As the physics appearing on different length scales is related, an effort has to be made to formally correlate information on different length scales.[24, 29]

Macromolecular liquids are complex, given the plethora of characteristic length scales that emerges from their investigation. Two fundamental, molecular length scales are relevant in the study of any macromolecular liquid, namely the monomer length scale, l, which is local, and the molecular radius-of-gyration, $R_g = l\sqrt{N/6}$, where N is the molecular degree of polymerization, which roughly represents the overall size of the polymer. Because R_g^2 increases linearly with the number of monomers in the chain, those two length scales can be separated by many orders of magnitude in real macromolecular systems of practical application.

The local scale is an effective length in which complicated local information is embedded. For example, in the simplest and most conventional description of the polymer local structure, inter- and intra-molecular forces balance each other leading to an unperturbed polymer chain statistics at any length scale.[30] However, simulations show that on the local scale entropic effects and chain connectivity produce a segmental correlation hole that manifests itself as local, intramolecular clustered, structures of monomers.[31] Because the liquid is almost incompressible and monomers from the same chain tend to cluster together due to connectivity, the ideality hypothesis does not hold on the local scale.

A second effect important on the local scale is the presence of rotational energy barriers.[32, 33] To describe liquids of semiflexible polymers, where the local dynamics is affected by conformational transitions, the bond length is modified into an effective segment length that includes the effect of hindered rotations. This length scale is commonly referred to as the polymer persistence length.[32]

Computer simulations are useful in providing detailed information about the macromolecular systems under study. Correlation functions can be readily calculated from simulation trajectories and compared with experiments. However, simulations are limited in the range of length scales they can cover, as the statistics is good up to the length scale defined by half the size of the simulation box. Increasing the box size, increases the number of interacting particles and the number of pair potentials that need to be calculated at any time step, dramatically slowing down the simulation.

For a system that is ergodic, where statistical averages over an ensemble of particles is equivalent to the average of one system over many computational time steps, one could think of limiting the number of particles simulated, while still being able to recover enough statistics by extending the length of the simulation run. Unfortunately, the problem of error build-up at each step during the simulation run makes calculated trajectories rapidly unreliable. This is due to the fact that trajectories are derived by numerical solutions of differential equations. These solutions are chaotic in nature, and small differences due to numerical uncertainty in the initial conditions produce large fluctuations in the output trajectory, which increase with time. The extent to which simulation trajectories are sensitive to small initial errors depends on the value of the Lyapunov exponent. Shadowing trajectories, which well represent the real ones, only last for a limited number of computational steps.[2, 34]

Other methods have been studied to improve the maximum number of computational steps that can be reliably simulated, including hybrid methods, e.g. implicit solvent methods, that conserve the atomistic description locally while assuming a meanfield description outside a local volume. However, these methods remain under discussion because of the errors that they can include in the procedure.[2]

In a nutshell, if the system is described at high resolution, a large number of instantaneous forces have to be calculated at each computational time step, which slows down the computational time. Computational time steps have to be short to avoid large initial errors, but because trajectories become increasingly unreliable with the number of steps, this limits the longest timescale that can be reached in the simulation, and so the quality of the simulation output.[2, 35]

A general strategy useful for increasing the timescale and the number of particles that can be simulated is to adopt a coarse-grained description of the system. The simulation of a coarse-grained system can include a significantly larger number of particles and can extend to a much longer time scale than simulations of the same system described with atomistic resolution. This is because internal degrees of freedom and local energy barriers are averaged out, allowing a larger elementary time step than for atomistic simulations. Moreover, in the coarse-grained description each molecule contains a number of atoms that can be considerably reduced with respect to the full atomistic descriptions, so that the number of pair interactions that have to be calculated, at each computational step between each pair of molecules, is reduced, allowing for the simulation of larger systems.

The trade-off of coarse-grained methods is that the local information is completely lost, and also that because the local energy barriers are averaged out and internal degrees of freedom are eliminated, the simulated dynamics is orders of magnitude faster than the real one, and there are not easy methods to recover the correct dynamics.[36]

Modeling of coarse-grained systems have recently received considerable attention[37] as simulations aspire to describe more and more complicated structures relevant for engineering applications as well as biophysical systems.[10, 38, 39] The key question in developing coarse-grained molecular models is the definition of the effective potential acting between units. The general strategy pursued to solve this problem is a bottom-up approach. First, atomistic simulations of the molecular liquid are performed. Once the coarse-grained structure is defined by lumping together adjacent atoms in the molecule, an effective numerical coarse-grained potential is obtained, which is parametrized by optimizing the agreement against properties measured in the atomistic simulation. For example, the parameters in the effective potential can be defined by the optimization of the mean-force potential, matching the forces, or by optimizing the free parameters against known physical properties. The potential, so derived, is used as an input to a new simulation of the coarse-grained system. The properties derived from this simulation are checked for consistency against physical properties, e.g. pair distribution functions, obtained from the atomistic simulation, and the process is repeated until a fully self-consistent description is achieved. The test quantity that is optimized is in most cases the pair distribution function, or analogously the total correlation function, as from this quantity all the properties of a liquid can be directly calculated.[40]

This numerical procedure has the limitation that the resulting optimized effective potentials are specific to the chemical structure considered and of the thermodynamics conditions in which the initial atomistic simulations were performed. In principle those potentials cannot be applied to describe the system in a different thermodynamic condition, which means that the potential is not transferable.

Several coarse-graining methods have been presented in the literature. An extremely successful approach has been the United Atom (UA) description where each moiety of type C, CH, CH_2, or CH_3 is represented as an effective unit.[41] Effective potentials between united atoms have been derived and parametrized to reproduce the properties of the system described at the atomic level. The UA description is useful because polyolefins, which constitute a great portion of the macromolecular systems of interest, can be fully represented as a collection of these sites. The UA description has been extensively tested and has been proven to be extremely reliable.[42–44]

Combined with new techniques that speed up the equilibration step, the UA description allows for MD simulations of polymer melts with long entangled chains.[45]

While UA simulations have proved successful in reproducing the structural and dynamical properties of polymers, there is an increasing need to extend simulations to even larger scales to capture other phenomena, such as cooperative self-assembly of supermolecular structures, dynamics of systems approaching their second order phase transitions, simulations of bulk properties, to name a few. Recently, we have developed an original coarse-grained method, which is analytical and represents polymers on the length scale of R_g as interpenetrating soft colloidal particles.[8, 46, 47] A more refined coarse-grained description has also been derived, where each macromolecule is represented as an elastic dumb-bell of interpenerating spheres.[48] The effective potential in these descriptions is derived by solving the Ornstein-Zernike equation in the monomer and effective unit sites, where the center-of-mass (com) of the effective unit is assumed to be an auxiliary site, i.e. there is no direct correlation between monomer and com. Relaxing this approximation does not change the outcome of the coarse-graining procedure.[47] Because the monomer intramolecular distribution follows a Gaussian statistics, the Ornstein-Zernike equation can be solved analytically to produce the pair distribution function for the effective units. From the latter, the effective coarse-grained potential is calculated by applying the hypernetted-chain closure approximation.[40] The advantage of our coarse-grained description is that the obtained potential is directly transferable to systems in different thermodynamic conditions and to polymers with different degree of polymerization or different chemical structure.[8, 46, 47] Comparison against UA simulations of several polymeric liquids and mixtures showed quantitative agreement between the total correlation functions in the two representations.

Because the trade-off of coarse-graining procedures is that the information on the local length scale is lost, techniques have been developed to merge the coarse-grained description with local information. In the so-called “multiscale modeling” procedures a hierarchy of simulations are performed on the system coarse-grained at different characteristic length scales, and then the information obtained from those simulations is combined into one overall description, which includes all the length scales of interest.

The method that we are presenting here is a multiscale modeling procedure for the simplest macromolecular liquids, i.e. of homopolymers. Here, the length scales of interest are the monomer and the radius-of-gyration, so that two simulations have to be combined, one at the monomer level of description, and one where polymers are represented at the R_g level, or mesoscopic simulation (MS-MD). We perform molecular dynamic simulations of the liquid of polymers described as soft colloidal particles in a MS-MD simulation and we combined those results with the outcome of a united atom molecular dynamic (UA-MD) simulation for the local description, through our multiscale modeling procedure. We test our procedure for a number of systems, which include polyethylene melts with different degrees of polymerization, as well as liquids of macromolecules with different monomeric structures. The procedure is optimized and shows quantitative agreement between the total correlation functions calculated by us, and the ones obtained in a test UA-MD simulation. The advantage of our procedure, with respect to running a full UA-MD simulation of the same system, is due to the gain in computational time.

Another advantage of our multiscale modeling procedure, with respect to other multiscale approaches, is that it is formally compatible with the first principle formalism used to coarse-grain the polymeric structure as both rely on the Ornstein-Zernike equation which includes auxiliary sites. Because it is analytical, the coarse-graining procedure can be used not only to remove internal degrees of freedom, but also in the opposite way to reintroduce "a posteriori" those internal degrees of freedom after the MS-MD is completed. It is shown that this approach reproduces pair correlation functions at a high computational efficiency, providing a method of extending simulations to large length scales of interest.

II.2. Coarse-Graining of a Polymer at the Radius-of-Gyration Length Scale

Our coarse-grain model, briefly revisited here, maps each macromolecule into an interacting soft-colloidal particle. We developed this model in a series of papers, where we reported coarse graining of polymer melts with different architectures as well as coarse graining of mixtures of those polymers.[8, 24, 46, 47, 49]

The first modeling of polymers as soft colloidal particles dates back to Flory and Krigbaum,[50] where repulsive monomer-monomer interactions are integrated over the Gaussian chain distribution. The resulting effective potential at contact is repulsive and becomes stronger with increasing chain length or polymer density, in disagreement with simulations, scaling theories and renormalization group calculations. Correct scaling behavior was obtained by Hansen and coworkers who derived pair distribution functions for polymers in dilute or semi-dilute solution, starting from first principles liquid state theory.[51] A more phenomenological form of this approach was implemented early on to describe polymer melts and mixtures by Dautenhahn and Hall,[52] and by Murat and Kremer.[53]

The choice of the monomer and radius-of-gyration as the two length scales at which the polymer liquid is coarse-grained in our multiscale procedure is motivated by the fact that the monomer pair distribution function, and the structure of the polymer liquid, are fully determined when these two length scales are known, as shown below.

Our coarse-graining procedure starts from Curro and Schweizer's polymer reference interaction site model (PRISM) Ornstein-Zernike equation, which for a homopolymer melt relates the monomer total pair correlation function, $h(r)$, to the direct correlation function, $c(r)$, in reciprocal space[54, 55]

$$\hat{h}(k) = \hat{\omega}(k)\hat{c}(k)[\hat{\omega}(k) + \rho\hat{h}(k)] \ , \tag{II.1}$$

where $\hat{\omega}(k)$ is the intramolecular structure factor, and ρ is the monomer site number density. The procedure is then extended to include the center-of-mass of the coarse-grained structures as auxiliary sites, using the formalism of Krakoviack *et al.*,[18] which starts from a matrix form of Eq.(II.1). The density of auxiliary sites is given by the molecular number density, $\rho_{ch} = \rho/N$. The solution of Eq.(II.1) is obtained under the assumptions that the direct correlation functions, $\hat{c}(k)$, only depend on interactions between real sites, while no interaction is assumed between auxiliary sites. Relaxing this condition does not modify the zeroth order result,[47] which yields the equation

$$h^{cc}(k) = \left[\frac{\omega^{cm}(k)}{\omega^{mm}(k)}\right]^2 h^{mm}(k) \ , \tag{II.2}$$

where $h^{mm}(k)$ is the total pair monomer-monomer correlation function, $\omega^{cm}(k)$ is the intrachain correlation function of monomers about the com, $\omega^{mm}(k)$ is the intramolecular monomer-monomer correlation function, and $h^{cc}(k)$ is the mesoscale com-com total correlation function. Eq.(II.2) is the basis for our coarse graining approach since it links the com and the monomer site correlation functions. The com representation corresponds to a mesoscale, coarse-grained description of the polymeric liquid, where each chain is a soft colloidal particle centered on the position of the polymer com. On the other hand, the monomer site description is related to the united atom representation of the polymer chain, where each site represents an united atom.

In order to obtain an expression for the coarse-grained description, we adopt for the monomer correlation function, $h^{mm}(r)$, the PRISM thread description, in which the polymer chain is treated as an infinite thread of vanishing thickness,

$$h^{mm}(r) \;=\; \frac{\xi'_\rho}{r}\left[\exp\left(-\frac{r}{\xi_\rho}\right)-\exp\left(-\frac{r}{\xi_c}\right)\right] \;, \tag{II.3}$$

with $\xi'_\rho = 3/(\pi\rho l^3)$ with ρ the monomer site density. Moreover, ξ_ρ is the length scale of density fluctuations defined as $\xi_\rho^{-1} = \xi_c^{-1} + \xi_\rho'^{-1}$, and $\xi_c = R_g/\sqrt{2}$ is the length scale of the correlation hole.[30] Eq.(II.3) shows how the structure of the macromolecular liquid is fully specified once the monomer and the radius-of-gyration length scales are known.

By assuming Gaussian intramolecular distributions for the monomer-monomer and monomer-com correlation functions, which is a well tested assumption, Yatsenko, *et al.* have shown that $h^{cc}(r)$ can be expressed in an analytical form in terms of molecular and thermodynamic parameters as[8]

$$\begin{aligned} h^{cc}(r) \;=\; & \frac{3}{4}\sqrt{\frac{3}{\pi}}\frac{\xi'_\rho}{R_g}\left(1-\frac{\xi_c^2}{\xi_\rho^2}\right)e^{-3r^2/(4R_g^2)} - \frac{1}{2}\frac{\xi'_\rho}{r}\left(1-\frac{\xi_c^2}{\xi_\rho^2}\right)^2 e^{R_g^2/(3\xi_\rho^2)} \\ & \times\left[e^{r/\xi_\rho}\mathrm{erfc}\left(\frac{R_g}{\sqrt{3}\xi_\rho}+\frac{\sqrt{3}r}{2R_g}\right) - e^{-r/\xi_\rho}\mathrm{erfc}\left(\frac{R_g}{\sqrt{3}\xi_\rho}-\frac{\sqrt{3}r}{2R_g}\right)\right] \end{aligned} \tag{II.4}$$

where $\mathrm{erfc}(x)$ is the complementary error function and ξ'_ρ can be expressed in terms of the radius of gyration as $R_g/(2\pi\rho^*_{ch})$ with $\rho^*_{ch} \equiv \rho_{ch}R_g^3$ being the reduced molecular number density. Although the PRISM-thread model employed at the monomer level description does not predict solvation shells, which are present in a polymeric liquid on the local scale, its description of the structure of the liquid at the center-of-mass length scale is correct. For example, Eq.(II.4) recovers the isothermal compressibility of the melt at the $k = 0$ limit[8] and it is thermodynamically consistent. This equation effectively maps the polymer melt into a liquid of soft colloidal particles of radius R_g and recovers, in its extension to the case of polymer mixtures, the formalism of Bhatia and Thornton for mixtures of colloidal particles.[23, 46, 56]

When compared against simulation data, the analytical expression of Eq.(II.4) reproduces well the com total correlation function obtained from UA-MD simulations for several polymeric systems that have different degrees of polymerization, different monomeric structure, and different density and temperature.[47] Theoretical calculations of $h^{cc}(k)$ do not contain any adjustable parameter because the parameters entering Eq.(II.4) are the ones used in the united atom simulation against which the formalism is tested.

Starting from Eq.(II.4) and enforcing for the closure equation the hypernetted chain approximation, which is the most reliable closure for soft potentials, the effective intermolecular potential between the coms of a pair of soft colloidal particles, $v^{cc}(r)$, is derived as[8, 46, 47]

$$\beta v^{cc}(r) = h^{cc}(r) - \ln[1 + h^{cc}(r)] - c^{cc}(r) \ , \tag{II.5}$$

with $\beta = (k_B T)^{-1}$ the inverse temperature of the system in Boltzman units. The direct pair correlation function, $c^{cc}(r)$ is given in reciprocal space in terms of $h^{cc}(k)$ as

$$c^{cc}(k) = \frac{h^{cc}(k)}{1 + \rho_{ch} h^{cc}(k)} \tag{II.6}$$

Substitution of Eq.(II.4) and Eq.(II.6) into Eq.(II.5) gives the effective pair potential acting between two soft colloidal particles. This is the potential needed as an input to the mesoscopic simulation of the coarse-grained units and is the potential we use in our MS-MD.

Because coarse-grained potentials result from the mapping of many-body interactions into pair interactions, through the averaging over microscopic degrees of freedom, they are parameter dependent. During the coarse-graining procedure, the potential acting between microscopic units, which is given by the Hamiltonian of the system, reduces to an effective potential, which is a free energy in the reference system of the microscopic coordinates. The coarse-grained potential so obtained contains contributions of entropic origin due to the microscopic, averaged-out degrees of freedom and is therefore state-dependent. This can be observed in the form of the total correlation function between coarse-grained sites, Eq.(II.4), which explicitly includes the structural parameters of the polymer, i.e. the radius-of-gyration and density screening length, as well as the thermodynamic parameter of the system number density. The temperature enters directly through Eq.(II.5) and indirectly through the molecular parameters, such as R_g.

The common procedure adopted to derive the effective potential between coarse-grained units is fully numerical. Once the level of coarse-graining is defined by the selection of the effective units, the pair distribution function between effective units, $g(r)$, is numerically calculated. From $g(r)$ the potential of mean force is derived as $-k_BT \ln g(r)$, and then used as an input to a coarse-grained simulation. By comparison against the UA simulation, corrections to the potential are obtained, and the new potential of mean-force is used as an input to a new simulation until full consistency is obtained between coarse-grained and UA simulations. Because numerically solved coarse-grained potentials have parameters that are defined through optimization against a specific UA simulation, they apply only for systems at thermodynamic conditions close to the one of the UA simulation, so they are not transferable. Moreover, because their form depends on the procedure used to derive them, if they are optimized against a given set of physical properties, it is not assured that they will reproduce other properties of the system. The numerical optimization of the potential against different physical properties could lead to different effective potentials, numerically optimized, even for the same system.

In this respect, an analytical potential such as the one we derive here has the advantage of being explicitly parameter dependent, and because it applies to systems defined by different values of the thermodynamic parameters, it is fully transferable. Moreover, because it is derived from a first principle approach, its properties are well defined. However, analytical potentials, as the ones we derived here, can be obtained only for a limited number of systems, thus implying that in most cases the numerical optimization procedure is the only option in deriving the effective coarse-grained potential. In conclusion, both analytical and numerically evaluated potentials are useful as they answer complementary questions in the process of building optimized coarse-grained descriptions of macromolecular systems.

Finally, it is important to notice that the mean-force potential is not the correct input potential for the mesoscale simulations, as the two agree only for systems at low density,[40] however it is a good first guess in the iterative numerical procedure commonly adopted. In Figure II.1 we show for the systems investigated the direct potential, which is input to our simulation, and the mean-force potential. The two appear to be related, even if their numerical value and the extent of the attractive contribution is quite different.

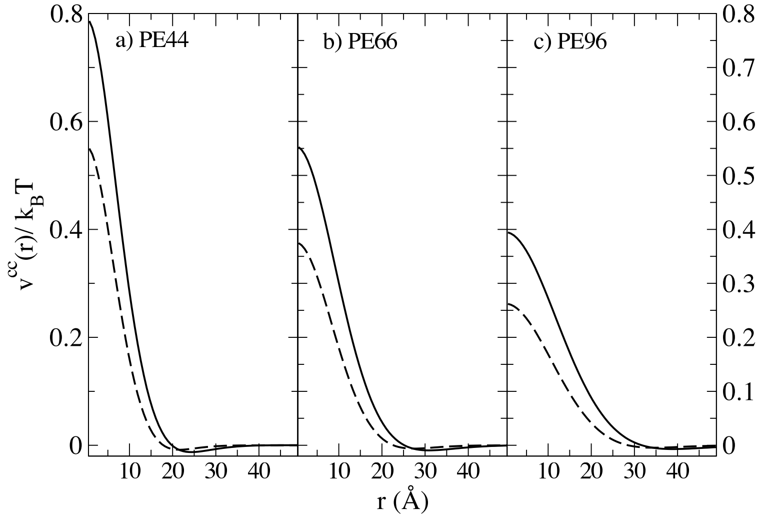

FIGURE II.1. The total pair potential, which is input into our MS-MD simulation, is shown for different chain lengths of polyethylene (solid line). For comparison, the dashed line represents the corresponding mean-force potential.

II.3. Mesoscale Simulation

Once the formalism to describe analytically the structure of a liquid of polymers in a coarse-grained representation is solved, and the effective potential between coarse-grained units is derived, it is possible to run directly mesoscale simulations of the coarse-grained systems. Our mesoscale simulations were performed by implementing classical MD simulations in the microcanonical (N, V, E) ensemble. We simulated liquids of point particles interacting through the soft potential resulting from Eqs.(II.4)-(II.6), which is repulsive at short range and slightly attractive at longer range. The interparticle potential differs depending on the chemical nature of the polymer investigated, as well as thermodynamic parameters of density and temperature. The systems we simulated included melts of polyethylene (PE) with $N = 44$ (PE44), $N = 48$ (PE48), $N = 66$ (PE66), and $N = 96$ (PE96) monomers. Other systems were melts of syndiotactic polypropylene (sPP), head-to-head polypropylene (hhPP), isotactic polypropylene (iPP), and polyisobutylene (PIB), all with 96 united atoms per chain. Each simulation was performed on a cubic box with periodic boundary conditions. We used reduced units in our simulation, such that all the units of length were scaled by R_g $(r^* = r/R_g)$ and energies were scaled by k_BT. The density was fixed at the value reported in Table II.1. Temperature and radius-of-gyration were utilized for dimensionalizing the results obtained from the MS-MD simulations, after they were performed.

TABLE II.1. Simulation Parameters for Polyolefin Melts

Polymer	Number of CH_x moieties	T [K]	ρ [sites/Å^3]	R_g [Å]
PE44	44	400	0.0324	10.50
PE48	48	448	0.0329	10.88
PE66	66	448	0.0329	13.32
PE96	96	453	0.0328	16.78
sPP	96	453	0.0328	13.93
hhPP	96	453	0.0336	13.54
iPP	96	453	0.0328	11.34
PIB	96	453	0.0357	9.68

The potential and its corresponding derivative entered as tabulated inputs to the program, and linear interpolation was used to determine function values not found in the supplied numerical data as the algorithm proceeds. In the initialization step, all particles were placed on a lattice, and each site was given an initial velocity pooled from a Mersenne Twister random number generator.[2] Subsequently, the system was evolved using a velocity Verlet integrator.

Equilibrium was induced in the ensemble by velocity rescaling. The desired temperature in the ensemble was attained by a quencing procedure, where velocities were forceably rescaled at regular intervals during the equilibration stage. We checked that the system had reached equilibrium when we observed a Maxwell-Boltzmann distribution of velocities, a steady temperature, a stabilized Boltzmann H-theorem function, and a decayed translational order parameter. At this stage, velocity rescaling was discontinued. We monitored the fluctuating steady temperature during the production stage to be sure that the system remains in equilibrium. During the production stage trajectories were collected over a traversal of $\sim 8R_g$.

A typical mesoscale simulation consisted of $\sim$ 3000 particles, evolving for about $30,000$ computational steps during $\sim$ 4 hours, and performed on a single-CPU workstation. We stress that our mesoscopic simulations represent an underestimate in the computational time since these have not been subjected yet to a parallelization. The large-scale (R_g length scale) pair distribution function resulting from the mesocale simulation has been shown to be in quantitative agreement with the one obtained from a full UA simulation, so that no precision is lost on the large scale during the coarse-graining procedure.[8, 46, 47] The mesoscale simulation, however, required a much smaller computational power than the full UA simulation. UA-MD simulations of polymer melts against which our MS-MD simulations are compared used $\approx 1,600$ chains with $N = 96$ units, where 1 ns of simulation required either 9 h of computer time on 512 processors of Sandia's ASCI Red Intel cluster or 25 h of computational time on 64 processors on a Cplant DEC alpha cluster.[15, 57, 58] The reduced computational time of the MS-MD allowed for improved precision in the large-scale regime as it was possible to increase the number of particles and the box size, with respect to the UA-MD, without dramatically affecting the computational time.

In this communication we test our multiscale procedure by comparing the resulting monomer total distribution function against the UA-MD simulation just described. We call this simulations the "full UA-MD". Those simulations were performed by Mondello et al.,[15] Jaramillo et al.,[57] and Heine et al.[58]

To capture properties on the monomer scale, the multiscale procedure requires information on the local scale, which must be extracted from simulations with atomic level resolution, here UA-MD. However, the UA simulation input to a multiscale modeling procedure only requires a number of polymers of the order of $\sqrt{N}$, which is much smaller than the number of polymers simulated in the full UA-MD, as we will discuss further in the communication. Henceforth we refer to the UA-MD simulation input to the multiscale procedure as the "local UA-MD".

II.4. Building the Full Structural Description at the Monomer Scale Using a Multiscale Approach

In a multiscale procedure, simulations are performed on a hierarchy of models where the same system is coarse-grained at different levels of resolution. The success of the method depends on the extent to which the system properties are modulated around distinct length scales. In the description of a polymer melt, the two length scales that are involved are the monomer segment length and the polymer radius-of-gyration. As it is shown in the left panels of Figures II.5-II.8 for the polymers considered in this study the peak on the local scale and the global properties are well separated. The multiscale procedure would not work if the local and global features superimpose, which could happen for short chains of stiff polymers. For those systems, however, the full UA-MD simulations are not too time consuming and there is no need to apply coarse-graining or to adopt a multiscale procedure.

In our mesoscale simulations polymers are represented as point particles interacting through a soft potential of the range of the polymer size. i.e. R_g. The MS-MD provide information for any length scale of the order and larger than the polymer radius-of-gyration. It should be noted that neither mesoscale nor UA simulations can accurately describe the system at a radius larger than half their simulation box length. However, because the box size can be considerably larger for mesoscale simulations than for UA-MD, the MS-MD can describe large-scale properties more efficiently than UA simulations (see Table II.2).

On the local scale, however, mesoscale simulations do not provide any information. To recover the structure of the liquid at length scales smaller than or equal to R_g, it is necessary to combine MS-MD with UA-MD simulations. These UA-MD, however, only need to provide information on the local scale, and they are run on a small number of molecules, of the order of $\sqrt{N}$, and are performed for a contained number of simulation steps. Even if UA-MD simulations have to be performed to provide the local information, the multiscale procedure efforts a net computational gain with respect to directly running a "full" UA-MD.

On the global scale, small k, the *monomer* total distribution function is calculated from the data of the mesoscale simulation, using the inverse of Eq.(II.2)

$$h^{mm}(k) = \left[\frac{\omega^{mm}(k)}{\omega^{cm}(k)} \right]^2 h^{cc}(k) \ , \tag{II.7}$$

where mesoscale simulations provide $h^{cc}(k)$ while UA MD simulations are used to determine the intramolecular form factors, $\omega^{mm}(k)$ and $\omega^{cm}(k)$.

Figure II.2 and II.3 show $h^{mm}(k)$ (solid line) calculated from the mesoscale simulation using Eq.(II.7) for several of the polymer melts of Table II.1, where each chain has 96 CH_x

TABLE II.2. Comparison of MS-MD Simulations with UA-MD Simulations

System	n_{MS}	L_{MS}[Å]	n_{UA}	L_{UA} [Å]
PE44	4000	175.7978	100	51.4033
PE48	4096	181.6127	400	83.634
PE66	5324	220.2708	100	58.5530
PE96	6859	271.7286	100	167.270
sPP	4394	234.2482	1600	167.27
hhPP	4096	227.5623	1600	165.966
iPP	3375	214.5239	1600	167.27
PIB	3375	208.6244	1600	162.676

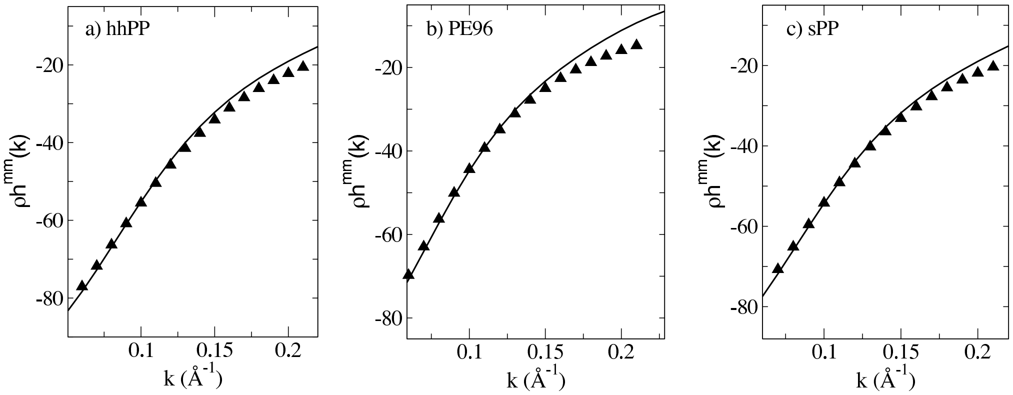

FIGURE II.2. Plot of $h^{mm}(k)$ for different polymer melts. Solid line depicts $h^{mm}(k)$ calculated using Eq.(II.7). Symbols represent data points from full UA MD simulation.

units, with $x = 1, 2$, or 3. The calculated $h^{mm}(k)$ (solid line) is compared to the full UA MD simulation (symbols). As expected, the theory compares well to UA MD simulations for the small k range (large r), and begins to diverge as k increases. This is a consequence of the coarse-graining procedure, Eq.(II.7). Since monomers can superimpose with the center-of-mass, $\omega^{cm}(k)$ approaches zero for large k, while $\omega^{mm}(k)$ has a finite value at contact due to the hard-core monomer-monomer repulsion. As a consequence the ratio: $[\omega^{mm}(k)/\omega^{cm}(k)]^2$ diverges at some large k value.

In general, $h^{mm}(k)$, calculated from Eq.(II.7), using data from mesoscale simulations and the intramolecular structure factors from UA simulations, accurately captures the structural properties of the polymer for small values of k (global structure), as it is shown in Figure II.2. However, the same quality of agreement observed between mesoscale simulations and data of the monomer total correlation function for most of the cases is not observed in two specific polymer structures, namely for iPP and for PIB, see Figure II.3. It is known that both PIB and iPP favor highly packed intramolecular structures because of the symmetry in the position of the sidechains in the monomeric unit.[47] Moreover, because of the presence of two side-groups in a PIB monomer, the number of monomers in a PIB chain containing 96 united atoms, is equal to 24 monomers. With such a small number of monomers the PIB sample can hardly exhibit Gaussian statistics for the intramolecular distribution. Because the assumption of having a Gaussian statistics is

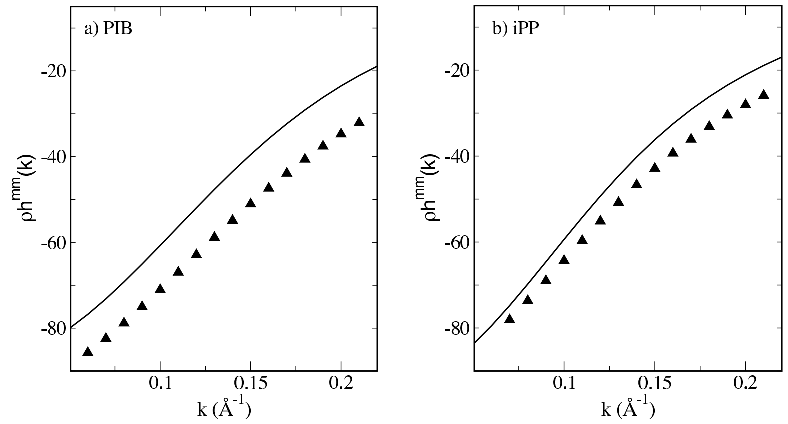

FIGURE II.3. Plot of $h^{mm}(k)$ for different polymer melts. Solid line depicts $h^{mm}(k)$ calculated using Eq.(II.7). Symbols represent data points from full UA MD simulation.

the starting point in our approach,[8,46,47] this accounts for the discrepancies between the coarse grained values and UA MD data that we observe for these systems.

II.5. Combining United Atoms and Coarse-Grained Simulations: The Crossover Length Scale

Since the mesoscale simulation only captures global properties, it is necessary to determine the length at which local, intramolecular effects become significant and cannot any longer be discarded. This defines the crossover length scale for the UA simulation at which data from UA-MD and MS-MD simulations are combined.

The extent to which intramolecular effects remain important on large length scales depends on the length of the polymer and its flexibility. If the length of the polymer is constant, stiffer polymers span a larger volume and therefore have a higher (lower) number of inter- (intra)molecular contacts than their more flexible counterparts. Furthermore, longer chains of polymers with identical chemical structure have a higher statistical number of interpenetrating molecules and a higher (lower) number of inter- (intra)molecular contacts than shorter chains. The iPP and PIB samples presented here are characterized by efficient intramolecular packing, which is due to the particular monomeric structure: for these chains intramolecular interactions are dominant over intermolecular ones for an extended range of length scales.

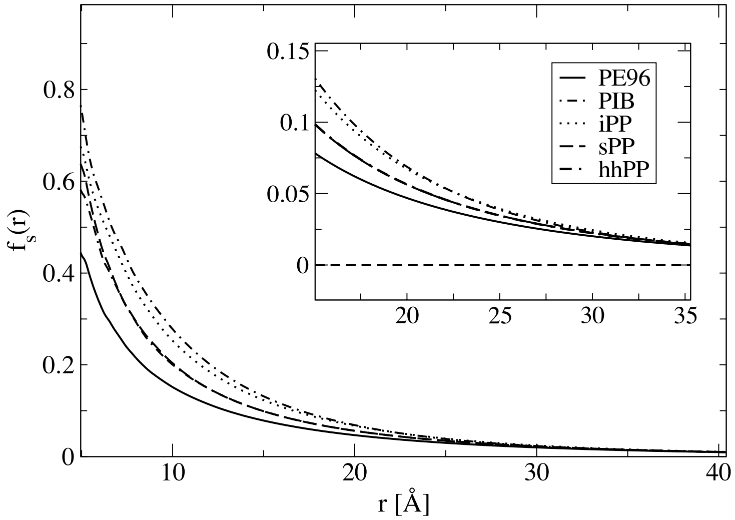

FIGURE II.4. Fraction of intramolecular contacts, $f_s(r)$, for melts of polymers with different monomer architectures.

The extent of intramolecular packing is quantified by calculating the ratio between the number of *intra* and *total* site/site contacts at a fixed radial distance, r,

$$f_s(r) = \frac{N_s(r)}{N_{total}(r)} \tag{II.8}$$

where $N_s(r)$ is the number of intramolecular contact sites defined as

$$N_s(r) = 4\pi\rho \int_0^r r'^2 \omega^{mm}(r')\, dr' \ . \tag{II.9}$$

The total number of sites in a given volume, $N_{total}(r)$, is given by

$$N_{total}(r) = \frac{4}{3}\pi\rho\, r^3 \, . \tag{II.10}$$

Figure II.4 shows $f_s(r)$ vs. r for different monomer architectures. As expected, iPP (dotted line) and PIB (dot-dashed line) show higher values of $f_s(r)$, whereas the stiffest molecule, PE (solid line), exhibits the lowest value at a given radius.

Following the reasoning presented at the end of this section, we assume that a fraction of intramolecular contacts equal to $f_s(r) = 0.025$, which corresponds to 2.5% of the total sites involved in intramolecular contacts, defines the value of the crossover distance. This corresponds to a distance r that is unique for a given polymer chain, and it defines the corresponding value in reciprocal space, $k = 2\pi/r$, at which the two simulations have to be combined.

Figures II.5-II.8 display the comparison of the total correlation function obtained with our procedure (Eq.(II.7)) and data from extended UA simulations. The left panel of the Figures show the total correlation function in reciprocal space, $h^{mm}(k)$, for various polymer melts, (sPP, hhPP, iPP, and PIB) and for varying chain lengths of polyethylene (PE). $h^{mm}(k)$ is obtained by combining the large scale data (small k) from the mesoscale simulations with the small scale data (large k) from united atom simulations. The vertical dashed line in Figures II.5-II.8 indicate the radius at which the MS-MD is combined with the UA MD simulation. Note that this occurs at an intermediate distance between the local peak and the global feature, so that neither information about the long range structure, nor the local structure is lost in extrapolating the connection between the two curves for $h^{mm}(k)$.

The right panels of Figures II.5-II.8 show the total correlation function, $h^{mm}(r)$, for polymer melts, obtained by taking the Fourier transform of $h^{mm}(k)$. The function, $h^{mm}(r)$, provides a complete description of the liquid structure and thermodynamic properties. In performing the discrete Fourier transform of the multiscale total correlation function, a sampling step of $\Delta k = 0.01\text{Å}^{-1}$ was used, which defines the resolution of the transformed function. Since we are combining two separate data sets, Δk must be large enough so that the Fourier transform is not affected by the small discontinuity at the point of intersection. As long as the interval of the discontinuity is of the same order as that of the sampling step there is no effect on the Fourier transform.

The calculated values for $h^{mm}(r)$ using our multiscaling approach (solid line) are presented along with data from the full UA MD simulations (symbols). The proposed method gives results in good agreement with the full UA simulation data and correctly captures all of the relevant structural features of the liquid, including solvation shells and the correlation hole observed in polymers.

Once this procedure is adopted, the iPP and PIB samples also give a good agreement with the full UA-MD simulation. Because in these samples, and in PE44, the chains are short, the total correlation function still shows a small numerical error. The error is clearly displayed by the

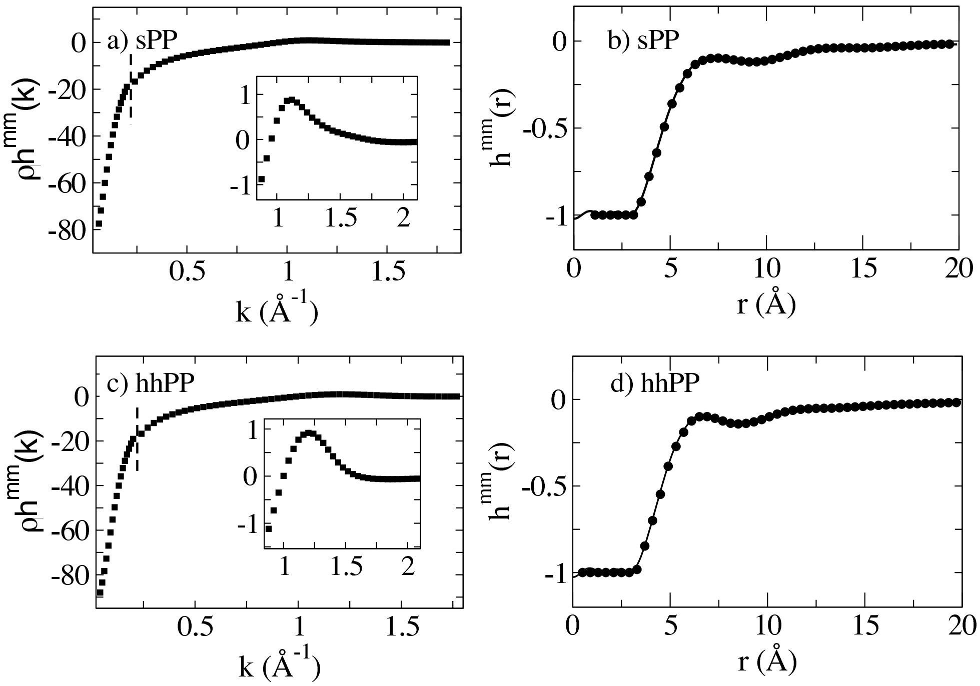

FIGURE II.5. (left) Plot of the total correlation function, $h^{mm}(k)$, for polymer melts of (a) sPP and (c) hhPP, obtained by combining mesoscale and UA MD simulations. Mesoscale simulation depicts $h^{mm}(k)$ over the small k range whereas UA simulation provides data over the large k range. The dashed line indicates the point at which the two simulations were combined. The inset depicts the local peak. (right) Plot of the related $h^{mm}(r)$, the total correlation function in real space for (b) sPP and (d) hhPP. The solid line depicts $h^{mm}(r)$ calculated using our multiscaling approach and the open circles represent data points from UA MD simulations.

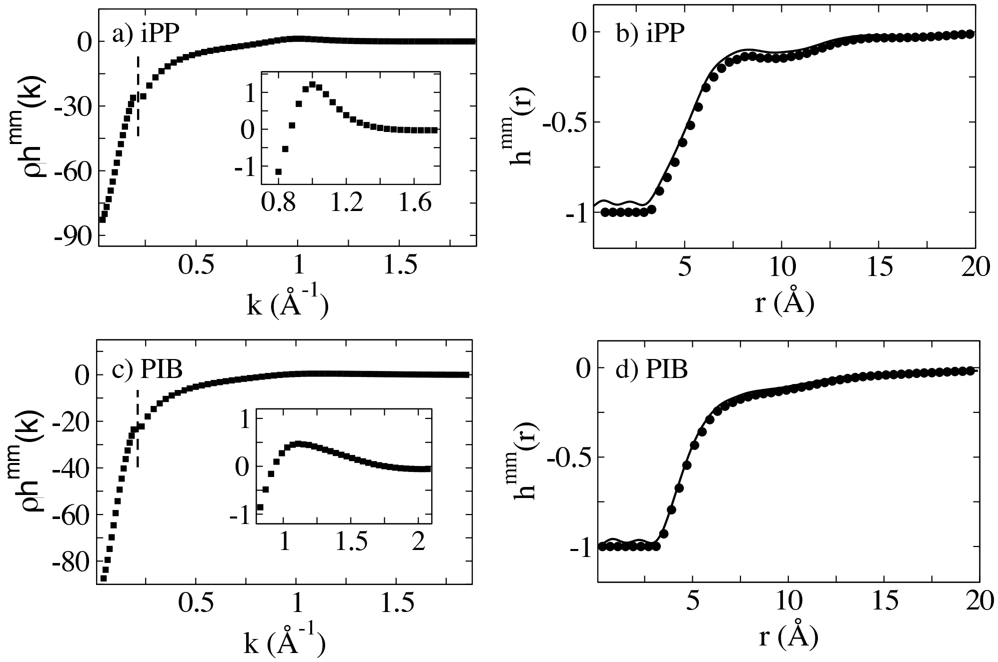

FIGURE II.6. Plot of $h^{mm}(k)$ and $h^{mm}(r)$. Combining theory and UA simulation (iPP, PIB). Same as in Figure II.5 for polymer melts of (a) iPP and (c) PIB

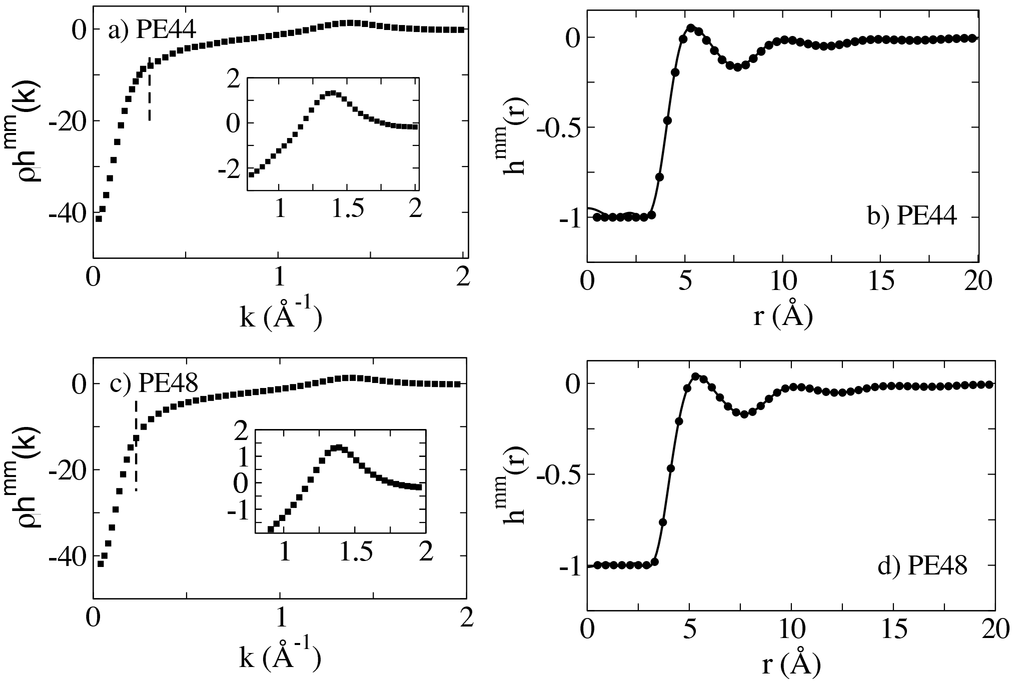

FIGURE II.7. Plot of $h^{mm}(k)$ and $h^{mm}(r)$ for polyethylene of different lengths (PE44, PE48). Same as in Figure II.5 for polymer melts of (a) PE44 and (c) PE48

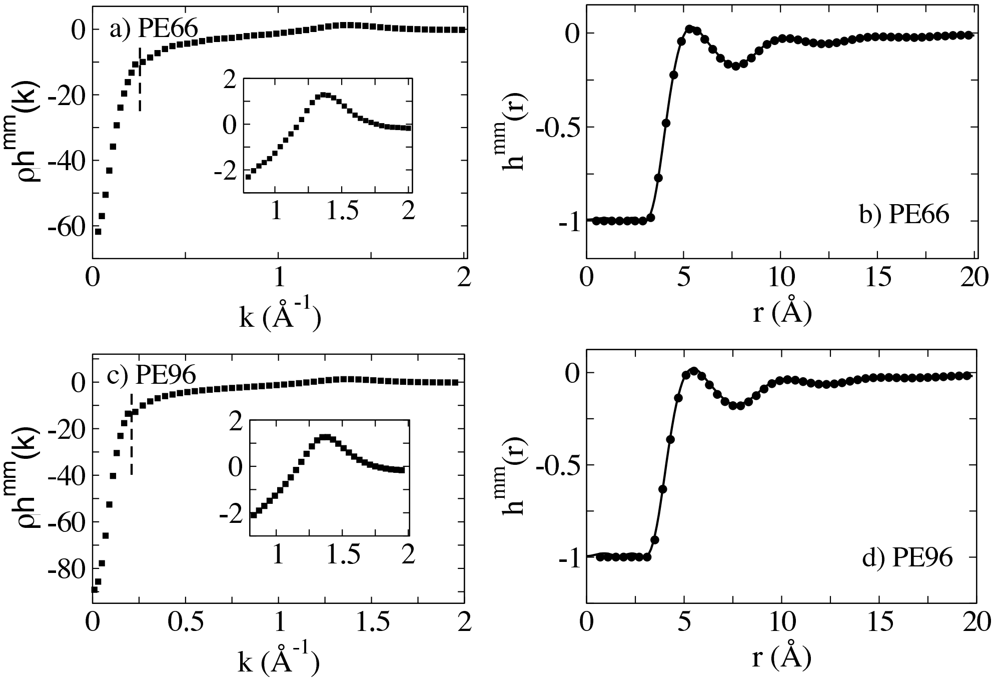

FIGURE II.8. Plot of $h^{mm}(k)$ and $h^{mm}(r)$ for polyethylene of different lengths (PE66, PE96). Same as in Figure II.5 for polymer melts of (a) PE66 and (c) PE96

function in the $r < d$ regime, with d the hard-core diameter of the repulsive inter-site interaction. This is the region of the excluded volume, and here it should be found that $h(r) = -1$.

The local chain structure, at large-k, is represented by the peak in the insets of Figures II.5-II.8, which has a shape that depends on the monomeric structure as well as on the thermodynamic parameters of density and temperature, as the local chain packing is affected by those quantities. Figure II.9 shows superimposed the local peaks for polyethylene chains with increasing degree of polymerization at constant temperature of 448 K. Because the chains have the same monomeric structure, and the thermodynamic parameters for each sample are close in value, the local peaks superimpose. This leads to a further computational gain for the multiscale procedure, with respect to performing the full UA-MD simulation. Because the local properties are largely independent on the global scale properties for samples with long polymer chains, the multiscale procedure allows one to obtain the local scale properties for all samples just from one local UA-MD, which can be performed on a melt of short polymer chains, e.g. $N \approx 40$.

Once the pair distribution function is obtained from the multiscale procedure any thermodynamic quantity of interest can be numerically derived, including the equation of

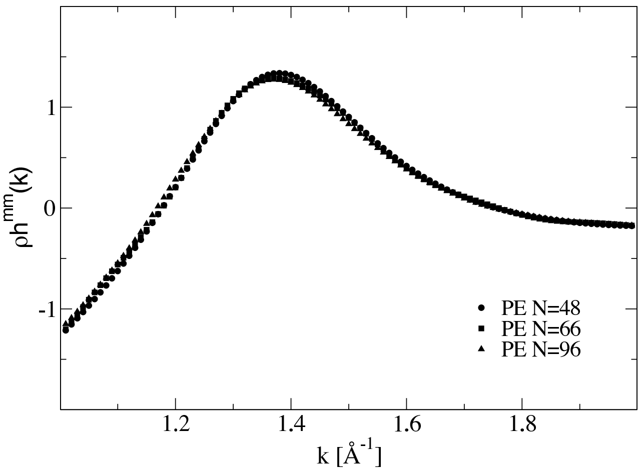

FIGURE II.9. Plot of the local peak for the total correlation function, $h^{mm}(k)$, for polymer melts of PE at increasing degree of polymerization, ($N = 48, 66, 96$) from local UA simulations at T=448 K.

state, the virial coefficient, internal energy, compressibility, and others.[40] Clearly the degree of precision of the multiscale total distribution function will affect the precision of the resulting thermodynamic quantities, so that care has to be taken in the choice of the crossover distance where local and global information is combined to optimize the agreement between UA-MD and multiscale data.

The crossover distance, at which the UA-MD ceases to provide relevant information on the local scale, is determined from the chosen value of the fraction of intramolecular contacts. In all the calculations reported above we adopted the value $f_s(r) = 0.025$. To determine this value, we investigated the extent of agreement between the total correlation function calculated through the multiscale procedure and the one from the full UA-MD data as a function of f_s.

Figure II.10 shows a correlation plot of $h^{mm}(r)$ from UA simulation and $h^{mm}(r)$ calculated from our theory when local UA-MD data were combined with MS-MD data at a radius corresponding to $f_s(r) = 0.05$ (top) and $f_s(r) = 0.025$ (bottom). Shown are the correlation plots for the stiffest chain, PE, and for the two most flexible ones, PIB and iPP. The degree of correlation between theory and simulation increases as $f_s(r)$ decreases, as expected; however already at $f_s(r) = 0.025$ there is a very high degree of positive correlation between the two. The correlation coefficients between theory and simulation for each polymer architecture are shown in Table II.3. As $f_s(r)$ decreases, the mesoscale picture of the liquid becomes increasingly accurate.

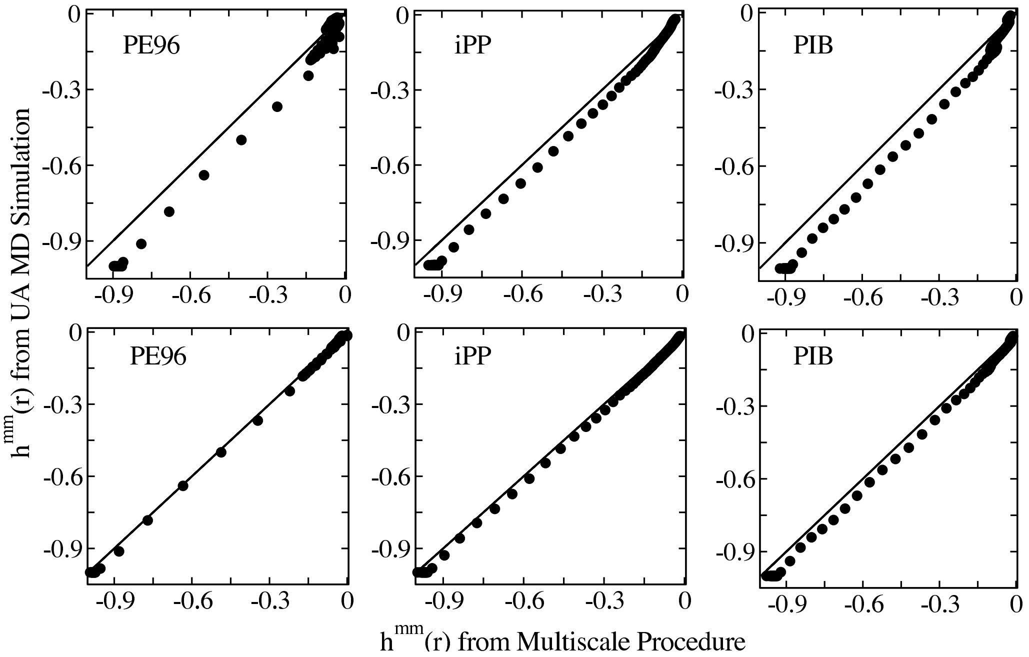

FIGURE II.10. Correlation coefficient for $h^{mm}(r)$ obtained from the full UA-MD simulation and its theoretical value calculated with $f_s(r) = 0.05$. Bottom panels: same as in top panels, but with $f_s(r) = 0.025$.

However, $f_s(r)$ only becomes appreciably small for a large radius, r, and so there is a trade-off between computational time in performing UA MD simulations and obtaining an accurate picture of the liquid structure.

TABLE II.3. Correlation coefficient for polyolefin melts

polymer	correlation coefficient at $f_s(r) = 0.025$
PE96	0.9998
sPP	0.9999
hhPP	0.9998
iPP	0.9998
PIB	0.9995

Because the correlation coefficient is close to unity in all polymer systems tested for $f_s(r) = 0.025$ and does not improve significantly for smaller values of $f_s(r)$, we propose that this value serves as a general rule of thumb for combining mesoscale and UA simulations.

A possible different criterion of selection of the crossover length scale could be to defined the point in which the UA-MD curve intersect the MS-MD (see Figure II.2). This leads to values of the distance r that are slightly larger than the ones established above, and for this reason requires more demanding local UA-MD, without adding precision to the calculated pair distribution functions. Furthermore, as mentioned above, for PIB and iPP, the curves never superimpose making an exact criterion of this sort for the combination of the two simulations unclear. By using the method adopted above of calculating the fraction of intramolecular contacts to determine the relevant crossover length scale, an exact distance, at which to combine the information, is readily obtained, and this distance does not depend on explicitly knowing the full UA MD simulation.

The value of $f_s(r) = 0.025$ is reached for a distance r that is polymer dependent. The number of polymer chains statistically comprised in the volume spanned by r defines an average number of chains, n, that we need to consider in a local UA-MD simulation to produce good statistical information. This number can be calculated from Eq.(II.10) using the crossover radius and dividing the number of particles so obtained by the number of CH_x, with $x = 0, 1, 2, 3$, units contained in a single chain. The number of sites, N_{UA}, and the number of polymer chains, n, contained in the volume defined by the given radius of intramolecular interactions, calculated for value of $f_s(r) = 0.025$, as well as for $f_s(r) = 0.05$, are presented in Table II.4. The number of chains n is also the statistical number of macromolecules that need to be considered in a local UA-MD simulation and is of the order of the number of chains interpenerating a "tagged" polymer, $\sqrt{N}$. This number of chains is one order of magnitude smaller than the number of molecules commonly used in the full UA simulations of polymer melts.

TABLE II.4. Total Number of Sites (N_{sites}) and Number of Molecules (n) included in a spherical volume of radius r, evaluated for $f_s(r) = 0.025$ and 0.05

System	$N_{sites}(0.025)$	$n(0.025)$	$N_{sites}(0.05)$	$n(0.05)$
PE96	2785	29	995	10
sPP	3547	37	1412	15
hhPP	3518	37	1511	16
iPP	3931	41	1758	18
PIB	3729	39	1749	18

II.6. Conclusion

In this communication we presented a new multiscale approach to simulate the structure of polymer melts in a computationally efficient way. We first identified the relevant length scales in which information has to be collected. For a liquid of uncharged homopolymer chains there are two length scales, which characterize all the structural properties of the macromolecular liquid, namely the monomer and the molecular radius of gyration.

Molecular Dynamics simulations are performed for each system in the two different coarse-grained representations. At the monomer level, the liquid is well represented through an United-Atom (UA) description, where each CH_x unit, with $x = 1, 2$, or 3, corresponds to an effective unit. At the molecular level, the coarse-graining is obtained through a soft-colloid representation, where each polymer molecule is depicted as a point particle centered at the polymer center-of-mass, and interacting with other particles through a soft repulsive potential of the range of R_g.

The two coarse-grained descriptions are formally connected through an Ornstein-Zernike equation, solved under the condition that the com's are fictitious sites, while the united atoms are real sites. An analytical solution of the OZ equation in terms of the total correlation function between the two representations has been derived, and this equation is used to combine local and global scale information in the proposed multiscale modeling procedure.

Information on large scale properties is collected from the MS-MD, soft-colloidal, simulation, which extends to large-scale and covers long-time regimes, as the dynamics is sped up because of the elimination of the internal degrees of freedom. The large-scale information has been shown to be quantitatively correct. However, because local degrees of freedom are averaged out, MS-MD simulations do not provide any information on local-scale properties.

To obtain a description of the macromolecular liquid at the monomer length scale, MS-MD simulations have to be combined with local UA-MD simulations. A crossover length scale between the two representation has to be defined. This is equivalent to establishing at which small length scale the coarse-grained description ceases to be valid. The local degrees of freedom are relevant up to a characteristic length scale, which is different depending on the chemical structure of the monomer, but which can be evaluated using short-time small-box united atom simulations. Once this crossover length scale is determined, it is adopted as the point at which global length scale information from MS simulations has to be combined with the local scale description from UA simulations, in reciprocal space. The resulting monomer total distribution function is Fourier transformed from reciprocal to real space to give the complete description of the system, through the total correlation function, $h(r)$.

We show that the resulting function, tested against data obtained from a full UA-MD simulation, exhibits quantitative agreement. Furthermore, a comparison of the needed computational time and resources of the multiscale procedure, against the requirements of the full UA simulation for the same system, highlights several favorable points.

In general, simulations of liquids necessitate the inclusion of a high number of molecules, n, to achieve a good statistical description, minimize finite-size effects, and approximate the thermodynamic limit ($n \rightarrow \infty$ and $V \rightarrow \infty$ while density, $\rho = n/V$, is constant). Moreover, macromolecules usually comprise a large number of monomers N, so that the overall computational time to simulate polymeric liquids increases rapidly, scaling as $(nN)^2$, if we assume the conventional scaling of computational steps with the square of the number of particles. This feature poses some limitations on the total number of polymers, their length, or the longest timescale that can be simulated.

Other techniques can be adopted to decrease the exponent in the scaling of the computational time, but these procedures usually cannot be translated into parallel calculations. Even with the most powerful resources, long-time UA-MD simulations of polymer melts usually can treat a maximum of 500 chains, for polymers comprised by less than 100 monomers. However, the best statistical description is reached for simulations of thousands of molecules, which is very time consuming and impossible to perform for long polymers.

A multiscale procedure is advantageous, because the mesoscale simulation provides the information on the large spatial and long-time scale, so that microscopic UA simulations can be limited in the number of particles that are monitored and in the computational time during which data are recorded.

In our procedure the number of molecules to be included in the UA simulation is of the order of the number of chains interpenetrating a single macromolecule ($\mathrm{O}(\sqrt{N})$), which is about one order of magnitude smaller than the number of particles needed if we perform a full UA simulation. For example, if we assume a scaling proportional to the square of the number of particles, the proposed procedure requires only $n^2 = N$ soft colloidal particles to calculate $h^{cc}(k)$

and only $(nN)^2 = N^3$ number of units in the local UA simulation, which is a dramatic gain with respect to the UA scaling of $(nN)^2$ where $n >> N$ for the full simulation.

If we assume a different scaling with the number of particles, for example because of adopting a more advanced sampling rule, the multiscale approach is still more convenient in the number of computational steps than the full UA MD simulations, since the gain in computational time when comparing the two procedures is due to the change in the total number of molecules to be tracked in the UA simulation, i.e. from $n \gg N$ in the full UA simulation to $n \propto \sqrt{N}$ in the local UA simulation.

Finally, computational time is further reduced when a family of homologous chains that only differ because of the degree of polymerization are under study: in this case local UA-MD only have to be performed for the shortest chain, as discussed in the previous section.

Having reduced the computational time necessary to obtain local information, the global scale description results from a mesoscale simulation, which can include a large number of particles and large box size without dramatically increasing the computational time, thus improving the statistics of the system on the global scale. Table II.2 shows the comparison of the number of molecules (n) and simulation box length (L) for UA simulations and MS simulations of different polyolefins.

For example, the full UA simulation for polyethylene with 66 united atoms includes 100 polymer chains, while our MS simulation includes over 5,000 polymers as soft colloids, providing a mesoscale liquid structure which is identical in the two simulations and a large scale description with improved statistics. This reinforces the point that only small UA simulations need to be performed to capture local properties, whereas the global properties may be deduced using a mesoscale approach which greatly extends the capabilities for computer simulations of macromolecules. The possibility of simulating systems on very large length scales while including a large number of particles can be useful in treating systems with diverging correlation lengths, such as mixtures approaching their spinodal decomposition.

In conclusion, Figures II.5-II.8 show that our method of combining mesoscale simulations at the coarse grained level with small UA simulations accurately captures both the large and small scale structure of a polymeric melt while remaining computationally advantageous. The approach is analytical and uses no adjustable parameters, and is therefore applicable to a large number of different polymer systems of varying chain length, density, and with different local chemical structure. As an example in this communication we investigate polyethylene chains with increasing degree of polymerization, as well as polymer chains with different monomeric structure. The same multiscale procedure is used for all of them, providing efficient calculations of monomer static properties across the many length scales of interest.

CHAPTER III

ANALYTICAL RESCALING OF POLYMER DYNAMICS FROM COARSE-GRAINED SIMULATIONS

The material of Chapter III is an overview of a theoretical approach to scale the artificially fast dynamics of simulated coarse-grained polymer liquids down to its realistic value. More comprehensive in-depth discussion of the formalism is given in Chapter IV and the application of the rescaling is on Chapter V. As coarse-graining affects entropy and dissipation, two factors enter the rescaling: inclusion of intramolecular vibrational degrees of freedom, and rescaling of the friction coefficient. Because our approach is analytical, it is general and transferable. Translational and rotational diffusion of unentangled and entangled polyethylene melts, predicted from mesoscale simulations of coarse-grained polymer melts using the rescaling procedure, are in quantitative agreement with united atom simulations and with experiments. My contribution to this chapter is in calculations of the rescaling factors, performing coarse-grained simulations, analyzing simulations data and preparing the illustrations. Anthony Clark participated in valuable discussions and James McCarty provided editorial assistance.

III.1. Introduction

The development of a systematic approach to bridge time scales between different hierarchical levels of description is an important goal in many areas of the physics of complex systems.[1] Furthermore, understanding the dynamics of polymeric liquids is relevant for many technological applications. Polymeric materials are processed in their liquid state, and the custom tailoring of new materials requires detailed predictions of their mechanical and dynamical properties to be made based on their chemical structure. To this end, molecular dynamics (MD) simulations shed light on the properties of complex systems; however, MD is limited by the precision of the calculations, which degrades with the number of computer iterations.[2] Quantitative predictions of the dynamics of unentangled polymer liquids are possible through simulation runs that are computationally demanding because the polymer self-diffusion coefficient, D, in melts scales with the degree of polymerization, N, as $D \propto N^{-1}$. Even more demanding are simulations of liquids of long, entangled, polymeric chains, where the diffusion coefficient scales as $D \propto N^{-2}$. For entangled polymer liquids it is therefore difficult to obtain well-equilibrated samples or to simulate the system for several relaxation cycles, which would improve the precision of the calculated time-correlation functions.

To reach the long time and length scales of interest, special strategies need to be employed. For example, some gain in computational time has been achieved by speeding up the equilibration process through an end-bridging Monte Carlo algorithm.[3] Moreover, if only qualitative, and not quantitative, predictions are sought, it is possible to adopt simplified intra- and intermolecular potentials, which can speed up each simulation step,[4,5] or purely phenomenological coarse-grained descriptions, which reproduce the expected dynamical scaling behavior.[5,6] However, quantitative computational methods that precisely relate chemical structure to the long-time properties of the polymeric liquid are still lacking.

There is a need for computationally efficient, predictive methods to simulate polymer liquids and complex fluids in the long-time regime. The strategy we are pursuing here is to develop coarse-graining methods and dynamical rescaling procedures which start from first-principles theory.[7,8] The goal is to obtain quantitative predictions of real polymer dynamics directly from properly rescaled fast mesoscale (MS) simulations of coarse-grained liquids.

In a coarse-grained description, the system is specified by a set of relevant mesoscopic variables while smaller length scale variables are omitted.[9] This is done at the expense of entropy and dissipation (friction), which are underestimated by coarse-graining.[7] Because of the reduced molecular degrees of freedom and the simplified energy landscape, MS-MD simulations require less computational time than atomistic simulations of the same systems.[8,10–12] However, because the effective energy landscape of the coarse-grained representation is artificially smooth, MS-MD simulations predict accelerated dynamics, which need to be rescaled to produce realistic values.

The enhanced diffusion in coarse-grained systems arises from the “soft” nature of the intermolecular potential. This is advantageous in enabling larger time steps to be used in integrating the equations of motion, and an efficient sampling of the energy landscape, which leads to good statistical averages of the structural properties on the large scale.[13] However, the measured dynamics of coarse-grained systems is too fast, and as of yet, there is no clear procedure to quantitatively re-scale these accelerated dynamics.

In an effort to develop quantitative rescaling methods, it is customary to build a numerical "calibration curve" obtained from direct comparison of MS-MD time correlation functions with atomistic simulations. The "calibration curves" are parametric, normal mode dependent, and specific to the system against which they are optimized, as well as to its thermodynamic conditions. Building these parametric curves in part defeats the purpose of the coarse-graining procedure as it requires running many atomistic simulations to optimize the fitting parameters. If the level of coarse-graining is low, i.e. if the average is performed over a small number of atoms, the correction to the dynamics is only perturbative and the parametric rescaling works well.[14] This explains the success of united-atom (UA) simulations.[3, 15] However, because the gain in computational time increases with the level of coarse-graining, simulations of slightly coarse-grained systems,e.g. UA-MD, afford a limited gain in time and length scales.

The most gain in computational efficiency is achieved through large-scale coarse-graining, as the one adopted in this communication. This is most useful when studying bulk physical quantities, e.g. viscosity, or systems with large-scale fluctuations, e.g. approaching spinodal decomposition.[16] Once simulations of heavily coarse-grained systems are combined with local scale simulations in a multiscale procedure, they provide the complete description of the system at all length scales of interest.[17]

This Chapter presents a derivation of a first-principles approach to rescale the dynamics from MS-MD simulations of a coarse-grained polymer melt to the values of an atomistic description. The rescaling is analytical, general and transferable. The favorable comparison with atomistic simulations and experimental data in different thermodynamic conditions supports the validity of the proposed procedure. The theoretical basis of the rescaling rests on the fact that the accelerated dynamics is a result of the missing dissipation due to the eliminated degrees of freedom.

The Chapter is organized as follows. In Section III.2 we briefly review our coarse-grained model, while the coarse-grained potential and mesoscale simulations are described in Section III.3. In the following section we present our atomistic model and the calculation of the energy due to the internal degrees of freedom. Rescaling of the friction coefficient is discussed in Section III.5, followed by a comparison of the diffusion coefficients predicted from MS-MD simulations after rescaling, with united-atom simulation and experimental data. A brief discussion concludes the communication.

III.2. Coarse-Grain Model

Our coarse-grained representation models polymers as interacting soft-colloidal particles with repulsive interaction range of the order of the size of the macromolecule, defined by the radius-of-gyration, R_g.[8] The total distribution function is derived from the solution of a generalized Ornstein-Zernike matrix equation

$$H(k) = \Omega(k)C(k)\left(\Omega(k) - H(k)\right) , \tag{III.1}$$

where $\Omega(k)$ is an intermolecular monomer distributions and $C(k)$ is a direct correlation function in reciprocal space. Eq. III.1 treats center-of-masses of coarse-grained sites as auxiliary sites, and monomer sites as real sites.[18] In reciprocal space, the total distribution function is

$$h(k) = \left[\omega^{cm}(k)/\omega^{mm}(k)\right]^2 h^{mm}(k) , \tag{III.2}$$

where the superscript "mm" identifies the monomer-monomer distribution, while "cm" indicates the distribution of monomers with respect to the center-of-mass. Eq.(III.2) is solved by assuming a Gaussian description of the intramolecular site distribution, which is an accepted approximation for polymer melts. The form factors entering Eq.(III.2) are approximated by $\omega^{cm}(k) = Ne^{-\frac{k^2R_g^2}{6}}$ and $\omega^{mm}(k) = N/(1 + k^2R_g^2/2)$, which is the Padé approximant of the Debye function $\omega^{mm}(k) = 2N(e^{-k^2R_g^2} + k^2R_g^2 - 1)/(k^4R_g^4)$. For the monomer-monomer total intermolecular correlation function $h^{mm}(k)$, we use the thread-limit polymer reference interaction site model description,[19] in which $h^{mm}(k) = h_0/(1 + \xi_\rho^2k^2)(1 + k^2\xi_c^2)$. Here, ξ_ρ is the length scale of density fluctuations defined as $\xi_\rho^{-1} = \xi_c^{-1} + \xi_\rho'^{-1}$, with $\xi_c = R_g/\sqrt{2}$ the length scale of the correlation hole, and $\xi_\rho' = R_g/(2\pi\rho_s^*)$ with $\rho_s^* = \rho_sR_g^3$ being the reduced molecular number density. The number density of soft colloidal particles $\rho_s = \rho/N$ with ρ being the monomer density and $h_0 = (\xi_\rho^2/\xi_c^2 - 1)/\rho_s$.

The structure of the coarse-grained polymer liquid is described by the total distribution function,[8] approximated for polymer chains with $N \geq 30$ as

$$h(r,\xi_\rho) \approx -\frac{39}{16}\sqrt{\frac{3}{\pi}}\frac{\xi_\rho}{R_g}\left(1+\sqrt{2}\frac{\xi_\rho}{R_g}\right)\left[1-\frac{9r^2}{26R_g^2}+\mathcal{O}\left(\frac{\xi_\rho^2}{R_g^2},\frac{r^4}{R_g^4}\right)\right]e^{-\frac{3r^2}{4R_g^2}}\ , \qquad \text{(III.3)}$$

which results from the analytical Fourier transform of $h(k)$. The structure of the liquid on length scales of the order of the polymer radius-of-gyration and larger, is well described by Eq.(III.3), which is in quantitative agreement with both atomistic and coarse-grained simulations.[8] The coarse-grained description of Eq.(III.3) is thermodynamically consistent with the atomistic representation, e.g. of the liquid compressibility.[8] Because the total correlation function of the coarse-grained representation is analytical, i.e. it depends explicitly on density and molecular parameters, it is also general and state-point transferable.

III.3. Coarse-Grained Potential and Mesoscale Simulations

Each soft-colloidal particle interacts with other colloids through an effective potential of the range of the overall polymer dimension, R_g. While hard-sphere systems are best described by a Percus-Yevick closure, the Hyper-Netted Chain (HNC) closure works best for systems with soft potentials,[20] including the mesoscopically coarse-grained polymer melts investigated here,[8, 21] and polymer coils in dilute or semidilute solutions.[22] The HNC potential between a pair of coarse-grained units is derived by applying the closure $\beta v(r) = h(r) - ln[h(r)+1] - c(r)$, where the direct correlation function is defined by the Ornstein-Zernike relation in reciprocal space $c(k) = h(k)/(1+\rho_s h(k))$.[23]

The potential between two spheres is calculated numerically, after Fourier transform, from the analytical expression, Eq.(III.2), by adopting the Debye form of the monomer intramolecular distribution, $\omega^{mm}(k)$. The Debye approximation has been shown to better represent simulation data than its Padé approximant.[21] Tabulated HNC potentials are input to the mesoscale simulations.

MS-MD simulations of polymer liquids are performed in the microcanonical ensemble, where each molecule is represented as an interacting soft-colloidal particle. In the initialization step, all particles are placed on a lattice with periodic boundary conditions. Each site is given an initial velocity and subsequently, the system is evolved using a velocity Verlet integrator. Equilibrium is induced in the ensemble by rescaling the velocity at regular intervals until the desired average temperature is reached. At this stage, velocity rescaling is discontinued and trajectories are collected over a traversal of $\sim 8R_g$, while the temperature is monitored to assure that it fluctuates around the desired equilibrium value. Because of the form of Eq.(III.3), the simulation uses reduced quantities of distance, $R_g = 1$, mass, $m = 1$, and energy, $k_BT = 1$.

A typical MS-MD simulation for our model is performed on a single-CPU workstation, and consists of $\sim$ 3000 polymers, evolving for a duration of $\sim$ 4 hours. The MS-MD simulation provides identical structural information to that of the analogous atomistic or united-atom (UA) simulations on length scales equal and larger than the polymer R_g. However, the MS-MD requires a much smaller computational power than the atomistic and UA-MD simulation, which is typically performed on a liquid of $\sim$ 500 polymers, on a parallel supercomputer. The convenient requirements in computational power of the MS-MD simulation allows one to increase considerably the number of particles and the simulation box size without dramatically affecting the computational time, thus improving the precision on the large-scale data collected.

III.4. Mapping of the Atomistic Description onto a Freely-Rotating-Chain Model

The correction in Helmholtz free energy, which accounts for the discarded internal degrees of freedom, is calculated starting from the atomistic representation of the liquid, where each chain is described as a collection of beads connected by springs defined by an effective intramolecular quadratic potential $U(r) = 3k_BT/(2l^2)\sum_{i,j=1}^{N} \mathbf{A}_{i,j}\mathbf{r}_i \cdot \mathbf{r}_j$. Here $\mathbf{A}$ is the connectivity matrix, which represents the structure and local flexibility of the polymer, $\mathbf{r}_i$ the position of unit i in a chain of N beads, and $\mathbf{l}_i = \mathbf{r}_{i+1} - \mathbf{r}_i$ the bond vector connecting two adjacent beads.[24] For polyethylene melts, each polymer is represented as a freely-rotating-chain (FRC), finite in size, with semiflexibility parameter $g = \langle(\mathbf{l}_i \cdot \mathbf{l}_{i+1})/(l_i l_{i+1})\rangle = 0.785$ and fixed bond length $l = 1.54$Å. This bead-and-spring model of the FRC has been shown to represent correctly the dynamics of polyethylene melts as measured in united-atom simulations[25] and in experiments.[26] A FRC model was also successfully adopted to model the dynamics of polymer melts with different molecular architectures,[27] and even proteins,[24, 28] once the proper semiflexibility parameters are selected.

To map the MS-MD simulation onto a real system, the reduced unit of time needs to be properly rescaled. Because energy is dissipated in internal degrees of freedom in the atomistic representation, the contribution due to the internal vibrational modes is included in the coarse-grained representation by rescaling the time in the MS-MD simulation, $\tilde{t}$, by the amount of internal free energy dispersed in vibrational modes in the atomistic description as $t = \tilde{t} R_g \sqrt{3mN/(2k_BT)}$, with the particle mass, m, and size R_g. By rescaling the internal free energy, we account for the change in entropy in the coarse-grained description. In the next section we derive the friction rescaling.

III.5. Rescaling of the Friction Coefficient

To account for the change in dissipation caused by coarse-graining, we start from the diffusion coefficient measured in the MS-MD simulation, D_t^{MS}, and we derive the center-of-mass (cm) diffusion coefficient of the polymer, D_{cm}, through the rescaling of the friction as

$$D_{cm} = D_t^{MS} \zeta_{\mathrm{s}}/(N\zeta_m)\,. \tag{III.4}$$

The correction factor is calculated from the ratio of the cm friction in the soft colloid representation ζ_s and the cm friction in the atomistic representation $N\zeta_m$, with ζ_m the monomer friction. Each friction coefficient is evaluated by solving the memory function in the corresponding Generalized Langevin Equation. These memory function definitions result from the straightforward application of Mori-Zwanzig projection operators to the Liouville equation, where either the monomer (atomistic description) or the center-of-mass (soft colloid description) of the polymer are assumed to be the “relevant slow variables.”[23, 24]

In the soft colloid representation the friction coefficient is defined as

$$\zeta_s \cong \frac{\beta}{3}\rho_s \int_0^\infty dt \int d\mathbf{r} \int d\mathbf{r}' g(r) g(r') F(r) F(r') \hat{\mathbf{r}} \cdot \hat{\mathbf{r}}' \int d\mathbf{R} S(R;t) S(|\mathbf{r}-\mathbf{r}'+\mathbf{R}|;t)\,, \tag{III.5}$$

where $\beta = 1/k_BT$, $g(r) = h(r) + 1$ is the radial distribution function, $F(r) = \beta^{-1}(d\ln g(r)/dr)$ is the total force exerted by the surrounding fluid on the colloid, and $S(k) = 1 + \rho_s h(k)$ is the structure factor of the fluid surrounding the colloid. The unit vectors $\hat{\mathbf{r}}$ and $\hat{\mathbf{r}}'$ define the direction of exerted forces.

In Eq.(III.5), the projected dynamics has been substituted with the real (unprojected) dynamics, which is a valid approximation when the Langevin equation is expressed as a function of slow variables for the diffusive regime.[23] In the long-time regime, the relaxation of the liquid is dominated by the polymer center-of-mass diffusion, D, here represented by the cm of the colloidal particle. In Fourier space the dynamic structure factor of the liquid reads $S(k;t) \approx S(k)exp(-k^2Dt)$. Evaluating the integral with use of Eq.(III.3) gives

$$D\beta\zeta_s \approx 4\sqrt{\pi}\rho_s R_g \xi_\rho^2 \left(1+\frac{\xi_\rho}{\xi_c}\right)^2 \frac{507}{512}\left[\sqrt{\frac{3}{2}}+\frac{1183}{507}\rho_s h_0+\frac{679\sqrt{3}}{1024}\rho_s^2 h_0^2\right] . \tag{III.6}$$

Eq.(III.6) expresses the friction coefficient of a soft colloidal particle.

In the atomistic description, the monomer friction coefficient is defined by the memory function as

$$\zeta_m \cong \frac{1}{N}\sum_{j,i=1}^{N}\int_0^\infty d\tau \frac{\beta}{3}\rho \int d\mathbf{r}\int d\mathbf{r}' g(r)g(r')F(r)F(r')\hat{\mathbf{r}}\cdot\hat{\mathbf{r}}' \int d\mathbf{R} S_{i,j}(R;t)S(|\mathbf{r}-\mathbf{r}'+\mathbf{R}|;t) , \tag{III.7}$$

where the dynamic structure factor of the surrounding liquid is approximated as $S(k;t) \approx S(k)exp(-k^2Dt) = [\omega(k)+\rho h(k)]\, exp(-k^2Dt)$, with $\omega(k)$ being the intramolecular static structure factor. This expression for $S(k;t)$ assumes that in the long time regime the relaxation of the liquid is dominated by the polymer center-of-mass diffusion, consistently with the soft-colloid representation.

To evaluate Eq.(III.7), we approximate the potential as an effective hard-core potential with a diameter d to be defined.[23] In hard-core fluids, $g(r)F(r) = g(d)\beta^{-1}\delta(r-d)$. Working in reciprocal space, the integrals in Eq. (III.7) can be performed analytically to give an expression for the dynamical quantity $D\beta\zeta_m$ depending on two length scales: R_g, and d. The result is lengthy, and it is not reported here. The values of R_g used are the ones reported in Tables III.1 and III.2.

The monomer hard-core diameter, $d = 2.1$Å, is identical for all the samples, and is obtained by reproducing the scaling with N of an unentangled melt, $D\beta\zeta_m = 1/N$, for the PE 44 sample. This sample is chosen because its degree of polymerization is smaller than the entanglement one,

$N_e = 130$, and it is large enough to ensure Gaussian chain statistics. Once d is defined, it is not changed for any other system considered, either unentangled or entangled. This is the only parameter that has to be fixed in our approach. Theoretically predicted values for unentangled systems recover the correct scaling behavior as $ND\beta\zeta_m \approx 1$. For entangled systems, we solve Eq. (III.7) by including a one-loop perturbation of the diffusion coefficient. For these entangled systems $ND\beta\zeta_m \propto N^{-1}$, in agreement with the known scaling behavior.

III.6. Comparison of Predicted Diffusive Dynamics with Simulations and Experiments

To test our approach we compare the rescaled dynamics, predicted from mesoscale simulations, with experiments and UA-MD simulations. Each sample that we investigate is in well-defined thermodynamic conditions of density and temperature, and has a specific radius of gyration. Those quantities enter as an input to our mesoscale simulation, and also in the expressions for the rescaling of the energy and friction coefficient (see Tables III.1 and III.2).

TABLE III.1. MS-MD Parameters - UA-MD data

Polymer	N	T [K]	ρ [sites/Å^3]	R_g [Å]
PE30[a]	30	400	0.0317	7.97
PE44[a]	44	400	0.0324	10.50
PE48[b]	48	450	0.0314	10.54
PE66[a]	66	448	0.0329	13.32
PE78[b]	78	450	0.0321	14.35
PE96[a]	96	448	0.0328	16.79
PE142[b]	142	450	0.0327	20.51
PE174[b]	174	450	0.0328	22.92
PE224[b]	224	450	0.0329	26.28
PE270[b]	270	450	0.0330	29.27
PE320[b]	320	450	0.0330	31.31

[a] data from ref.;[15] [b] data from ref.[3]

Comparison with simulation data are limited here to United-Atom simulations, but our theory is general and comparison could be made with atomistic simulations as well. The UA-MD simulations reported in this communication cover a regime from unentangled,[15] to slightly entangled dynamics (two entanglements per chain).[3] We use as an input of our approach the radius of gyration, as measured in each simulation. These values are very close to the theoretical R_g values calculated using a FRC model with semiflexibility parameter $g = 0.785$.

TABLE III.2. MS-MD Parameters - Experimental Data

System	N	R_g^{FRC}[Å]
PE 36	36	10.07
PE 72	72	14.82
PE 106	106	18.20
PE 130	130	20.25
PE 143	143	21.27
PE 192	192	24.77
PE 242	242	27.88

$T = 509$K, $\rho = 0.0315$ [sites/Å^3]. Data from Ref.[26]

The experimental samples considered in this paper[26] cover a region at the crossover from unentangled to entangled dynamics comparable to the one in UA-MD simulations. However, the values of the radius-of-gyration for those samples are not known, because only the degree of polymerization is reported. For those samples we assume as input values of R_g those calculated using a FRC approach.

The predicted cm diffusion coefficient of a polymer chain, D_{cm} is compared in Figure III.1 against the data from simulations,[3, 15] and from experiments.[26] We also show, as a guide to the eye, lines with the scaling behavior of unentangled and entangled systems. The agreement between calculated and measured diffusion coefficients is good over a range of the degree-of-polymerization, covering unentangled as well as entangled polymer melts. Because each simulation and experimental value is taken in slightly different thermodynamic conditions, the data points do not perfectly align along the lines of the scaling exponents in the figure. However we observe a good agreement between predicted theoretical values and measured ones in simulations or experiments.

To test further the validity of our procedure, we calculate the decay of the rotational time-correlation function for the molecular end-to-end vector with input parameters for polyethylene and the rescaled monomer friction coefficient $\zeta = k_B T/(N D_{cm})$, and compare it against UA-MD simulations (see Figure III.2). Predicted and measured decays are in excellent agreement for the unentangled samples, suggesting that the proposed procedure holds for different normal modes of motion.

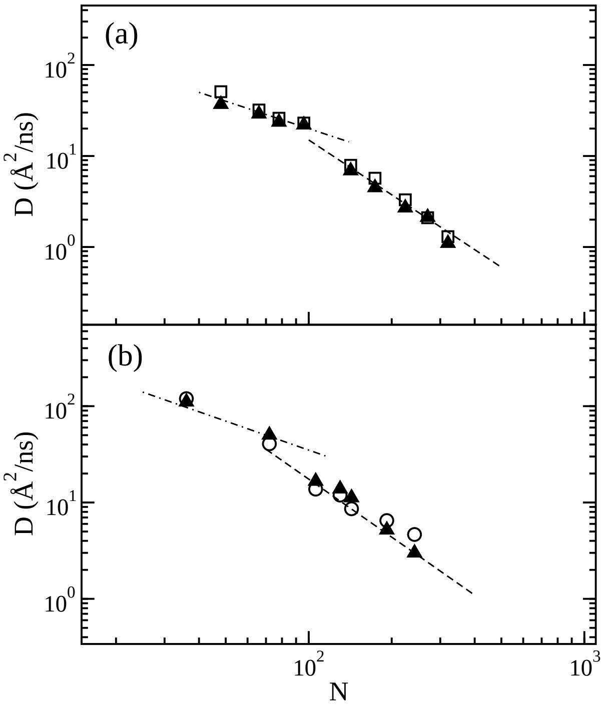

FIGURE III.1. Plot of diffusion coefficients as a function of degree of polymerization, N. Comparison between the theoretically predicted values (triangle), simulations (square) from,[3,15] and experiments (circle) from[26] and references therein. Also shown is the scaling for unentangled, N^{-1} (dot-dashed line), and entangled systems, N^{-2} (dashed line)

III.7. Conclusion

Mesoscale simulations of coarse-grained systems are becoming increasingly important, as they are computationally efficient and allow for the study of systems on larger length and time scales than their atomistic counterparts. However, while structural properties on large length scales are well described by MS-MD simulations, the dynamics is unrealistically fast due to the simplified free energy landscape. In this communication we have presented an analytical, first-principles, approach to scale the dynamics measured in mesoscale simulations down to realistic atomistic values. The rescaling procedure takes into account the averaged internal degrees of freedom and enhanced dissipation due to the coarse-graining procedure. The agreement of predicted long-time dynamics with data from simulations and experiments is quantitative. Whereas previous efforts at dynamical rescaling have used numerical calibration curves, which are specific of the system under study, our approach is analytical and thus general and transferable: it

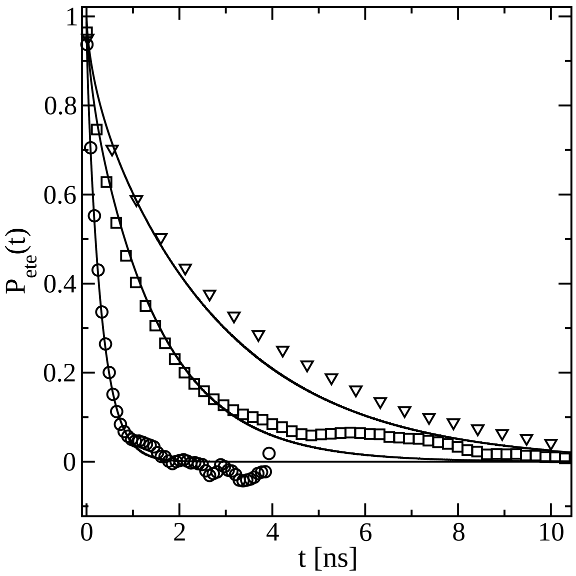

FIGURE III.2. Normalized rotational time decorrelation function for the end-to-end vector for the semiflexible chains with rescaled friction (solid lines) compared against simulations (symbols) for polyethylene melts of increasing length; $N = 30$ (circles), $N = 66$ (squares), $N = 96$ (triangles)

is readily applicable to systems with different thermodynamic parameters and to polymer chains of increasing degree of polymerization crossing from the unentangled to the entangled regime. The development of a general scheme to rescale the dynamics from MS-MD simulations promises to be useful in multiscale modeling techniques and fast equilibration methods employed in computer simulations of complex fluids.

In summary, the development of schemes to rescale the dynamics from MS-MD simulations will certainly be beneficial in the advancement of multiscale modeling techniques of complex fluids. Equilibrium and non equilibrium simulations of polymer melts with different architectures should be natural implementations of the approach for future work. It should also be possible to extend this model to rescale systems represented at an intermediate level of coarse-graining as collections of soft colloidal beads, so that the internal dynamics of entangled chains can be simulated.

CHAPTER IV

THEORETICAL DEVELOPMENT OF FRAMEWORK FOR RECONSTRUCTION OF DYNAMICS OF COARSE-GRAINED MACROMOLECULAR LIQUIDS

Presented in Chapter IV is a detailed derivation and testing of our approach to rescale the dynamics of mesoscale simulations of coarse-grained polymer melts briefly reviewed in Chapter III. Starting from the first-principle Liouville equation and applying the Mori-Zwanzig projection operator technique, the Generalized Langevin Equations (GLE) for the coarse-grained representations of the liquid is derived. Each polymer is represented at two levels of coarse-graining: monomeric as a bead-and-spring model and molecular as a soft-colloid. In the long-time regime where the center-of-mass follows Brownian motion and the internal dynamics is completely relaxed, the two descriptions must be equivalent. By enforcing this formal relation we derive from the GLEs the analytical rescaling factors to be applied to dynamical data in the coarse-grained representation to recover the monomeric description. Change in entropy and change in friction are the two corrections to be accounted for to compensate the effects of coarse-graining on the polymer dynamics. The solution of the memory functions in the coarse-grained representations provides the dynamical rescaling of the friction coefficient. The calculation of the internal degrees of freedom provides the correction of the change in entropy due to coarse-graining. The resulting rescaling formalism is a function of the coarse-grained model and thermodynamic parameters of the system simulated. The material from Chapter IV has been published with my advisor, Marina Guenza, as co-author.

IV.1. Introduction

The last few years have witnessed a growing interest in the design and application of coarse-graining methods to simulate complex fluids.[29] This effort has been motivated by the need for improving computational efficiency with the purpose of investigating complex systems on the numerous length scales on which their properties develop.[10, 11, 39, 59, 60] Computer simulations have the capability of providing detailed microscopic information on the static and dynamics of the systems under study,[35] but they are limited in the range of timescales and in the number of molecules that can be simulated because the precision of the calculations degrades with the number of computer iterations with a behavior that depends on the Lyapunov exponent of the system. Once the number of particles is set, the window of achievable timescales that can be investigated becomes defined.[2, 34] Because the maximum number of iterations decreases with increasing number of simulated particles, it is particularly difficult to simulate systems where characteristic length scales are diverging, such as a system approaching a second order phase transition.[61, 62]

Recent improvements of computational machines have lead to a considerable extension of the maximum time- and length scales that can be reached by simulations where the system is described at the atomistic level. However, for many complex systems, including liquids of high-molecular weight macromolecules, the computational power is still inadequate to describe, at the atomistic level, the long-time dynamics. For example, the most recent and advanced simulations of long chains that have an extended number of entanglements adopt a simplified model, which treats the structure of the polymer as a collection of beads and springs interacting through a finite extensible nonlinear elastic (FENE) potential. This model allows for the simulations of a large number of polymers, which is important for the proper calculation of viscoelastic properties, and reaches full relaxation for all but the longest chains simulated.[63]

Progress has been made when the focus is on qualitative behavior and scaling exponents.[61, 64] For example, if the complex intra- and inter-molecular non-bonded interactions are simplified into an identical potential, the computational efficiency improves dramatically as the code does not need to identify and treat uniquely different pairs of interacting sites. This strategy, however, has the disadvantage that the thermodynamics of the system is not properly described because the interactions are too drastically simplified.

The need for methods that are fully predictive of the physical properties of a system on the basis of the specific chemical structure of the sample and its thermodynamic conditions has stimulated new interest in developing fast quantitative simulations. Such predictive approaches are useful, for example, to evaluate *a priori* the structure and dynamics of newly synthesized polymeric materials, in relation to their technological applications. Following this perspective, several procedures have been proposed to speed up atomistic simulations, while conserving their power of predicting quantitative properties.[3, 65] A few simulations of long entangled chains have been performed using united atoms (UAs).[3,66–68] For UAs the effective unit is very close to the atom is size, i.e. CH_x with $x = 1, 2, 3$, which allows for some gain in the computational time.

A useful strategy to improve the outcome of simulations on the long timescale and large length scale is the use of coarse-graining procedures.[9,59] A coarse-graining procedure averages out irrelevant degrees of freedom, which occur on length scales smaller than a designated cutoff length, and this allows for the extension towards large scales of the simulations. Another way to put it is that, because the interaction potentials become softer, the maximum time and length scale increase as the basic time step of the mesoscale (MS) simulations becomes larger. The characteristic length scale of coarse-graining has to be defined on the basis of the properties that need to be investigated. In this communication we discuss a first-principles way of selecting meaningful length scales for the structural and dynamical coarse-graining.

Several considerations need to be made to properly develop a coarse-graining procedure. As the coarse-grained liquid is represented as a function of new coordinates, an effective potential needs to be derived to be used as an input to the MS simulation. Care has to be taken to make the potential reproduce the structure of the system, namely pair distribution functions, and to be thermodynamically consistent. A common procedure to optimize the coarse-grained description is to use self-consistent numerical methods that are optimized to reproduce atomistic descriptions through iterative procedures. Usually the target is the optimization of specific quantities, such as the pair distribution function,[69] the forces generated by the soft potential,[39] or directly the thermodynamic properties.[70]

We recently proposed an approach that starts from the Ornstein-Zernike (OZ) equation where the atomistic sites are defined as real sites, and the coarse-grained sites are defined as auxiliary sites.[8,71–76] Because our procedure is analytical, and no optimization of parameters is needed in our approach as the potential is explicitly dependent on the thermodynamic and molecular parameters, it opens up the possibility of deriving a formal solution to key problems. For example, it is straightforward to show that the structural properties are consistent between the two levels of description, i.e. atomistic and coarse-grained.[8] Moreover, the thermodynamic properties of the coarse-grained polymer liquid (e.g. isothermal compressibility,[8] pressure in the virial and in the compressibility routes, total and cohesive energy) are shown to be formally consistent in the two levels of coarse-graining.Local structure is easily included *a posteriori* through a multiscale modeling procedure.[17,76] Finally, it is possible to derive an analytical rescaling factor for the dynamics, which is the main focus of this communication.

While the structure is well described by simulations of the coarse-grained system on the scale larger than the scale of coarse-graining, the dynamics in MS simulations is unrealistically fast. Because local degrees of freedom are averaged out, the coarse-grained molecules move rapidly over a simplified free energy landscape. As the system explores efficiently this "reduced" configurational landscape, the measured dynamics is artificially sped up by the smoothness of the potential. This is useful when coarse-grained representations are used to rapidly reach an equilibrated state of the system before starting the atomistic molecular dynamics (MD) simulation. However, to directly collect information on the dynamics of systems from MS MD simulations, it is necessary to develop formalisms that rescale the unrealistically fast dynamics into the slower dynamics at atomistic resolution. In this communication we discuss in details an analytical procedure we recently proposed to rescale the mesoscale dynamics. The procedure is able to predict center-of-mass dynamics in quantitative agreement with experiments and atomistic simulations.[36]

The common strategy to rescale the dynamics is to build a "calibration curve". The latter is obtained through the numerical fitting of dynamical quantities and optimization of the related parameters until the agreement of dynamical properties calculated in an all-atom and in a MS simulations is obtained.[13,77] However, the numerical calculation of optimized calibration curves for the dynamics is quite difficult to achieve for macromolecular systems, as the dynamics is mode dependent: there are in principle N internal modes in any molecule formed by N units and the degree of polymerization of a long chain can be of the order of one million monomers. Moreover, numerically optimized parametric quantities are in general not transferable between systems in different thermodynamic conditions or with different chemical structure or increasing degree of polymerization. To overcome this problem, it is common to select as coarse-grained units ones that are very close in size to the atomistic units, so that the needed corrections to reach consistency in dynamic properties are minimal. In this case, corrections to the measured dynamics can be evaluated through a perturbative formalism which should rapidly converge to the desired value. The resulting computational gain is, however, still limited. Recently a numerical Ornstein-Zernike-based approach, with atomistic-level coarse-graining and the Percus -Yevick closure approximation, has been proposed, which shows different rescaling factors depending on the time correlation function under study.[78] Another coarse-grained approach for polyethylene melts describes a polymer chain as a collection of soft blobs connected by elastic bands, which enforce chain-chain uncrossability. Simulations follow an effective Langevin equation, whose parameters, i.e. effective potential, frictions and random forces, are obtained by numerical optimization from an atomistic MD simulation. The optimized equation of motion (EOM) reproduces well experimental data of the system.[79]

Our approach is different from others in several ways. First of all it is analytical rather than numerical, providing the formal rescaling factor by solving the EOMs in the two levels of representation. In this way, there is no need of performing an atomistic simulation to input numerical quantities in our formalism. Second, thermodynamic and molecular parameters enter directly into the rescaling procedure, which therefore can be applied directly to predict diffusion coefficients in different thermodynamic conditions and for homopolymer melts with different degrees of polymerization. It is important to note that the molecular radius of gyration, which is an input to the theory, is also density and temperature dependent: this has to be taken into account when the theory is used as a predictive tool. The tests of our rescaling approach, presented in this communication and in the previous publication,[36] show that the proposed procedure is accurate in the range of temperatures ($T = 400K \div 509K$) and densities ($\rho_m = 0.031$ sites/Å^3 $\div \rho_m = 0.033$ sites/Å^3) considered.

The dynamics measured in MS simulations of coarse-grained systems is directly rescaled into its atomistic counterpart using approximate closed-form expressions of friction and entropy. The two levels of coarse-graining, which allow for a straightforward analytical solution, are here two simple isotropic models: a soft sphere description for the molecular coarse-graining, and a bead-and-spring description for the monomer level coarse-graining. More sophisticated coarse-grained models can be developed for intermediate length scales;[74,75] however, the formalism can become more involved.[80] At the atomistic level the polymer is described as a "bead-and-spring" type of approach where the chain is a collection of friction points connected by harmonic springs. This is an implementation of the most popular model to treat unentangled polymer melt dynamics, i.e. the Rouse model, and maps well into the dynamics of polymers described not only by UA simulations, but also by atomistic simulations and experiments, as it contains both local chemical structure, semiflexibility, and finite size effects.[24,26,82] It is a very accurate and molecular specific model, which has been shown to describe well, for example, the dynamics of the protein CheY, by testing its predictions of NMR relaxation against experiments.[24,83]

In our coarse-grained model a polymer chain is represented as a soft-colloidal particle.[8,52,53,85] Because the length scale of the coarse-graining is of the order of the molecular radius of gyration, i.e. the size of the molecule, the *direct* predictions of the rescaling procedure are suitable for properties on length scales larger than R_g and on timescales longer than the longest time of intramolecular relaxation, i.e. the longest correlation time in the Rouse theory. Internal dynamics cannot be obtained directly from the coarse-grained simulation; however, the rescaled diffusion coefficient leads to the monomer friction coefficient, which can be used as an input to well-tested theories of polymer dynamics, and *indirectly* recovering the dynamics in the complete spectrum of polymer relaxation. An example of this kind of calculation is presented in this communication in Section V.4. The extended level of coarse-graining provides a good test of our procedure, as large deviations could result from the rescaling if the method were not correct. Furthermore, our procedure can be useful in the study of long-time relaxation, given that large length scales and long timescales are most difficult to simulate for polymeric systems.

Although the outline of our rescaling theory has been published recently in a short paper,[36] this communication presents a detailed derivation and discussion of our approach, which includes the prediction of the dynamics for new samples. After introducing our coarse-grained model input to the mesoscale simulations, we formally derive the rescaling approach for the dynamics, starting from the Liouville equation and using projection operators. Friction coefficients in the two descriptions are derived from the solution of the memory functions, while the rescaling of the simulation time is obtained from the entropic contribution, which accounts for the intramolecular degrees of freedom neglected in the soft colloid representation. Theoretical predictions compare well against UA MD simulations,[3,15,57,58] and experiments,.[26,86–89] We also calculate the diffusion coefficient for new PE samples in thermodynamics conditions for which UA-MD data are not available. The purpose of these calculations is to show that our method is not a simple rescaling of the mesoscale data through a shift of the diffusion coefficient to bring dynamical results to coincide with atomistic simulations, as is conventionally done. Instead our approach is fully predictive and can be used to calculated the diffusion coefficient, and the monomer friction, for new samples.

The communication is structured as follows: after introducing our coarse-grained model in Section IV.2 and the projection operator technique to derive the equations of motion in the two levels of coarse graining in Section IV.3, we formally derive the rescaling approach for the dynamics from the solution of the memory functions in Section IV.7. We then present the MS simulations (Section V.1), as well as the results obtained from the same, and apply the rescaling procedure to the data from MS simulations (Chapter V). Predictions of dynamical quantities and direct comparison for several samples, both from atomistic simulations and from experiments, provide a stringent test of the approach and show good quantitative agreement. A brief discussion in Section V.6 concludes the communication.

IV.2. Coarse-Graining of Polymeric Liquids: Structural Properties

In this section we briefly review the theoretical background of the pair distribution functions that are input to our rescaling equation. The structure of a polymeric liquid, at length scales equal or larger than the monomer size, is fully specified by the monomer total distribution function, $h(r)$, which for polymer melts depends on two characteristic length scales, namely the density fluctuation lenthscale, which is the atomic length, and De Gennes' correlation hole length scale.[30] The latter is of the order of the molecular radius-of-gyration, $R_g = \sqrt{N/6}l$, which is the overall dimension of the polymer, where N is the degree of polymerization and l is the statistical bond length. We select l and R_g because these are the two length scales that define the structural properties of the polymeric liquid.

At the monomer level traditional dynamical approaches, such as the Rouse model and semiflexible models, adopt a bead-and-spring representation where each monomer can be modeled as a friction point connected by springs (see Figure IV.1). A similar model, where the polymeric chain is described as a collection of "sites" centered at the center of the monomeric unit, is also in conventional theories of polymer liquids.[54, 55] Although "site" is the word most used in the liquid state community and "monomer" or "bead" is the common wording in the literature on polymer dynamics, in this communication they identify the same CH_x unit and henceforth they

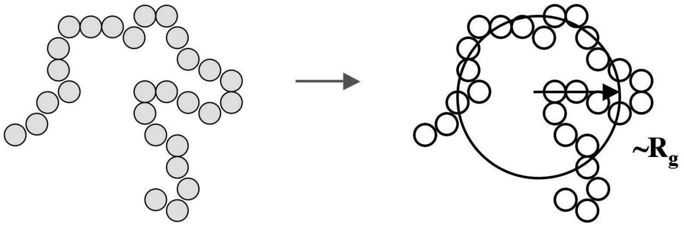

FIGURE IV.1. Illustration of monomer and overall coarse-graining of a homopolymer linear chain.

will be used interchangeably. It is important to notice that all the CH_2 units are assumed to be equivalent and independent of the position along the chain.

The coarse-graining of a polymer at the R_g length scale represents each molecule as an interacting soft colloidal particle with symmetric or asymmetric shape.[52,53,85] In our model,[8,71–73] the macromolecular liquid is represented as a liquid of symmetric soft colloidal particles interacting through a pair potential. This potential has a range of the order of few R_g, and each soft-colloidal particle is centered at the center-of-mass of a polymer (see Figure IV.1).

The coarse-graining procedure that translates the monomer description into the soft-colloidal representation is performed starting from an Ornstein-Zernike equation where monomers are assumed to be real sites, while the center-of-mass (cm) are auxiliary sites.[84] The cm-cm total intermolecular correlation function is expressed as a function of the polymer parameters as[8,71]

$$\begin{aligned} h^{cc}(r) \;=\; & \frac{3}{4}\sqrt{\frac{3}{\pi}}\frac{\xi'_\rho}{R_g}\left(1-\frac{\xi_c^2}{\xi_\rho^2}\right)e^{-3r^2/(4R_g^2)} - \frac{1}{2}\frac{\xi'_\rho}{r}\left(1-\frac{\xi_c^2}{\xi_\rho^2}\right)^2 e^{R_g^2/(3\xi_\rho^2)} \\ & \times\left[e^{r/\xi_\rho}\mathrm{erfc}\left(\frac{R_g}{\sqrt{3}\xi_\rho}+\frac{\sqrt{3}r}{2R_g}\right) - e^{-r/\xi_\rho}\mathrm{erfc}\left(\frac{R_g}{\sqrt{3}\xi_\rho}-\frac{\sqrt{3}r}{2R_g}\right)\right] \;, \end{aligned} \tag{IV.1}$$

where erfc(x) is the complementary error function. Here $\xi'_\rho \;=\; R_g/(2\pi\rho^*_{ch}) \;=\; 3/(\pi\rho l^2)$ with $\rho^*_{ch} \equiv \rho_{ch}R_g^3$ being the reduced molecular number density, $\rho_{ch} = \rho/N$ is the molecular density, ρ the site number density, and l is the statistical segment length. The length scale of density fluctuations, ξ_ρ, is defined as $\xi_\rho^{-1} \;=\; \xi_c^{-1} + \xi'^{-1}_\rho$, and $\xi_c \;=\; R_g/\sqrt{2}$ is the length scale of the correlation hole.[30]

In the limit of long chains, $N \to \infty$, Eq.(IV.1) reduces to

$$h^{cc}(r) \approx -\frac{39}{16}\sqrt{\frac{3}{\pi}}\frac{\xi_\rho}{R_g}\left(1+\sqrt{2}\frac{\xi_\rho}{R_g}\right)\left(1-\frac{9r^2}{26R_g^2}\right)e^{-\frac{3r^2}{4R_g^2}} . \tag{IV.2}$$

For polymers with $N \geq 30$, a plot of $h(r)$ shows that the two equations, Eqs.(IV.1) and (IV.2), are indistinguishable.[8, 71]

The structure of the liquid on the length scale of the polymer radius-of-gyration and larger, as represented by $h^{cc}(r)$, is in quantitative agreement with the output of both the atomistic UA MD and the MS MD simulation of the coarse-grained liquid. The theory recovers identical analytical expressions of the compressibility in the atomistic and the coarse-grained representations, indicating thermodynamic consistency between the two levels of description.[8, 71]

Eqs.(IV.1) and (IV.2) are *de facto* coarse-graining equations, which translate the atomistic description of a polymer liquid, onto its representation as a liquid of interacting soft colloidal particles of size R_g. The advantage of our coarse-graining approach is that it is analytical and general as it applies to systems with different thermodynamic conditions, different degree of polymerization and different bond length.[8, 17, 71–76]

IV.3. Dynamical Coarse-Graining: From the Liouville to the Langevin Equations

While the structure of the polymeric liquid, as represented by the total correlation function, is identical in the atomistic and coarse-grained descriptions,[8, 71] the dynamics of the coarse-grained system, as measured in the MS MD simulations of the soft-colloidal particles, is unrealistically accelerated. In Figure (IV.2) we show, for a polyethylene chain with $N = 44$, the mean-square-displacement of the center-of-mass obtained in MS MD simulations of the polymer liquid represented as soft-colloidal particles and the mean-square-displacement directly measured in UA MD simulations . The dynamics in the coarse-grained representation is several orders of magnitude faster than the atomistic description. Because the level of coarse-graining of the model presented here is extended, this effect is more evident than in other models; however, accelerated dynamics is present in any simulation of coarse-grained systems.

It has been argued that there are two main effects of coarse-graining that accelerate the dynamics: namely, the change in entropy and the change in the friction coefficient. Öttinger

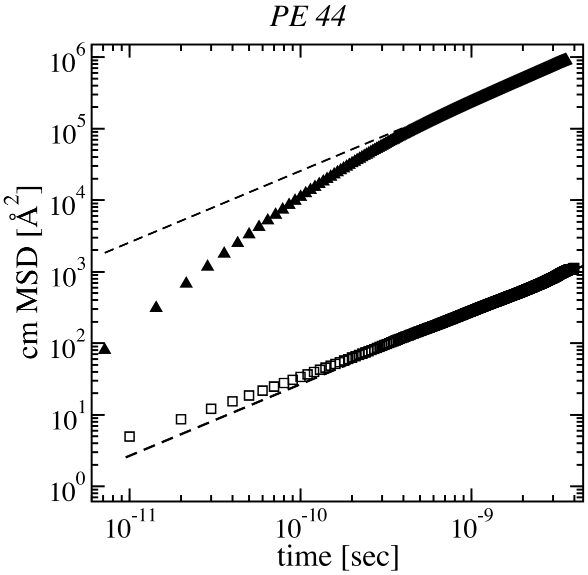

FIGURE IV.2. Cm mean-square displacement, for a polyethylene melt with $N = 44$, from MS MD simulations (triangles) and UA MD simulations (squares). Dashed lines show the diffusive limits of the two samples.

has presented an approach for systems far from equilibrium that accounts for those effects.[7] We propose here a procedure, based on first-principles theory to properly account for both contributions through the introduction of the necessary corrections for systems where the fluctuation dissipation theorem applies, e.g. close to equilibrium.

To coarse-grain the dynamics of the polymeric liquid on the length scale of the radius of gyration, we adopt a Mori-Zwanzig projection operator technique, where the selected slow variables are the position and momentum coordinates of the polymer center-of-mass. This description should represent well center-of-mass diffusion.[23, 90, 91]

The atomistic level representation is obtained following the same Mori-Zwanzing procedure, but choosing as the slow relevant variables the ensemble of position and momentum coordinates of the center of mass of the monomeric unit, which for a polyolefin is the CH_x unit, with $x = 1, 2,$ or 3. This model is consistent with the representation of the polyethylene chain in UA MD simulations,[92, 93] and it has been shown to describe at a high level of accuracy the dynamics of polyolefins at the monomer lenghtscale.[24, 95, 96]

In the long-time regime the two descriptions, soft-colloid and monomeric/UA, should be identical as they both recover the diffusive dynamics of the center-of-mass.[97] In fact, they are not, as the soft-colloidal description is heavily coarse-grained and its dynamics is accelerated. The analytical rescaling factor is derived directly from the comparison between the soft-colloid and the monomer dynamical equations.

As this coarse-graining and rescaling procedure is general, it can be adopted to formalize the dynamics of the molecular liquid at the desired level of coarse-graining. However, the projection operator technique rests on a separation of timescales between the slow relevant variables onto which the dynamics is projected, and the fast irrelevant variables that are averaged out. If no separation of timescales is observed, it is necessary to include corrections to the projected dynamics, which appear as contributions to the friction coefficient, expressed as memory functions. In the system investigated here, polymer melt dynamics, no clear separation of timescales occurs between the dynamics of the "tagged" chain and the dynamics of the surrounding molecules.[92] For this reason, the Generalized Langevin Equation generated from this procedure needs to account for the correction terms to the projected dynamics, which are represented by the memory function contributions.[98]

For a liquid of n macromolecules containing N monomers, the first-principle Liouville equation is simply written as

$$\frac{\partial f\left(\mathbf{R},\mathbf{P},t\right)}{\partial t}=iLf\left(\mathbf{R},\mathbf{P},t\right)\ , \tag{IV.3}$$

with

$$f\left(\mathbf{R},\mathbf{P},t\right)=\prod_{j=1}^{n}\left[\prod_{a=1}^{N}\delta(\mathbf{r}_a^j(t)-\mathbf{R}_a^j)\delta(\mathbf{p}_a^j(t)-\mathbf{P}_a^j)\right]\ , \tag{IV.4}$$

the instantaneous distribution in reduced phase space, and $\mathbf{R}_a^i$ and $\mathbf{P}_a^i$ are the phase-space variables associated with the Cartesian position and momentum coordinates of the bead a belonging to molecule i, namely $\mathbf{r}_a^i(t)$ and $\mathbf{p}_a^i(t)$. The formal solution of Eq.(IV.3) is

$$f\left(\mathbf{R},\mathbf{P},t\right)=e^{-iLt}f\left(\mathbf{R},\mathbf{P}\right)\ , \tag{IV.5}$$

with the shorthand notation $f\left(\mathbf{R},\mathbf{P}\right)=f\left(\mathbf{R},\mathbf{P},0\right)$

The Liouville operator is defined as

$$iL = -\sum_{j=1}^{n}\sum_{a=1}^{N}\left[\frac{\partial U_j}{\partial \mathbf{r}_a^j}\cdot\frac{\partial}{\partial \mathbf{p}_a^j}-\frac{\mathbf{p}_a^j}{m}\cdot\frac{\partial}{\partial \mathbf{r}_a^j}\right] \ , \tag{IV.6}$$

where the total energy U_j in the Hamiltonian, H, contains both intramolecular, U_j^0, and intermolecular, W_{ij}, pairwise decomposable potential contributions. The intermolecular potential contains both interactions between the n tagged chains, W_{jk}^0, and between the tagged chains and the surrounding ones, W_{jk}, so that the usual condition applies that $L_0 f(\mathbf{R},\mathbf{P}) = 0$. The statistical average of the phase space density is defined as

$$< f\left(\mathbf{R},\mathbf{P}\right) >= \int d\mathbf{r}\int d\mathbf{p} f\left(\mathbf{R},\mathbf{P}\right)\psi\left(\mathbf{r},\mathbf{p}\right) \ , \tag{IV.7}$$

with the equilibrium distribution of particle positions and coordinates

$$\psi\left(\mathbf{r},\mathbf{p}\right) = e^{-\beta H}\left[\int d\mathbf{r}\int d\mathbf{p} e^{-\beta H}\right]^{-1} \ , \tag{IV.8}$$

where $\beta = (k_B T)^{-1}$, k_B the Boltzman's constant, and T the absolute temperature. Following Mori-Zwanzig, we define the projection operator, $\hat{P}$, for the coarse-grained model we adopt, namely the monomer and the soft-colloidal.

IV.4. Monomer Level Representation of the Polymer Chain

In our atomic-level description each macromolecule is represented as a collection of connected beads, or friction points. In the field variables for one molecule ($n = 1$),

$$g\left(\mathbf{R},\mathbf{P},t\right) = \left[\prod_{a=1}^{N}\delta\left(\mathbf{r}_a(t)-\mathbf{R}_a\right)\delta\left(\mathbf{p}_a(t)-\mathbf{P}_a\right)\right] \ , \tag{IV.9}$$

the projection operator is defined as

$$\hat{P}h\left(\mathbf{R},\mathbf{P},t\right) = \int d\mathbf{R}'\int d\mathbf{P}'\int d\mathbf{R}''\int d\mathbf{P}'' < h\left(\mathbf{R},\mathbf{P},t\right)g\left(\mathbf{R}',\mathbf{P}'\right) > \\ < g\left(\mathbf{R}',\mathbf{P}'\right)g\left(\mathbf{R}'',\mathbf{P}''\right) >^{-1} g\left(\mathbf{R}'',\mathbf{P}''\right) \ , \tag{IV.10}$$

where $\hat{P} = (\hat{P})^2$ and $\hat{P}g\left(\mathbf{R},\mathbf{P}\right) = g\left(\mathbf{R},\mathbf{P}\right)$. Here we use for the field variable the symbol $g\left(\mathbf{R},\mathbf{P},t\right)$ to indicate that the slow variables in the projection operator can be different than the ones in the general formalism of the preceding section. By applying the projection operator to both the left and the right sides of the Liouville equation, one recovers a generalized Langevin equation.[90–93]

Briefly, the generalized Langevin equation in the phase space is then transformed into its analog equation in space coordinates,

$$m\frac{d^2\mathbf{r}_a(t)}{dt^2} = \beta^{-1}\frac{\partial}{\partial\mathbf{r}_a(t)}\ln\psi(\mathbf{r}) - \int_0^t d\tau\sum_{b=1}^{N}\frac{\beta\mathbf{p}_b}{3m} < \mathbf{F}_a(t)\cdot\mathbf{F}_b^{\hat{Q}}(t-\tau) > +\mathbf{F}_a^{\hat{Q}}(t) \ , \tag{IV.11}$$

where $\psi(\mathbf{r}(t))$ is the intramolecular distribution function. The inertial contribution in Eq.(IV.11) can be discarded, as the liquid has a low Reynolds number and the dynamics is overdamped. The Generalized Langevin Equation is simply written as

$$\zeta_m\frac{d\mathbf{r}_a(t)}{dt} = \frac{1}{\beta}\frac{\partial}{\partial\mathbf{r}_a(t)}\ln\psi(\mathbf{r}) + \mathbf{F}_a^{\hat{Q}}(t) \ , \tag{IV.12}$$

with the averaged friction coefficient, in the Markov limit,

$$\zeta_m \approx \beta/3\ N^{-1}\sum_{a,b=1}^{N}\int_0^\infty d\tau < \mathbf{F}_a(t)\cdot\mathbf{F}_b^{\hat{Q}}(t-\tau) > \ . \tag{IV.13}$$

This equation describes how the monomer friction coefficient is generated from the space and time correlation of the random forces that act on two different segments of the “tagged” polymer chain, a and b. The extent of the correlation depends on the propagation of the forces through the macromolecule, its structure and local flexibility. The forces are generated by the monomers of the surrounding molecules randomly colliding with the monomers of the tagged chain: the collision strength depends on the structure of the liquid and on the interparticle potential. A more explicit definition of the friction coefficient is given in the following sections.

IV.5. Solution of the Generalized Langevin Equation in the Monomer Representation

The intramolecular distribution function is approximated in our description by a Gaussian distribution

$$\psi(\mathbf{r}) = \left[(2\pi)^N \det(\mathbf{A}^{-1})\right]^{-3/2} e^{-\frac{3}{2l^2}\mathbf{r}^T\mathbf{A}\mathbf{r}} \ , \tag{IV.14}$$

which holds for polymer chains longer than about 30 monomers.[81] This leads to a Generalized Langevin Equation where the intramolecular contribution is linear in the monomer coordinates

$$\zeta_m \frac{d\mathbf{r}_a(t)}{dt} = -\frac{3k_BT}{l^2}\sum_{b=1}^{N}\mathbf{A}_{a,b}\mathbf{r}_b(t) + \mathbf{F}_a^{\hat{Q}}(t) \ , \tag{IV.15}$$

and is simply solved through transformation into normal modes of motion.[24,97] The matrix $\mathbf{A}$ is defined, for a semiflexible polymer represented as a Freely Rotating Chain (FRC), as the product of two matrices, $\mathbf{M}$ and $\mathbf{U}$,

$$\mathbf{A} = \mathbf{M}^T \begin{pmatrix} 0 & 0 \\ 0 & \mathbf{U}^{-1} \end{pmatrix} \mathbf{M} \ , \tag{IV.16}$$

with the connectivity matrix, with dimensions $N \times N$, defined as

$$\mathbf{M} = \begin{pmatrix} N^{-1} & N^{-1} & N^{-1} & ... & N^{-1} \\ -1 & 1 & 0 & ... & 0 \\ 0 & -1 & 1 & ... & 0 \\ ... & ... & ... & ... & ... \\ 0 & ... & 0 & -1 & 1 \end{pmatrix} , \tag{IV.17}$$

and the $\mathbf{U}$ matrix defined as a function of the stiffness parameter g as

$$\mathbf{U}_{ij} =< \frac{\mathbf{l}_i \cdot \mathbf{l}_j}{|\mathbf{l}_i||\mathbf{l}_j|} >= g^{|j-i|} \ . \tag{IV.18}$$

Here, $g = - < \cos\theta >$ and θ is the angle between two consecutive bonds in the FRC representation of a homopolymer.[97] The stiffness parameter, g, is specific of the chemical structure and thermodynamic conditions of the sample under study.

IV.6. Center-of-Mass Level Representation of the Polymer Chain

In the soft colloidal particle representation the projection operator targets the center-of-mass of the polymer. The field variable ($n = 1$, $N = 1$, $a = cm$) is simply defined as

$$g(\mathbf{R}, \mathbf{P}, t) = [\delta(\mathbf{r}_{cm}(t) - \mathbf{R})\, \delta(\mathbf{p}_{cm}(t) - \mathbf{P})] \ . \tag{IV.19}$$

Applying the projection operator in the new field variable to the Liouville equation, where $U = 0$ and $W_{ij} \neq 0$, leads to the generalized Langevin equation

$$\begin{aligned} \frac{\partial}{\partial t} g(\mathbf{R}, \mathbf{P}, t) &= -\int_0^t ds \int d\mathbf{R}' \int d\mathbf{P}' M(\mathbf{R}, \mathbf{P}, \mathbf{R}', \mathbf{P}') g\left(\mathbf{R}', \mathbf{P}', (t-s)\right) \\ &+ F(\mathbf{R}, \mathbf{P}, t) \ , \end{aligned} \tag{IV.20}$$

which reduces, following the procedure briefly outlined in Section IV.4, to

$$m\frac{d^2\mathbf{r}_{cm}(t)}{dt^2} = -\int_0^t d\tau \frac{\beta \mathbf{p}_{cm}}{3m} < \mathbf{F}_{cm}(t) \cdot \mathbf{F}_{cm}^{\hat{Q}}(t-\tau) > + \mathbf{F}_{cm}^{\hat{Q}}(t) \ . \tag{IV.21}$$

In the overdamped regime,

$$\zeta_{soft}\frac{d\mathbf{r}_{cm}(t)}{dt} = \mathbf{F}_{cm}^{\hat{Q}}(t) \ , \tag{IV.22}$$

where ζ_{soft} is the friction coefficient for the colloidal particle, $\zeta_{soft} \cong \beta/3 \int_0^\infty d\tau < \mathbf{F}_{cm}(t) \cdot \mathbf{F}_{cm}^{\hat{Q}}(t-\tau) >$. Eq.(IV.22) obeys the fluctuation-dissipation relation $\langle \mathbf{F}_{cm}(t) \cdot \mathbf{F}_{cm}(t') \rangle = \delta_{t-t'} 6 k_B T \zeta_{soft}$.

The choice of the field variables in the projection operator defines the length scale of coarse-graining and the variables in which the resulting Generalized Langevin Equation is expressed. Because the derivation just presented depends on the basic assumption that the correlation function of the bath variables are short lived in the presence of heavy particles, and correction terms represented by the memory functions are minimized when a clear separation of timescale is observed between the slow variables in the projection operator and the fast variables that are averaged out, this criteria provides a way of selecting the relevant length scales for the coarse-graining, when dynamical properties are under study.

For example, as far as polymer dynamics is concerned, we know that for times longer than the longest Rouse correlation time, $\tau_R \approx R_g^2/D$, polymer internal dynamics is fully relaxed and the monomer dynamics follows the motion of the center-of-mass, which is long lived. This suggests that the center-of-mass coordinates are a good choice to represent the projected slow dynamics for time $t >> \tau_R$. This reasoning holds for both unentangled and entangled polymer dynamics as the longest relaxation time, after which free diffusion and Brownian motion set in, is τ_R with the proper diffusion coefficient, i.e. for unentangled chains $D_{unent} \propto N^{-1}$ and for entangled chains $D_{ent} \propto N^{-2}$.

IV.7. Analytical Rescaling of the Coarse-Grained Dynamics due to Free Energy Change

The two Langevin equations, Eqs.(IV.15) and (IV.22), display the two levels of coarse-graining of the macromolecular liquid, which are adopted in this paper. The comparison of the two equations, which in the longtime regime should predict identical dynamics for the polymer center-of-mass, shows that the two equations differ because of the presence of the intramolecular free energy in the monomer description, which is absent in the soft colloidal approximation, and because of the different friction coefficients in the two representations.

The elimination of degrees of freedom increases the entropy of the system, as every coarse-grained state corresponds to a number of preaveraged microstates. In an extreme picture we can imagine that the preaveraging due to the coarse-graining procedure is in effect transforming the energy of the system, expressed for example in the Liouville equation by an Hamiltonian, into a free energy in the corresponding Langevin equation. While the Hamiltonian contains kinetics and potential energy, the free energy includes an entropic contribution due to the preaveraged microstates for each coarse-grained state.

As far as the free energy correction is concerned, the system described by the larger cutoff lenghtscale is the one where the level of coarse-graining is most extensive and the highest entropic correction has to be included. This correction can be calculated from the comparison of the two equations. Because the system described at the monomer level is exploring in time the intramolecular energy states of the configurational landscape, its dynamics is slowed down with respect to the colloid representation where intramolecular degrees of freedom are not present. To take this effect into account we calculate the correction that has to be included in the soft-colloid representation to take into account the time spent by the atomic system to explore the internal degrees of freedom.

Consistent with the monomer-level model adopted in our study and with UA MD simulations, the polymer is described as a collections of beads, or friction points, connected by harmonic springs. Each bead corresponds to a CH_x moiety, with $x = 2$ or 3, depending if the unit is imbedded in the chain or is terminal. This model has been shown to provide a realistic representation of the dynamics of numerous polymeric systems with different chemical structure.[24, 82, 83, 95, 96]

The intramolecular potential is defined as

$$U(r) = \frac{3k_BT}{2l^2}\sum_{i,j=1}^{N}\mathbf{A}_{i,j}\mathbf{r}_i\cdot\mathbf{r}_j\ , \tag{IV.23}$$

with $U(r)$ not to be confused with the semiflexibility matrix of Eq.(IV.18). Here $\mathbf{A}$ is the connectivity matrix of Eq.(IV.16), which represents the structure and local flexibility of the polymer,[99, 100] $\mathbf{r}_i$ the position of bead i in a chain of N beads or united atoms, and $\mathbf{l}_i = \mathbf{r}_{i+1} - \mathbf{r}_i$ the bond vector connecting two adjacent beads.

The statistically averaged internal energy for one molecule consisting of N monomers is given by

$$\left\langle \frac{U}{k_BT}\right\rangle = N\int Ue^{-\frac{3}{2l^2}\mathbf{r}^T\mathbf{A}\mathbf{r}}dr = \frac{3N}{2l^2}\int \mathbf{r}^T\mathbf{A}\mathbf{r}e^{-\frac{3}{2l^2}\mathbf{r}^T\mathbf{A}\mathbf{r}}\ . \tag{IV.24}$$

After solving the integral by normal mode transformation, as reported in Appendix A, this model predicts the average energy dissipated in the internal modes to be $\langle U/(k_BT)\rangle = 3N/2$. The soft-colloidal representation, instead, has no internal degrees of freedom.

The simulation time $\tilde{t}$, as measured in the MS simulation of the coarse-grained system, translates into the real time t after including the rescaling due to the energy, which is reduced by the amount of energy dissipated in the fluctuations due to internal degrees of freedom.[101] For our model

$$t = \tilde{t}R_g\sqrt{\frac{m}{k_BT}\frac{3}{2}N}\ , \tag{IV.25}$$

with the particle mass, m, and size R_g. This rescaling slows down the coarse-grained dynamics, but only partially accounts for the observed phenomenon because the rescaling of the friction needs to be included.

IV.8. Theoretical Derivation for Monomer Friction Coefficient

The rescaling of the friction coefficient is calculated considering the friction of the polymer center-of-mass in the monomer/UA representation, and comparing the result with the friction of the cm of a soft colloidal particle. The expression for each of the friction coefficients is derived from its definition as the integral of the memory function contribution to the Generalized Langevin Equation (GLE) in the two levels of representation.

The effect of coarse-graining the Liouville equation, or projection onto the slow degree of freedoms, is the appearance in the Langevin equation of the dissipation terms, given by the random force and the friction coefficient. Systems with different levels of coarse graining have different friction and, as a consequence, different diffusion coefficients.

For a particle in a liquid, the center of mass mean-square displacement is defined as

$$\langle \Delta R^2(t) \rangle = 6\, D\, t \ , \tag{IV.26}$$

with D the diffusion coefficient. For a polymer, the cm diffusion coefficient is given by $D = k_B T/(N\zeta_m)$, where ζ_m is the friction coefficient of a monomer, while for a liquid of soft colloidal particles $D_{soft} = k_B T/\zeta_{soft}$, with ζ_{soft} the friction coefficient of the colloidal particle. The two should be identical in the long-time limit, but they are not, as the diffusion coefficient obtained from MS MD simulation is much larger (much faster dynamics) than the one obtained from UA MD. The correction factor to scale down the MS MD diffusion coefficient, D^{MS}, is $\zeta_{soft}/(N\zeta_m)$, which yields the rescaled mean-square displacement

$$\langle \Delta R^2(t) \rangle = 6\, D^{MS} \frac{\zeta_{\text{soft}}}{N\zeta_m}\, t \ . \tag{IV.27}$$

The thermodynamic conditions of the system under study, i.e. density and temperature, and its molecular structure, i.e. the radius-of-gyration, enter the equation above both directly through the definitions of the friction coefficients, Eqs.(IV.44) and (IV.49) and indirectly through the mesoscale simulation from which the diffusion coefficient, D^{MS}, is measured.

To solve Eq.(IV.27) we start from the definition of the monomer friction coefficient, ζ_m, which is given in the Markov limit by the memory function

$$\zeta_m \ \cong \ \frac{1}{N} \sum_{a,b=1}^{N} \int_0^{\infty} d\tau \Gamma_{a,b}(\tau) \ . \tag{IV.28}$$

$\Gamma_{a,b}(t)$ is the function that describes the correlation, through the polymer chain between monomers a and b, of the random forces generated from the random collisions of the surrounding molecules undergoing Brownian motion, with[91–93]

$$\Gamma_{a,b}(t) \;\cong\; \frac{\beta}{3}\rho \int d\mathbf{r} \int d\mathbf{r}' g(r) g(r') F(r) F(r')\, \hat{\mathbf{r}} \cdot \hat{\mathbf{r}}' \int d\mathbf{R}\, S^{Q}_{a,b}(R;t) S^{Q}(|\mathbf{r} - \mathbf{r}' + \mathbf{R}|;t)\,, \tag{IV.29}$$

where $g(r) = h(r) + 1$ is the monomer radial distribution function, $F(r)$ is the total force exerted by all the matrix polymer on the monomer, and $S^{Q}(r;t)$ is the projected dynamic structure factor of the matrix fluid surrounding the polymer. The unit vectors $\hat{\mathbf{r}}$ and $\hat{\mathbf{r}}'$ define the directions of the total exerted forces. The derivation of Eq.(IV.29) is not completely new and is briefly reported in Appendix B.

Eq.(IV.29) rests on the approximations that the fluid is isotropic and that many-body correlation functions can be described with good accuracy as products of pair distribution functions. The solution of this equation is sometimes carried on by introducing a mode-coupling approximation,[92–94] however we follow a different procedure. The dynamic structure factor, which is ruled by the projected dynamics, is approximated by its real dynamics counterpart, $S^{Q}(r;t) \approx S(r;t)$, simplifying the solution of Eq.(IV.29). This is an acceptable approximation when the Langevin equation is expressed as a function of the slow variables[98] and holds for our system in the long-time, diffusive regime.[95]

In order to separate the spatial coordinates of $S(|\mathbf{r}-\mathbf{r}'+\mathbf{R}|;t)$ in Eq.(IV.29) it is convenient to use the Fourier transform

$$S(r;t) = \frac{1}{(2\pi)^3} \int e^{i\mathbf{kr}} S(k;t)\, d\mathbf{k}\ , \tag{IV.30}$$

where the dynamic structure factor is calculated in reciprocal space as the sum of intra- and intermolecular contributions

$$S(k,t) = \frac{1}{N}\sum_{\alpha\gamma} S_{\alpha\gamma}(k,t) = \frac{1}{N}\sum_{\alpha\gamma} \omega_{\alpha\gamma}(k,t) + \rho\frac{1}{N}\sum_{\alpha\gamma} h_{\alpha\gamma}(k,t)\,. \tag{IV.31}$$

Here $\omega_{\alpha\gamma}(k,t)$ is the time dependent intramolecular probability distribution functions for monomers α and γ, on the same molecule, to be separated by a reciprocal distance k, while $h_{\alpha\gamma}(k,t)$ is the corresponding intermolecular contribution.

Given that the dynamics on the global scale is driven by the polymer diffusion, the intramolecular probability distribution function in reciprocal space can be expressed, in the limit of large length scales, $k \leq 1/R_g$, as

$$\omega_{\alpha\gamma}(k;t) \approx \exp\left[-\frac{k^2 l^2 |\alpha-\gamma|}{6}\right] \exp\left[-k^2 D t\right] \ , \tag{IV.32}$$

where D is the polymer center-of-mass diffusion coefficient and $l = N^{-1}\sum_{i=1}^{N}|\mathbf{l_i}|$ is the average segmental length.

Because in Eqs.(IV.28) and (IV.29) the order of the summation and time integrals can be changed, the double summation reduces the inter- and intramolecular distributions to their averages over the bead distribution. The site-averaged intramolecular probability distribution function, $\omega_0(k)$, is well approximated by the Debye formula,[97]

$$\omega_0(k) = \frac{1}{N}\sum_{\alpha\gamma}\omega_{\alpha\gamma}(k) = \frac{2N(e^{k^2R_g^2} + k^2R_g^2 - 1)}{k^4R_g^4} \ , \tag{IV.33}$$

or by its Pade' approximant

$$\omega_0(k) \approx \frac{N}{1+k^2\xi_c^2} \ . \tag{IV.34}$$

The site-averaged intermolecular probability distribution is defined by the Ornstein-Zernike equation

$$h(k) = \frac{1}{N}\sum_{\alpha\gamma}h_{\alpha\gamma}(k) = \frac{\omega_0^2(k)c(k)}{1-\rho c(k)\omega_0(k)} \ , \tag{IV.35}$$

where $c(k)$ is the direct correlation function. At the monomer level we follow Curro and Schweizer's PRISM thread approach,[54,55] where the polymer chain is modeled as a thread of vanishing thickness, $c(k) \approx c_0$, with $c_0 = -(1 - 2\xi_\rho^2/R_g^2)/(2N^2\rho_{ch}\xi_\rho^2/R_g^2)$. Substitution of c_0 and Eq. (IV.34) into Eq. (IV.35) gives

$$h(k) = \frac{h_0}{(1+k^2\xi_\rho^2)(1+k^2\xi_c^2)} \ , \tag{IV.36}$$

where $h_0 = h(k=0) = (\xi_\rho^2/\xi_c^2 - 1)/\rho_{ch}$ is related to the compressibility of the system.[8,71]

Because in the large length scale regime, of interest here, the relaxation of the liquid is dominated by the polymer diffusion, the dynamic structure factor is approximated as

$$S(k;t) \approx S(k)\exp\left[-k^2Dt\right] . \tag{IV.37}$$

Finally, after introducing the integral representation of the delta function

$$\int d\mathbf{R}\; e^{i\mathbf{R}(\mathbf{k}_1+\mathbf{k}_2)} = (2\pi)^3\; \delta(\mathbf{k}_1+\mathbf{k}_2)\,, \tag{IV.38}$$

the last integral in Eq.(IV.29) simplifies to

$$\int d\mathbf{R}\, S(R;t)S(|\mathbf{r}-\mathbf{r}'+\mathbf{R}|;t) = \frac{1}{(2\pi)^6}\int d\mathbf{k}_1 \int d\mathbf{k}_2\; S(k_1;t)\; S(k_2;t)e^{i\mathbf{k}_2(\mathbf{r}-\mathbf{r}')}\int d\mathbf{R}\; e^{i\mathbf{R}(\mathbf{k}_1+\mathbf{k}_2)}\;. \tag{IV.39}$$

Because the functions $\omega_0(k)$ and $h(k)$ are even with respect to k, the equation reduces to three contributions: the first is due to intramolecular interactions $\omega_0^2(k)$, the second includes the cross product $\omega_0(k)h(k)$, and the last is due to the intermolecular contribution $h^2(k)$. This leads to the following expression

$$\int d\mathbf{R}\, S(R;t)S(|\mathbf{r}-\mathbf{r}'+\mathbf{R}|;t) = \frac{1}{(2\pi)^3}\int d\mathbf{k}\; (\omega_0^2(k)+2\rho h(k)\omega_0(k)+\rho^2h^2(k))e^{-2k^2Dt}e^{i\;\mathbf{k}(\mathbf{r}-\mathbf{r}')}\;. \tag{IV.40}$$

Because we are assuming that monomers are interacting through a hard core potential, which is consistent with the PRISM thread model,[54, 55] the force is a delta function and therefore

$$g(r)F(r) = g(d)\beta^{-1}\delta(r-d)\,. \tag{IV.41}$$

where d is a hard core diameter, identical for any CH_2 bead in the chain, in the spirit of the UA-MD description and PRISM approach. When we compare our equations with data of experimental or simulated systems, where monomers interact through a Lennard-Jones potential, the latter has to be mapped onto a hard-core potential with the effective diameter, d.[102]

The final expression for the monomer friction coefficient is given by

$$\zeta_m = \frac{1}{48\,\pi^3}\,\rho g^2(d)\,(\beta D)^{-1}\left\{J[\omega_0(k),\omega_0(k)]+2\rho J[\omega_0(k),h(k)]+\rho^2 J[h(k),h(k)]\right\}\;, \tag{IV.42}$$

with the function

$$J[\alpha(k),\beta(k)] \;=\; \int d\mathbf{r}\int d\mathbf{r}'\int_0^\infty dk\,\frac{\sin(k|\mathbf{r}-\mathbf{r}'|)}{k|\mathbf{r}-\mathbf{r}'|}\,\hat{\mathbf{r}}\cdot\hat{\mathbf{r}}'\,\delta(r-d)\delta(r'-d)\,\alpha(k)\beta(k)\;. \tag{IV.43}$$

The solution of Eqs.(IV.42) and (IV.43) is given by a lengthy but analytical expression, which is a function of the molecular parameters, ξ_ρ, R_g, thermodynamic parameters, ρ, β, the diffusion coefficient, D, and of the hard-core diameter d, as

$$
\begin{aligned}
\zeta_m \approx\ & \frac{2}{3}(D\beta)^{-1}\rho g^2(d)\Bigg(\frac{1}{12}\pi N^2 d^2 R_g\left[15\sqrt{2}+40\frac{d}{R_g}+12\sqrt{2}\left(\frac{d}{R_g}\right)^2\right]+ \\
& \rho\pi N h_0\frac{1}{3\sqrt{2}(R_g^2-2\xi_\rho^2)^2}\Bigg[12\sqrt{2}\xi_\rho^7+12d^4R_g^3\left(1-2\left(\frac{\xi_\rho}{R_g}\right)^2\right)+ \\
& 4\sqrt{2}d^3R_g^4\left(5-14\left(\frac{\xi_\rho}{R_g}\right)^2+2\left(\frac{\xi_\rho}{R_g}\right)^4\right)+3d^2R_g^5\left(5-14\left(\frac{\xi_\rho}{R_g}\right)^2-4\sqrt{2}\left(\frac{\xi_\rho}{R_g}\right)^5\right) \\
& -12\sqrt{2}e^{-\frac{2d}{\xi_\rho}}\xi_\rho^7\left(1+\frac{d}{\xi_\rho}\right)^2\Bigg]+\rho^2\pi h_0^2\frac{1}{12(R_g^2-2\xi_\rho^2)^3}\Bigg[40d^3R_g^6+15\sqrt{2}d^2R_g^7 \\
& -24\sqrt{2}d^4R_g^3\xi_\rho^2-144d^3R_g^4\xi_\rho^2+6\sqrt{2}d^4R_g^5\left(2-9\left(\frac{\xi_\rho}{d}\right)^2\right)+ \\
& 12R_g^2\xi_\rho^7\left(4\left(\frac{d}{\xi_\rho}\right)^3-7\left(\frac{d}{\xi_\rho}\right)^2+9\right)-8\xi_\rho^9\left(4\left(\frac{d}{\xi_\rho}\right)^3-9\left(\frac{d}{\xi_\rho}\right)^2+15\right)- \\
& e^{-\frac{2d}{\xi_\rho}}12\xi_\rho^4(d+\xi_\rho)\left(R_g^2(d+3\xi_\rho)(2d+3\xi_\rho)-2\xi_\rho^2(2d^2+5\xi_\rho d+5\xi_\rho^2)\right)\Bigg]\Bigg)\ .
\end{aligned}
\tag{IV.44}
$$

This expression is general and holds for any homopolymer melt represented as a collection of identical beads interaction through a hard-core potential of range d. The value of d is specific of the monomeric structure of the homopolymer.

IV.9. Friction Coefficient for a Liquid of Interacting Soft Colloidal Particles

The friction coefficient for a point particle interacting through a soft repulsive potential is much smaller than the friction of the macromolecule before coarse-graining. In fact, the friction coefficient of an object can be estimated using Stokes' formula where $\zeta = 6\pi\eta r_H$, with η the fluid viscosity and r_H the hydrodynamic radius. The latter can be evaluated from the surface area of the object exposed to the solvent, which can be estimated by "rolling" a solvent molecule on the object. It is evident that the surface available to the solvent in a bead-spring representation of a polymer is much higher than the surface available to the solvent for a point particle interacting through a soft, long-ranged potential.

To calculate the friction coefficient for a soft colloidal particle, we start from the Generalized Langevin Equation that describes the time evolution for the position coordinate of the molecular center-of-mass, i.e. Eq.(IV.22) where the friction coefficient for soft particles is given by

$$\zeta_{\text{soft}} \cong (\beta/3)\ \rho_{ch} \int_0^\infty d\,t\ \int d\mathbf{r} \int d\mathbf{r}' g(r) g(r') F(r) F(r')\, \hat{\mathbf{r}} \cdot \hat{\mathbf{r}}' \int d\mathbf{R}\, S(R;t) S(|\mathbf{r} - \mathbf{r}' + \mathbf{R}|;t)\,. \quad \text{(IV.45)}$$

Eqs.(IV.29) and (IV.45) look identical, with just a different form of the density prefactor. In reality the form of the pair-distribution function, $g(r)$, the force exerted by the surrounding molecules on the tagged chain, $F(r)$, and the dynamic structure factors, $S(\mathbf{R}, t)$, are different quantities in the monomer and soft-colloid representations.

We assume that the dynamic structure factor in reciprocal space has the form

$$S(k;t) \approx S(k)\ e^{-Dtk^2} = (1 + \rho_{ch} h^{cc}(k))\ e^{-Dtk^2} \quad \text{(IV.46)}$$

where $h^{cc}(k)$ is the center of mass total pair correlation function

$$h^{cc}(k) = h_0 \left[\frac{1 + k^2 R_g^2/2}{1 + k^2 \xi_\rho^2} \right] e^{-\frac{k^2 R_g^2}{3}}\,. \quad \text{(IV.47)}$$

with $h_0 = (\xi_\rho^2/\xi_c^2 - 1)/\rho_{ch}$, as defined in the previous section. Eq.(IV.47) is just the Fourier transform of Eq.(IV.1). Eq.(IV.46) indicates that in the long-time regime, which is of interest here, the relaxation of the liquid is largely driven by the center-of-mass diffusion, while internal dynamics and local modes of motion are already fully relaxed. This is a reasonable assumption given that the length scale of our treatment is the overall polymer dimension, and no structural or dynamical information is retained on the local scale.

To perform our calculation we need to defined an approximate analytical form of the effective force. To do so we adopt the simplified form of $h^{cc}(r)$, Eq.(IV.2). Then, we reduce further the expression by neglecting the small attractive component of the potential. Finally we approximated the real potential, $v(r)$, with its mean-force counterpart $w(r) \approx -k_B T \ln[h(r) + 1]$ properly rescaled. The real potential, calculated through the HNC approximation as described in the following section, is a complicated function of $h(r)$. However it can be related, in an approximated way, to the simpler potential of mean force through the equation

$$v(r) \approx \frac{v(0)}{w(0)} w(r) \; , \tag{IV.48}$$

where $v(r) \approx \sqrt{3} w(r)$ for all the samples considered in this study. These approximations define the force $F(r)$ and the pair distribution function, $g(r) = h(r) + 1$, entering the equation for the friction coefficient.

The resulting expression for the friction coefficient of the soft colloidal particle is expressed as a function of the diffusion coefficient D, β, ρ_{ch} and the two length scales R_g and ξ_ρ as

$$\zeta_{\text{soft}} \cong 4\sqrt{\pi}(D\beta)^{-1} \rho_{ch} R_g \xi_\rho^2 \left(1 + \frac{\sqrt{2}\xi_\rho}{R_g}\right)^2 \frac{507}{512} \left[\sqrt{\frac{3}{2}} + \frac{1183}{507} \rho_{ch} h_0 + \frac{679\sqrt{3}}{1024} \rho_{ch}^2 h_0^2\right] \; . \tag{IV.49}$$

This expression is an approximated analytical form for the friction coefficient of a soft colloidal particle.

CHAPTER V

APPLICATION OF THE RECONSTRUCTION PROCEDURE TO SIMULATED COARSE-GRAINED POLYMER MELTS

In Chapter V rescaling method developed in previous chapter is applied to dynamics obtained from mesoscale simulations of polyethylene, represented as soft colloidal particles. The results of rescaling approach show a good agreement with data of translational diffusion measured experimentally and from simulations. The proposed method is used to predict self-diffusion coefficients of new polyethylene samples. My contribution to this chapter are all performed simulations and calculations of rescaling factors, derivation of the friction coefficients in two representations. The material from Chapter V has been published with my advisor, Marina Guenza, as co-author.

As stated above, the accelerated dynamics that is a consequence of the coarse graining of the system can be rescaled by taking into account the two main effects of the procedure, namely the change in the entropic contribution to the free energy of the system due to the averaging of the internal degrees of freedom and the change in the friction coefficient due to the different shapes of the molecule in the two different levels of coarse-graining. The difference in shape relates to the change in the molecular surface available to the surrounding molecules, and to the correlation of the random forces generated by intermolecular collisions.

The first rescaling is given by the inclusion *a posteriori* of the internal degrees of freedom, averaged out during the coarse-graining procedure, as a correction term in the free energy of the system, which accounts for the difference in entropy. The energy correction affects the time of the measured dynamics as the change from a bead-spring description to a soft-colloid representation leads to the rescaling of the time reported in Eq.(IV.25), also taking into account the fact that because the potential is expressed in normalized quantities, the simulation runs using reduced units of energy, $k_B T = 1$ and the normalized length r/R_g.

The second rescaling of the dynamics is calculated starting from the ratio between the friction coefficients in the two coarse-grained representations, as described in Eq.(IV.27).

V.1. Coarse-Grained Interparticle Soft Potential and Accelerated Dynamics in Mesoscale Simulations

Here we present numerical calculations to illustrate and discuss the rescaling procedure of the preceding sections. We first perform MS MD simulations of the coarse-grained polymer liquid, where each chain is represented as a soft colloidal particle, centered at the center-of-mass of a chain, and interacting with the surrounding particles through a soft repulsive potential of the order of few times the chain dimension, R_g. The simulations of the soft colloidal liquid produce dynamical properties that are accelerated due to the soft nature of the potential in the coarse-grained representation. These properties are rescaled following our procedure, and then compared with existing data, when they are available.

In a previous paper we briefly presented calculations of the rescaled dynamics for a variety of systems including UA MD simulations and experimental data of PE diffusion available in the literature, that we use to test the accuracy of our procedure. We selected UA MD simulations as our test (see Table V.1) because they have been shown to reproduce with a high level of accuracy the dynamical properties of PE melts, such as diffusion and viscosity.[104, 105] We also compared predictions of rescaled MS-MD simulations with experiments for samples with temperature $T = 509\ K$, monomer site density $\rho = 0.0315302$ sites/Å^3 and $N = 36,\ 72,\ 106,\ 130,\ 143,\ 192,$ and 242.[26, 86–89] Our MS-MD simulations, properly rescaled, provided good quantitative predictions of the diffusion coefficient for those systems.[36]

TABLE V.1. Polyolefin melts UA MD simulation parameters

System	T[K]	ρ[sites/Å^3]	$(R_g^{UA})^2$[Å^2]
PE 30[a]	400	0.0317094	63.5695
PE 44[a]	400	0.0323951	110.3197
PE 48[b]	450	0.0314487	111.0832
PE 66[a]	448	0.0328993	177.5348
PE 78[b]	450	0.0321465	205.9221
PE 96[a]	448	0.0328194	281.7989
PE 122[b]	450	0.0325479	346.2655
PE 142[b]	450	0.0326600	420.7070
PE 174[b]	450	0.0327680	525.1816
PE 224[b]	450	0.0328835	690.5038
PE 270[b]	450	0.0329520	856.4648
PE 320[b]	450	0.0330034	980.1088

[a] from Refs.;[15, 57, 58] [b] from Ref.[3, 65]

In this paper we use those same systems to illustrate our procedure. Moreover we present new results for PE samples, not present in the literature, to underline the predictive power of the theory, where no calibration curve is necessary. Once a system is selected, its structural and thermodynamic parameters are defined and are used as input to the MS MD simulation so that the whole procedure is free of adjustable parameters, with the exception of the parameter d that is fixed for PE once and for all samples.[3, 15, 57, 58]

Systems that we simulated include liquids of chains with increasing degree of polymerization, as described above. As the molecular weight of the polymer increases, the systems cross the threshold from unentangled to entangled dynamics. For entangled systems the dynamical rescaling approach that we propose is modified to include a one-loop perturbation that accounts for the presence of entanglements. Simulations of soft colloidal liquids are performed for entangled systems, and the rescaling applied to predict diffusion.

Details about our MS MD simulations have been reported in previous papers of ours and will not be repeated here.[17, 36, 76] Briefly, MS MD simulations were implemented in the microcanonical (N, V, E) ensemble on a cubic box with periodic boundary conditions. We used reduced units such that all the units of length were scaled by R_g $(\tilde{r} = r/R_g)$ and energies were scaled by k_BT. Temperature and radius-of-gyration were utilized for dimensionalizing the results obtained from the MS MD simulations, after they were performed.

The number of particles, i.e. polymer chains, in our simulations varies from 1728 $(N = 40)$ to 85184 $(N = 1000)$ depending on the system. This number is determined by the box size, which is larger than twice the range of the potential, and by the liquid density. The potential is long-ranged, due to the many-body effects entering through the OZ equation.

Each simulation evolves for about $50,000$ computational steps. For the entangled melts the potential is longer ranged than for the unentangled systems, and therefore it is cut at larger distances requiring a bigger box size. The reduced density used in simulations, $\rho^{sim} = \rho R_g^3$ where ρ is the site density, varies around 1 for unentangled melts, and exceeds 2 for weakly entangled melts. A typical MS simulation takes between 2 hours $(N = 40)$ to 4 days $(N = 200)$ on one CPU workstation, while using the code that works in parallel, the computational time is further reduced, 2 days for $N = 1000$ and 46654 particles.

The pair potential acting between two effective coarse-grained units is formally derived from the colloidal representation of the liquid, specifically $h(r)$, using an hyper-netted-chain (HNC) closure approximation to the Ornstein-Zernike equation.[23] This approximation is known to work well for liquids of particles interacting through a soft potential.[102] The potential input to the MS MD simulation, $v^{cc}(r)$, is derived from the total correlation function for the soft colloidal representation of the liquid, $h^{cc}(r)$, defined in the limit of long chains, $N \rightarrow \infty$, as in Eq.(IV.2). The potential is calculated using the hypernetted chain approximation as

$$\beta v^{cc}(r) = h^{cc}(r) - ln[1 + h^{cc}(r)] - c^{cc}(r) \ . \tag{V.1}$$

Here the direct correlation function, $c^{cc}(r)$ is given in reciprocal space in terms of $h^{cc}(k)$ as:

$$c^{cc}(k) = \frac{h^{cc}(k)}{1 + \rho_{ch} h^{cc}(k)} \ . \tag{V.2}$$

It is important to define the correct potential acting between the coarse-grained units to achieve a realistic representation of the large scale properties of a system through MS MD. Because coarse-grained potentials result from the mapping of many-body interactions into pair interactions, through the averaging over microscopic degrees of freedom, they are parameter dependent. During the coarse-graining procedure, the potential acting between microscopic units, which is given by the Hamiltonian of the system, reduces to an effective potential, which is a free energy in the reference system of the microscopic coordinates. The coarse-grained potential so obtained contains contributions of entropic origin due to the microscopic, averaged-out degrees of freedom and is therefore state-dependent. This can be observed in the form of the total correlation function between coarse-grained sites, Eq.(IV.2) from which the potential is derived. The correlation function explicitly includes the structural and thermodynamic parameters of the polymer, i.e. the radius-of-gyration, density screening length, and number density. The temperature enters directly through Eq.(V.1) and indirectly through the molecular parameters, such as R_g. The radius of gyration is also density dependent.

Before entering the details of applying our rescaling approach we focus on the “raw” dynamics obtained directly from the MS MD simulations. Figure V.1 displays the mean-square displacement for the MS MD simulation of a polyethylene melt with $N = 44$. At short times the inertial term in the Langevin equation is dominant as the particles undergo ballistic dynamics, while in the long-time regime the system crosses over to diffusive dynamics. The diffusion coefficient is higher than the value measured in UA MD simulations, and the transition from ballistic to diffusive regime happens after about 5000 simulation steps (dot-dot vertical line on top panel of Figure V.1), which corresponds to a distance of roughly $30R_g$. Such a large distance reflects the fact that in MS MD simulation the point particles interact through a very soft potential and the density is also very low. Because the particle has to “collide” many times to undergo the crossover to diffusive dynamics the latter takes place at a large length scale.

Moreover, the bottom panel in Figure V.1 displays the velocity correlation function $\left\langle (v(t) - v(0))^2 \right\rangle$ and shows that, consistent with the mean-square-displacement, once more the inertial term becomes negligible at the same crossover time that the diffusive regime sets in. Since our MS MD simulation are performed at equilibrium, the average kinetic energy per particle $\left\langle mv^2(t)/2 \right\rangle = 3/2\, k_BT$, and therefore

$$\lim_{t\to\infty} \left\langle (v(t) - v(0))^2 \right\rangle = \lim_{t\to\infty} \left[2 \left\langle v^2(t) \right\rangle - 2 \left\langle v(t)v(0) \right\rangle \right] = 6k_BT/m\,. \tag{V.3}$$

The dynamical transition is displayed as a dashed line on the bottom panel of Figure V.1, taking into account that our simulations are in reduced units and $m = 1$, $k_BT = 1$. The figure shows that the velocity autocorrelation function reaches it’s asymptotic value at about the same time as the diffusive regime sets in for the mean-square-displacement.

V.2. Calculations of the Monomer Friction Coefficient, ζ_m

Because our formalism maps the Lennard-Jones liquid described by the UA MD simulation into a liquid of polymers interacting through a monomer hard-core repulsive potential, it is necessary to define an effective hard-core diameter, d. This is done by requiring the friction of the chain with $N = 44$ to follow the expected scaling behavior for the diffusion of an unentangled polymer chain, $D = k_BT/(N\zeta_m)$. Since all except two of the atoms in our PE chains are CH_2 monomers, we assume that the potential is identical for all the units along the homopolymer chain. Moreover we assume that the range of the repulsive interaction, d, is independent of liquid density.[103]

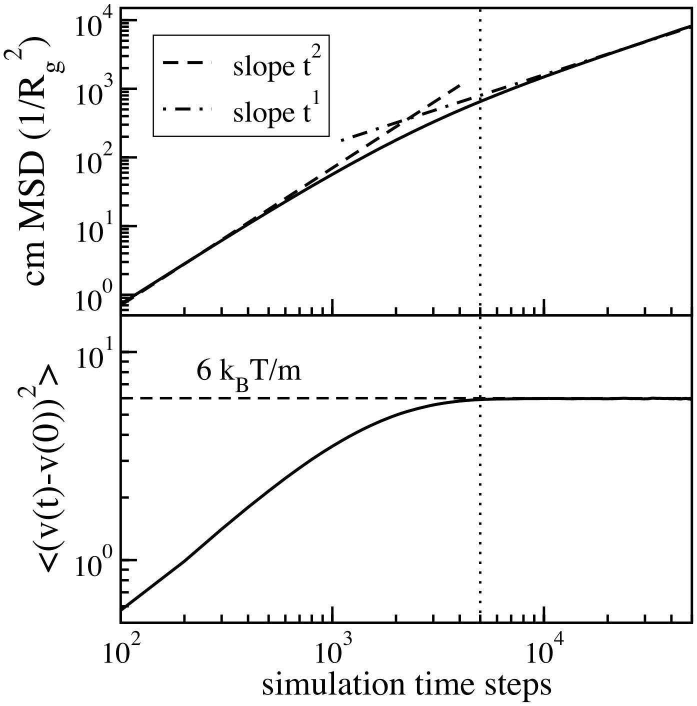

FIGURE V.1. Top panel: Cm mean-square displacement (solid line) from MS MD simulation in reduced units as a function of simulation time steps for the $PE44$ melt sample. The slopes for the ballistic and the diffusive regimes are shown as dashed and dot-dashed lines correspondingly. Bottom panel: Cm velocity time correlation function showing when the inertial term becomes negligible. The asymptotic value of 6 k_BT/m is depicted as a dashed line.

Among the different samples, we selected the chain with $N = 44$ to optimize d, because this sample follows unentangled dynamics while the polymer is long enough to obey the Gaussian intramolecular distribution of monomer positions, which justifies the analytical form of the intramolecular structure factors used in our formalism. Figure V.2 displays the monomer friction coefficient, from Eq.(IV.44), expressed as the dimensionless quantity $D\beta\zeta_m$, as a function of the hard sphere diameter d, for polyethylene melts of three different degrees of polymerization. The $1/N$ scaling is reported as a dot-dashed line in the figure.

In these calculations, the numerical values of N, ρ and R_g were taken from the data of the UA MD simulation against which the proposed approach is tested. The value of the radial distribution function at the contact was set to $g(d) = 1/2$, which is the conventional value assumed in the PRISM thread theory for polyethylene chains. This value is intermediate between zero and the first solvation shell value. The optimized hard-core diameter for $N = 44$ is $d = 2.1\mathring{A}$, which is an intermediate value between the bond length, $l = 1.54$ Å, and the Lennard-Jones σ-parameter, $\sigma = 3.95$ Å, in the intermonomer potential of the UA MD.[57,58] The unentangled scaling is fulfilled for PE30 at $d = 2.07$ Å and for PE96 at $d = 1.96$ Å, which are close to the one for PE44. Because the PE96 sample has a degree of polymerization that is close to the entanglement value of $N_e = 130$, its dynamics is likely to be in the crossover regime where the effect of entanglements start to be felt, since the transition from the unentangled to the entangled dynamics is very broad.

Table V.2 displays the numerical values of the dimensionless monomer friction coefficient, $D\beta\zeta_m$, for polymeric liquids with different degree of polymerization, N, across the unentangled-to-entangled transition. For both unentangled and entangled systems the hard sphere diameter has been fixed to the value of the unentangled ones, $d = 2.1$Å, so that the intermolecular monomer potential is not changed as a function of N. While for unentangled systems the monomer friction coefficient was calculated from Eq.(IV.44), for entangled chains we adopted a perturbative approach to account for the effect of entanglements. Let's denote

$$D\beta\zeta_m = J(\rho, N, R_g, d)\,, \tag{V.4}$$

where for unentangled systems $J(\rho, N, R_g, d) \approx N^{-1}$. Following a one-loop perturbation, and including the definition of the diffusion coefficient for a macromolecule comprised of N monomers

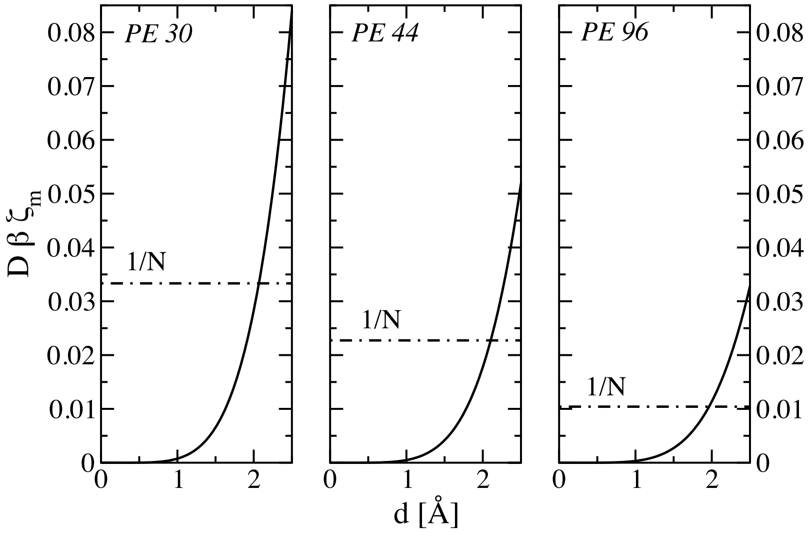

FIGURE V.2. Plot of $D\beta\zeta_m$ as a function of hard core diameter d. From left to right, the three panels show curves for polyethylene melt with $N = 30$, $N = 44$, and $N = 96$.

with ζ_m the monomer friction coefficient $D = (\beta\zeta_m N)^{-1}$, the normalized and perturbed friction coefficient becomes

$$D\beta\zeta_m' = ND\beta\zeta_m J(\rho, N, R_g, d) = N(D\beta\zeta_m)^2 \ . \tag{V.5}$$

The one loop perturbation is in the spirit of the reptation model where both the chain reptating and the chains involved in the entanglements relax with the same diffusive mechanism: each brings a N^{-1} scaling contribution, which is the trademark of polymer Brownian motion. Interestingly, in our model the diffusion coefficient of entangled polymers under certain fixed monomer density and temperature shows apparent scaling exponents different from -2 (see Figure V.4). The resulting scaling exponents emerge cumulatively from output of mesoscale simulations and both steps of rescaling.

Because Eq.(V.5) applies only when the systems are entangled, to predict the diffusive behavior of new samples it is necessary to estimate a priori the crossover degree of polymerization, N_e. Several methods have been presented in the literature to estimate N_e from thermodynamic conditions and molecular parameters.[106] Those methods provide similar values of N_e. Moreover, the expressions for the unentangled and entangled frictions, Eqs.(IV.44) and (V.5), predict values that differ only slightly in the crossover region. In this way, selecting the unentangled

TABLE V.2. Monomer friction coefficient contributions with hard sphere potential for $d = 2.1$Å

System	$D\beta\zeta_m(\omega_{\alpha\alpha})$	$D\beta\zeta_m(\omega_{\alpha\gamma})$	$D\beta\zeta_m(h_{\alpha\gamma})$	$D\beta\zeta_m$	$ND\beta\zeta_m$
PE 30	0.03378	0.08484	-0.04883	0.03601	1.0804
PE 44	0.02744	0.06244	-0.03991	0.02253	1
PE 48	0.03101	0.07984	-0.04904	0.03080	1.4782
PE 66	0.02539	0.05703	-0.03823	0.01880	1.2409
PE 78	0.02632	0.06287	-0.04179	0.02107	1.6439
PE 96	0.02239	0.04766	-0.03325	0.01441	1.3834
PE 122	0.02400	0.05533	-0.03831	0.01701	2.0757
PE 142	0.02245	0.04967	-0.03501	0.01466	2.0815
PE 174	0.02193	0.04827	-0.03438	0.01389	2.4170
PE 224	0.02133	0.04664	-0.03359	0.01304	2.9219
PE 270	0.02039	0.04344	-0.03164	0.01180	3.1849
PE 320	0.02184	0.04956	-0.03585	0.01371	4.3874

expression to represent entangled systems, or vice versa, in the crossover region would result in small inconsistencies in the calculated diffusion coefficients.

Table V.2 includes intra- ($D\beta\zeta_m(\omega_{\alpha\gamma})$) and inter-molecular ($D\beta\zeta_m(h_{\alpha\gamma})$) contributions to the monomer friction coefficient, as well as the self intramolecular contribution, $D\beta\zeta_m(\omega_{\alpha\alpha})$. In general, the calculated total friction is comparable in magnitude to the self intramolecular contribution, $D\beta\zeta_m(\omega_{\alpha\alpha})$. Moreover, the total intramolecular contribution, $D\beta\zeta_m(\omega_{\alpha,\gamma})$, is of the same order of magnitude of the intermolecular contribution, $D\beta\zeta_m(h_{\alpha,\gamma})$, but with the opposite sign, which is reasonable as the liquid is almost incompressible. This result shows that the conventional approximation of replacing the structure factor, $S_{\alpha,\gamma}(k)$, by the single chain analog, $\omega_{\alpha,\gamma}(k)$, can lead to errors in the evaluation of the memory function for macromolecular liquids.[107] The table also displays the value of the dimensionless friction coefficient $ND\beta\zeta_m$, which for unentangled systems should be ≈ 1. As expected, we see deviation from the unentangled behavior in the very short chains and in the crossover to entangled dynamics at $N \approx 100$.

V.3. Calculation of the Friction Coefficient of a Soft Colloid, ζ_{soft}

Starting from Eq.(IV.49) we calculated the friction coefficient, $D\beta\zeta_{soft}$, for polymer liquids represented as soft colloidal particles. Table V.3 shows the dimensionless friction coefficient for several systems. The molecular parameters, N and R_g, and the thermodynamic conditions of density ρ and temperature T, are taken from the UA MD simulations, see Table V.1. The

TABLE V.3. Soft-colloids friction coefficient contributions

System	$D\beta\zeta_{\text{soft}}^{\text{self}}$	$D\beta\zeta_{\text{soft}}(h^{cc})$	$D\beta\zeta_{\text{soft}}(1+h^{cc})$
PE 30	0.044273	-0.029932	0.014341
PE 44	0.020769	-0.012441	0.008328
PE 48	0.024639	-0.015289	0.009349
PE 66	0.012619	-0.006659	0.005960
PE 78	0.012019	-0.006254	0.005765
PE 96	0.008055	-0.003712	0.004344
PE 122	0.007423	-0.003334	0.004089
PE 142	0.006159	-0.002612	0.003546
PE 174	0.005218	-0.002108	0.003109
PE 224	0.004298	-0.001648	0.002650
PE 270	0.003660	-0.001351	0.002310
PE 320	0.003521	-0.001288	0.002233

dimensionless friction coefficient for these systems is $D\beta\zeta_{\text{soft}}(1+h^{cc}) \approx 0.002 - 0.01$, while we would expect $D\beta\zeta_{\text{soft}}(1+h^{cc}) \approx 1$ for unentangled systems, see Table V.3. These data show that the theoretically calculated friction coefficient (without rescaling) for the soft colloidal systems greatly underestimate the friction coefficient, as also observed in the MS MD simulations, and hence give rise to accelerated dynamics as discussed previously. It also shows that intra- and inter-molecular contributions to the friction coefficient are comparable in magnitude: both of them need to be taken into account when calculating dynamical properties of polymer melts.

V.4. Results from the Rescaling Procedure: Comparison with Simulation and Experimental Data

Some of the results reported in this section were already briefly presented in our short paper.[36] Our discussion here makes use of some of those data as a starting point to illustrate with an example the details of the proposed rescaling procedure and highlight its strengths and weaknesses.

In order to rescale the unrealistic fast dynamics of MS MD simulations we applied our rescaling procedure and compare the predicted dynamics with data from UA MD simulations and experiments. We use as input parameters the thermodynamic conditions and molecular parameters of each sample under study. The rescaling procedure is given by Eq.(IV.27), where D^{MS} is the diffusion coefficient from the MS-MD simulation, the soft colloid friction coefficient is calculated using Eq.(IV.49), and the monomer friction coefficient is given by Eq.(IV.44) for unentangled chains, and Eq.(V.5)with Eq.(IV.44) for entangled ones. Eq.(IV.27) depends on the temperature and density of the system investigated and on its molecular radius-of-gyration.

Indirectly those parameters enter our procedure through the diffusion coefficient from mesoscale simulations, D^{MS}. Specifically temperature enters through the rescaling of the time, as the time step in the mesoscale simulation is adimensional and becomes dimensional once it is rescaled by the energy, following a well-established procedure. Moreover, thermodynamic and molecular parameters enter indirectly through the soft potential, Eq.(V.1), which is parametric and includes density, temperature, and the molecular radius-of-gyration.

Finally, thermodynamic parameters enter directly through the definitions of the friction coefficients in the monomer and soft-sphere descriptions, Eqs.(IV.44) and (IV.49) respectively. Specifically, the monomer friction coefficient is a function of ρ, N, R_g, plus a hard sphere diameter, d, which is used to map the Lennard-Jones potential of the united atom simulation onto a repulsive hard-core potential with an effective bead diameter. The hard sphere diameter d is assumed to be independent of the thermodynamic conditions, for the range of temperature and density simulated here, and constant for all the monomers in the homopolymer chain. The criteria of choosing numerical value for d have been already explained and discussed.

In an analogous way, the soft-sphere friction coefficient depends on the chain number density, which relates to the monomer number density through N as $\rho_{ch} = \rho/N$, and R_g is the radius of gyration of the polymer chain. It also depends on the density fluctuation length scale ξ_ρ, which is expressed as a function of R_g and ρ_{ch} as $\xi_\rho = R_g/(\sqrt{2} + 2\pi\rho_{ch}R_g^3)$, and on the parameter $h_0 = h(k = 0) = -(1 - 2\xi_\rho^2/R_g^2)/\rho_{ch}$. In fact, the dimensionless combination $D\beta\zeta_{\text{soft}}$ is determined by only three parameters: ρ, N and R_g. In conclusion, once thermodynamic parameters, R_g and d are defined, there are no adjustable parameters in our method.

The predicted diffusion coefficients from our rescaled MS MD simulations are in good agreement with the data for all the test systems. As an example, Table V.4 displays the diffusion coefficients obtained directly from the MS MD, D^{MS}, once they are rescaled to include the internal degrees of freedom, and after the second rescaling of the friction, D_{cm}, as well as the values of the diffusion coefficient from the UA MD simulations, D^{UA}, against which we compare our predicted diffusion. The table shows that while the initial values of the diffusion are orders of magnitude larger than the data from UA MDs, the rescaled coefficients are very close to the real values. For the entangled systems we adopt the perturbative approach described in Section V.2 obtaining predicted values that are in quantitative agreement with the UA MD simulations. Entangled samples are from references,[3,65] and are mostly in the weakly entangled regime. For these samples the UA MD simulations include a small number of chains: $n = 40$ for $N = 78$, $n = 22$ for $N = 142$, $n = 32$ for $N = 174$, $N = 224$, $N = 270$ and $N = 320$, with n the number of chains in the simulation and N the degree of polymerization. These numbers show one advantage of adopting a coarse-grained description as typically our samples include thousands of chains. Simulating a large ensemble of molecules is necessary, for example, when the goal is to investigate large-scale fluctuations or the relative relevance of intra- vs inter-molecular contributions to the dynamics.

TABLE V.4. Diffusion coefficients in Å^2/ns from MS MD compared with UA MD simulation

System	T[K]	D^{MS}	D_{cm}	D^{UA}
PE 30	400	4.44×10^3	58.9	82.9
PE 44	400	5.29×10^3	44.5	46.0
PE 48	450	5.80×10^3	36.7	50.8
PE 66	448	6.04×10^3	29.0	31.8
PE 78	450	6.73×10^3	23.6	26.0
PE 96	448	6.98×10^3	21.9	23.3
PE 142	450	8.45×10^3	6.92	7.93
PE 174	450	8.51×10^3	4.53	5.70
PE 224	450	8.80×10^3	2.73	3.28
PE 270	450	9.39×10^3	2.14	2.06
PE 320	450	8.73×10^3	1.03	1.30

Figure V.3 illustrates how our approach can be used to calculate dynamics also in the short time regime. The figure shows the mean-square-displacement of the center-of-mass from UA MD in comparison with the one calculated from the diffusion coefficient rescaled from the MS MD. The agreement is quantitative in the long time regime. In the short time regime, the UA MD simulation data exhibit a subdiffusive behavior, even if polymers are unentangled. In a series of papers we have shown that the subdiffusive regime is a consequence of the presence of cooperative dynamics involving several polymer chains moving in a correlated way inside the dynamically heterogeneous liquid of macromolecules.[92,95] A detailed discussion of this phenomenon, which is of intermolecular origin, has been provided before and will not be repeated here. Our theory, the Cooperative Dynamics Generalized Langevin Equation (CD-GLE), needs as an input the diffusion

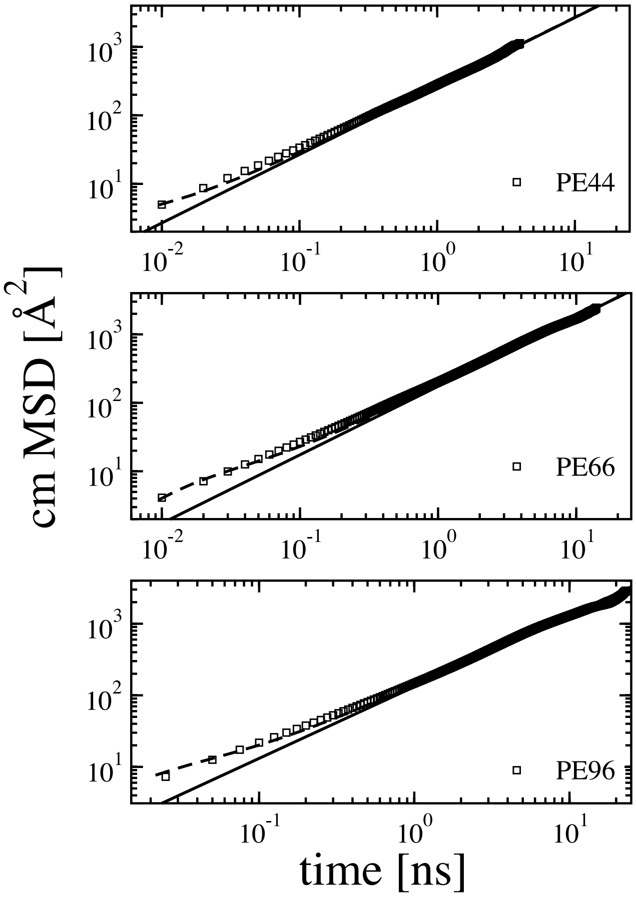

FIGURE V.3. Plot of mean-square displacement as a function of time for unentangled PE melts. The rescaled MS MD simulation (line) is compared with UA MD simulation (symbols) for $N = 44, 66, 96$. Also shown is the outcome of the theory for cooperative dynamics (dashed lines).

coefficient and predicts the subdiffusive behavior for times shorter than the longest correlation time as a function of the number, $n' \propto \sqrt{N}$, of macromolecular chains moving in a cooperative way. Figure V.3 shows the results from our CD-GLE calculations as dashed lines. Here, the input monomer friction coefficient is calculated from MS MD using the rescaling procedure. The number of chains undergoing cooperative dynamics is $n' = 30$ for $N = 96$, $n' = 25$ for $N = 66$, and $n' = 14$ for $N = 44$.

The subdiffusive behavior shown in UA-MD data is not visible in the rescaled MS MD data as the dynamics are accelerated. The effective temperature experienced by the polymer is much higher than the temperature in UA MD simulations as the energy is not dissipated in the internal degrees of freedom.

Finally we discuss the calculations of the monomer and soft-colloid friction coefficients for a set of polyethylene chains investigated experimentally.[26,86–89] The experimental data do not report the values of R_g at the desired thermodynamic conditions, $T = 509$ K and density $\rho = 0.0315302$ sites/Å^3, while it is known that the chain conformation, and R_g, are temperature dependent. To calculate the input parameters for our MS MD simulations we adopt a freely rotating chain model, for which the mean-square end-to-end polymer distance is given by[100]

$$\left\langle R_{ete}^2 \right\rangle = Nl^2 \left[\frac{1+g}{1-g} - \frac{2g}{N} \frac{1-g^N}{(1-g)^2} \right] \ , \tag{V.6}$$

and $R_g^2 \approx \left\langle R_{ete}^2 \right\rangle /6$ for a chain with Gaussian statistics. For polyethylene melts at this temperature and density the stiffness parameter is $g = 0.785$.[26]

The values of the monomer and soft-colloid friction coefficients for the experimental samples, calculated from Eqs.(IV.44) and (IV.49) respectively, are presented in Table V.5. The Table shows the large difference between the predicted dimensionless friction coefficients, $D\beta\zeta_{soft}$ and $ND\beta\zeta_m$, for the same macromolecule coarse-grained at two different length scales. From the values displayed in Table V.5 we calculate the rescaling factor for the friction coefficient measured in MS MD simulations, following the procedure described in this communication. Because the data have different thermodynamic parameters of density and temperature, their scaling behavior cannot be inferred from their plot, even if an apparent N^{-1} scaling is followed by the unentangled samples and the typical reptation N^{-2} scaling by the entangled ones.

TABLE V.5. Theoretically calculated dimensionless friction coefficient for monomer ($d = 2.1$Å) and soft colloid with R_g^{FRC} for experimental samples

System	$(R_g^{FRC})^2$[Å^2]	$D\beta\zeta_{soft}$	$ND\beta\zeta_m$
PE 36	101.4350	0.007846	0.5153
PE 72	219.5710	0.004927	0.8946
PE 106	331.1465	0.004543	1.8407
PE 130	409.9056	0.003497	1.5354
PE 143	452.5669	0.003318	1.6822
PE 192	613.3669	0.002828	2.2412
PE 242	777.4485	0.002500	2.8186

$T = 509$K, $\rho = 0.0315302$ [sites/Å^3]

TABLE V.6. Predicted diffusion coefficients in Å^2/ns from MS MD and experimental data from Refs.[26, 86–89]

System	PE36	PE72	PE106	PE130	PE143	PE192	PE242
D_{cm}	111	50	23	14	11	5.6	3.2
D^{exp}	120	41	14	12	8.6	6.5	4.5

V.5. Theoretical Predictions of Diffusion Coefficients for Polyethylene Samples

In this section we report theoretical predictions from rescaled mesoscale simulations of the diffusion coefficients for a series of PE samples for which data of chain dynamics, either from simulations or from experiments, are not available in the literature. The degree of polymerization of each sample is not larger than the ones already investigated. However, because there are no data to fit any parameter, these calculations illustrate the predictive power of our method. Diffusion coefficients calculated by combining the mesoscale simulations with the rescaling procedure presented in this manuscript, are displayed in Figure V.4 as a function of the degree of polymerization (triangles down).

MS MD simulations are performed for $N = 44, 60, 80, 100, 200, 300, 400, 500$ and $1,000$, at constant monomer density $\rho_m = 0.0323951$ [sites/Å^3] and temperature $T = 400\ K$. The value of R_g at increasing N is calculated using a freely rotating chain model with the stiffness parameter from the UA MD data for PE44 (see Table V.1). The hard sphere diameter is fixed to the value reported in the previous sections for PE, $d = 2.1$Å, and the pair distribution function at contact is $g(0) = 1/2$ as described early on in this communication. While the simulations of

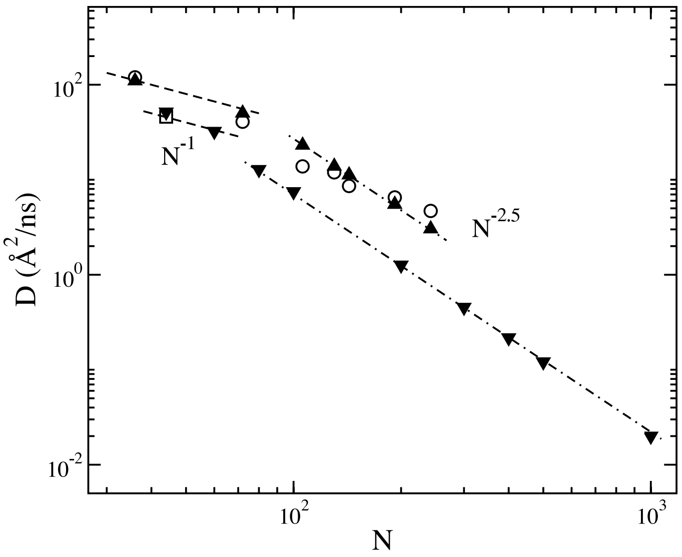

FIGURE V.4. Plot of diffusion coefficients as a function of degree of polymerization, N. The rescaled results from MS MD simulations at $\rho_m = 0.0324$ sites/Å^3 and $T = 400$K (triangles down) are compared with simulations data for $N = 44$ (square). Also reported are MS-MD data at $\rho_m = 0.0315$ sites/Å^3 and $T = 509$K (triangles up) which match the experimental data (circles) from Ref.[26] The scaling exponents for unentangled, N^{-1} (dashed line), and entangled dynamics, $N^{-2.5}$ (dot-dashed line) are also displayed.

the small samples can be performed on a single CPU machine, for systems with a higher degree of polymerization is convenient to adopt parallel computing. For those systems, simulations were run using the LAMMPS code,[108] with our potential as an input, remotely on a 64 CPU machine available through the TeraGrid.[109] The simulation for the PE1000 sample included 46,656 molecules and required about 2 days of computer time. By comparison with our single CPU calculations, running the simulation in parallel reduces the computer time by a factor of 10^2. The number of particles in the simulation is determined by the length of the box size, which for the PE1000 sample is equal to 22 R_g, i.e. larger than twice the range of the potential, to eliminate molecular self-interaction through the periodic boundary conditions.

While we assume that small changes of density and temperature do not affect the hard-core diameter, d, even a small difference in ρ_m can noticeably change the prefactor in Eq.(IV.27). The monomer friction coefficient is calculated using Eq.(IV.44) for unentangled systems and Eq.(V.5) for entangled ones.

In conclusion, the data set just discussed (triangles down in Figure V.4) is for samples at $\rho_m = 0.0324$ sites/Å^3 and $T = 400$K. Here the semiflexibility parameter and bond length are calculated from the radius-of-gyration of the $N = 44$ sample measured in UA MD simulations. All the other data at increasing N are predicted while keeping the semiflexibility parameter and the bond length constant in the freely-rotating-chain expression, as discussed above.

Moreover, Figure V.4 displays data from a second set of MS MD simulations (triangles up) performed at $\rho_m = 0.0315$ sites/Å^3 and $T = 509$ K and increasing N. This set of simulations, rescaled with our method, quantitatively reproduces the experimental data (circles) reported in Ref.[26] Note that the value of D reported here for $N = 106$ is slightly different than the one reported in our previous paper,[36] which was incorrectly calculated. All the other points are identical to the ones reported previously.[36] The predicted values of the diffusion coefficient appear to be consistent with the known experimental behavior.

Finally, if we assume that the change in diffusion coefficient from one set, with $\rho_m = 0.0324$ sites/Å^3 and $T = 400$K, to the other, with $\rho_m = 0.0315$ sites/Å^3 and $T = 509$K, is mostly due to the difference in temperature, the behavior illustrated in Figure V.4 is consistent in the entangled regime with the analysis performed in Ref.[110] The diffusion coefficients of unentangled chains follow the scaling behavior of the Rouse approach, while the entangled chains show a scaling with degree of polymerization of -2.5. Although the latter scaling exponent disagrees with the "reptation model", it is known that experimental samples of weakly entangled chains also show a scaling exponent of -2.5. For those polymer chains, which are just across the transition from unentangled to entangled dynamics, constraint release and "tube" fluctuations are relevant. The observed scaling behavior is also consistent with the scaling of the viscosity observed experimentally.[111] The advantage of our method with respect to UA-MD simulations is that even in the case of long entangled chains it is possible to include a large number of molecules, improving the statistics of calculated correlation functions. Overall this plot shows that it is possible to provide reasonable predictions of large scale dynamical properties by properly rescaling mesoscale simulations.

V.6. Conclusion

The need for developing a fundamental approach to rescale dynamical data obtained from MS simulations of coarse-grained systems has been a long-standing problem from the time that coarse-graining approaches started being developed. Because MS simulations are less computational demanding than atomistic simulations, it is possible to investigate larger systems for longer times than in all-atom simulations, allowing one to extend the maximum time and length scales accessible through simulations and to improve the statistics of measured averaged quantities. Considering that the number of particles in a simulation should be large enough to ensure proximity to the thermodynamic limit, MS simulations of coarse-grained systems could become an indispensable tool to investigate the structure and dynamics of macromolecular liquids.

One advantage of a MS simulation of a coarse-grained system is that the simulation speeds up because of the averaging of the internal degrees of freedom, leading to a softer potential and allowing the study of longer timescales than in a fully atomistic simulation. This implies, however, that the dynamical properties resulting from the MS MD are faster than their real counterpart, for example the ones from UA MD and need to be rescaled.

It is the common procedure to rescale the measured dynamics numerically by bringing a time correlation function to agree with the one measured in atomic level simulations, however we adopt a different strategy. We have proposed a first principle approach to derive an analytical form of the rescaling procedure to be applied to the dynamics measured directly from MS MD of a coarse-grained polymer liquid. Our approach allows for the reliable prediction of the long-time diffusion of a polymer melt as it would be measured in an atomistic or UA-MD simulation. The rescaling procedure has been tested so far against simulations and experiments of polyethylene liquids both unentangled and entangled. Calculated diffusion coefficients for samples for which we do not have data either experimental or simulated, show consistent behavior.

We start by running MS MD simulations of coarse-grained polyethylene melts where each polymer is represented as a point particle. The analytical intermolecular potential, input to the MS MD, is derived from the Ornstein-Zernike equation with the hypernetted closure approximation. The correction term to the measured dynamics of the MS MD simulations, is calculated from the solution of the Generalized Langevin Equations written for the coarse-grained and for the monomer-level representations of the macromolecular liquid. Those equations are formally derived from the Liouville equation by assuming two different length scales characterizing the relevant slow dynamics, i.e. monomer and center-of-mass, onto which the Liouville equation is projected.

While the Mori-Zwanzig projection operator technique suggests a reliable criteria to select the proper length scale of coarse-graining for dynamical properties, the GLEs thus generated allow one to derive analytical forms of the rescaling contributions associated with the coarse-grained dynamical equations. The rescaling procedure includes two contributions, given by the changes in entropy and in the friction coefficient during coarse-graining. The entropic contribution emerges from the averaging of the internal degrees of freedom, while the friction is due to the change in shape, and as a consequence the change of the molecular surface exposed to the surrounding molecules. Both corrections depend on the thermodynamic conditions of the system simulated, and on the molecular structure through the radius-of-gyration of the macromolecule. Thermodynamic and molecular quantities enter both directly through the rescaling equations and indirectly through the effective potential in the mesoscale simulations. In this way the dynamics predicted from the rescaling of each mesoscale simulation is specific of the system under study.

A feature of the coarse-graining models we study is the mapping of the polymeric liquid onto simple representations, which are isotropic. At the molecular level the polymer is described as a soft isotropic sphere. At the monomer level, the bead-and spring description affords equivalent beads in the chain, which is a reliable approximation due to the high number of statistically equivalent structural configuration of the molecule. Chain end effects enter in the model through the finite size of the polymer in the matrix representation of the equations. Moreover, because the monomers in a homopolymer are structurally identical, with the exception of the two end monomers, the intermolecular monomer-monomer hard-core interaction potential is assumed to be identical for any pair of monomers, and each monomer is supposed to have identical friction coefficient.

Although the theoretical picture is straightforward, our approach has the advantage of being described in closed-form expressions, even if approximated, which allows for an analytical solution of the rescaling formalism. This has the potential of being useful in improving our understanding of the nature of coarse-graining procedures.

CHAPTER VI

RECONSTRUCTION OF GLOBAL AND LOCAL DYNAMICS FROM COARSE-GRAINED SIMULATIONS AND COOPERATIVE DYNAMICS THEORY

In Chapter VI the dynamical rescaling procedure we developed in Chapter IV is applied to polymer with different monomeric chemical structure. The dynamical data obtained from mesoscale molecular dynamic simulations of polymer liquids is scaled down to its realistic values in the atomistic description. The rescaling formalism accounts for the change in entropy and change in friction that are a consequence of the coarse-graining of the polymeric structure. The rescaled diffusion coefficient obtained from mesoscale simulations of coarse-grained *cis*-1,4-Polybutadiene melts shows good agreement with data from united atom simulations performed by Tsolou et al. The derived monomer friction coefficient is used in calculations of the internal polymer dynamics performed by means of the theory of cooperative dynamics. Theoretically predicted time correlation functions show good agreement with simulations in the whole range of length and time scales in which simulation data are available. Predictions for new data for which atomistic level simulations are not available are also presented.

VI.1. Introduction

Computer simulations of macromolecular liquids described at the atomistic level are extremely useful because they bridge information between the microscopic molecular structure of the polymeric system, at the given thermodynamic conditions, and its macroscopic properties, such as viscosity, diffusion, and dynamical-mechanical response, which are observed experimentally. Unfortunately, the study of the dynamics of polymeric liquids by atomistic computer simulations is limited by the impossibility of reproducing with accuracy the dynamics in the wide range of time and length scales relevant for samples of long polymeric chains, despite the tremendous progress already occurred in the development of novel computational hardware and software. It is known that long simulation trajectories deteriorate with time, following a law defined by the Lyapunov exponent characteristic of the system, and the resulting long-time dynamics is affected by errors.

Atomistic simulations of polymeric liquids are limited either in the length of the macromolecular system, or in the maximum timescale that can be reached. Unfortunately the long timescale is a regime of great interest for the physics of macromolecular liquids, because of the relevance of dynamical-mechanical properties of macromolecules in that regime for their industrial applications. Because the limitation concerns only the region of long-time, large-scale properties, it is possible to shift the focus of a simulation to this region of interest by the reduction of the simulated degrees of freedom through the averaging of local scale properties, i.e adopting a so-called "coarse-graining" procedure.

While simulations of coarse-grained systems afford to represent larger length and longer time-scales than atomistic simulations, they also are marred by the shortcoming that the measured dynamics is unphysically fast. This is the advantage that allows one to perform simulations in the long-time regime, but it is also a problem because the dynamics in the simulation becomes too fast and it is unreliable. Depending on the level of coarse-graining the dynamics can become even orders of magnitude faster than the atomistic dynamics. Being aware that the dynamics has to be rescaled to recover the correct timescale, one resorts to the most conventional method, which is to build a calibration curve calculated by superimposing the long-time dynamics of the coarse-grained and atomistic simulations. The hope is for this calibration curve to be transferable to other systems, or to be identical, and so applicable, for thermodynamic conditions close to, but different from the phase point for which the curve was optimized in the first place. Otherwise, if an atomistic simulation has to be ran every time we need to rescale a coarse-grained simulation there is no advantage in running simulations of coarse-grained (CG) systems. Moreover the mesoscale simulation of the coarse-grained system is supposed to reach timescales longer than the atomistic simulation. However, if a calibration curve has to be derived by running atomistic simulations, then the whole procedure defeats its purpose.

Recently we have proposed an original procedure to rescale the dynamics measured in simulations of coarse-grained polymer melts.[112, 113] The procedure we proposed does not require to run atomistic simulations to calibrate the dynamics of the coarse-grained simulation. Once one parameter, specifically the diameter of the hard-core monomer potential, is fixed the rescaling factors are fully determined. The advantage of this method is clear, given that the coarse-grained simulation can reach larger-scale longer-time properties than the atomistic simulation. Because no atomistic simulations are needed, the measured dynamics can be directly rescaled to obtain the dynamics of the real system we wanted to study.

The method has been formally derived, and then applied to systems of polyethylene (PE) melts. The choice of PE as a test system was motivated by the wealth of experimental and simulation data available in the literature. We have shown that the proposed theory is able to predict diffusion coefficients in agreement with both atomistic simulations and experiments for systems in the unentangled and in the entangled regimes, and for a range of temperatures and densities. One of the questions that still needed to be answered was if our method was able to generate high quality predictions also for macromolecular liquids with a more complex monomeric structure than the simple polyethylene. A first study of this issue is presented in this manuscript which investigates the agreement between theoretically predicted diffusion coefficients for polybutadiene (PB) chains and data from molecular dynamics simulations performed by Tsolou, Mavrantzas and coworkers.[114–116]

Our rescaling method considers two contributions emeging from the consequence of applying the coarse-graining process and derives the theoretical corrections that need to be applied to the dynamics of the coarse-grained description to recover the modalities of the original atomistic system. The first correction emerges from the consideration that due to the process of averaging the intramolecular degrees of freedom, the coarse-grained system experiences a change in its energy, because a number of local states are neglected. While the atomistic system devotes time to explore local configurations, the coarse-grained system doesn't. To recover the correct dynamics those states need to be included *a posteriori* in the form of an entropic contribution to the free energy that rescales the time measured in the CG simulations.

The second correction comes from the change of the "shape" of the molecule once it is coarse-grained. Macromolecules described at the atomistic level become represented by chains of effective atoms, or as bead-and-springs, chains of soft blobs, or even each molecule as a soft sphere. In all these multiple forms the surface of each molecule available to the surrounding molecules, i.e. the "solvent", is different. The hydrodynamic radius, r_{hydr}, of the coarse-grained unit in each description is different and so is its friction coefficient, ζ, defined by Stokes' law as $\zeta = 6\pi\eta_s r_{hydr}$, where η_s is the viscosity of the medium. By solving the memory function for the friction coefficient in each description we are able to calculate the correction factor that has to be applied to each friction coefficient to recover the description at a different level of coarse-graining.

In this communication our rescaling method is first briefly summarized and then applied to study the dynamics of cis-1,4-PB and compared with simulation data by Tsolou et.al.[68] who also investigated the effect of temperature and pressure on the simulations.[115] Other data are contained in a paper where UA MD simulations of melts in the entangled regime was performed to quantify reptation parameters and compare them with the tube model.[116] In that paper primitive path analysis was applied to three different polymer melts: PE (up to C_{500}), cis-1,4-PB (up to C_{800}), and trans-1,4-PB (up to C_{400}).

VI.2. Rescaling of the Free-Energy and Rescaling of the Friction

In this section we briefly present an overview of the main steps in our procedure. A complete and detailed presentation of the same has been already published[112, 113] and will not be repeated here. We start from the consideration that the procedure of coarse-graining corresponds to eliminating some internal degrees of freedom, by combining groups of atoms into one effective CG unit. Specifically, our rescaling theory has been developed for an extended level of coarse-graining as intramolecular coordinates are fully averaged out and the polymer is represented as an isotropic sphere centered on the center-of-mass (com) of the macromolecule. There are some advantages in the choice of this description. First, the CG representation is fully isotropic, and even if it is known that the shape of a polymer is closer to an ellipsoid than to a sphere,[117] the total correlation function of the polymeric liquid, i.e. the structure of the polymeric liquid, is well reproduced by this model; second the formalism is analytical, which allows us to derive formally many of the physical quantities of interest for both the static and the dynamic properties of the coarse-grained system as a function of the atomistic description; third all the consequences of the coarse-graining procedure are enhanced with this extreme level of coarse-graining and are easier to study in such a description. If the procedure adopted is not precise, its negative effects would be maximized in this coarse-gained description: the fact that the theory, which is predictive, is found to be in quantitative agreement with both simulated and experimental data is encouraging.

In every CG model, the averaging of the intramolecular degrees of freedom leads to a speeding up of the dynamics. When a polymer is represented as a soft sphere the dynamics in the mesoscopic simulation (MS) is orders of magnitude faster than in the atomistic description. One of the reasons for this acceleration is the fact that while a macromolecule needs to explore a large number of internal chain configurations for each position of the center-of-mass, the soft sphere instead is free to move in the three-dimensional space. To take into account this contribution the time measured in the mesoscale simulation of the soft sphere is multiplied by a rescaling factor that is calculated as the ratio of the energy due to the internal degrees of freedom in the two representations, i.e a chain of beads and a soft sphere.

From the definition of the internal energy for a simple bead-and-spring model and for a soft sphere, the correction term is calculated. The dimensionless simulation time, $\tilde{t}$, from mesoscale (MS) simulations is rescaled according to

$$t = \tilde{t} R_g \sqrt{\frac{m}{k_B T} \frac{3}{2} N} \ , \tag{VI.1}$$

where m is particle mass and $R_g = \sqrt{N/6} l$ is the radius-of-gyration of the molecules, i.e. its characteristic size. The internal degree-of-freedom averaged out in the coarse-grained description are accounted for by introducing the $\frac{3}{2}N$ factor.

The second rescaling is due to the change in the shape of the molecule represented in the two levels of coarse-graining, and so the effective friction in the two representations. In the long time the com mean-square displacement is related to the molecular diffusion coefficient as

$$\langle \Delta R^2(t) \rangle = 6 \, D \, t \ , \tag{VI.2}$$

where $D = k_B T/(N \zeta_m)$ is the diffusion coefficient of the system, which has to be calculated. If we use as a starting point the diffusion coefficient measured in the mesoscale simulation $D^{MS} = k_B T/\zeta_{soft}$, the rescaled diffusion coefficient is simply given by

$$\langle \Delta R^2(t) \rangle = 6 \, D^{MS} \frac{\zeta_{\text{soft}}}{N \zeta_m} \, t \ , \tag{VI.3}$$

where the problem reduces to the calculation of the friction coefficient in the monomer and soft-sphere representations. The friction coefficients are calculated from the solution of the memory function in the two representations (bead-and-spring and soft-sphere).

For a bead-and-spring model the friction is given by:

$$\zeta_m \cong \frac{1}{N} \sum_{a,b=1}^{N} \int_0^{\infty} d\tau \Gamma_{a,b}(\tau) \ . \tag{VI.4}$$

where the memory function is defined as[118]

$$\Gamma_{a,b}(t) \cong \frac{\beta}{3}\rho \int d\mathbf{r} \int d\mathbf{r}' g(r) g(r') F(r) F(r') \, \hat{\mathbf{r}} \cdot \hat{\mathbf{r}}' \int d\mathbf{R} \, S^{Q}_{a,b}(R;t) S^{Q}(|\mathbf{r} - \mathbf{r}' + \mathbf{R}|;t) \, . \tag{VI.5}$$

$S^Q(r,t)$ is the dynamic structure factor, which includes both intra- and inter-molecular contributions, i.e. incoherent and coherent scattering. This function is assumed to decay with the same diffusion coefficient in the long-time bead-and-spring model, when all internal dynamics are fully relaxed, and in the soft-sphere representation, where there is no internal dynamics. As a consequence, in the ratio of the two frictions, the term containing the diffusive decay of $S^Q(r,t)$ is simplified and does not appear in the final solution.

In Eq.(VI.5) $g(r)$ is the pair distribution function of the molecular liquid, and $F(r)$ is the force due to the effective potential, obtained from the solution of the Ornstein-Zernike equation by applying the Percus Yevick closure. The monomer potential, which in the atomistic-level simulation is a Lennard-Jones potential, is here approximated by an effective hard-sphere with an effective diameter, d, to mimic the properties of the L-J potential. All the physical quantities that appear in the equation are known and the analytical expression for the monomer friction is[113]

$$
\begin{aligned}
\zeta_m \approx\ & \frac{2}{3}(D\beta)^{-1}\rho g^2(d)\Bigg(\frac{1}{12}\pi N^2 d^2 R_g\left[15\sqrt{2}+40\frac{d}{R_g}+12\sqrt{2}\left(\frac{d}{R_g}\right)^2\right]+ \\
& \rho\pi N h_0\frac{1}{3\sqrt{2}(R_g^2-2\xi_\rho^2)^2}\Bigg[12\sqrt{2}\xi_\rho^7+12d^4R_g^3\left(1-2\left(\frac{\xi_\rho}{R_g}\right)^2\right)+ \\
& 4\sqrt{2}d^3R_g^4\left(5-14\left(\frac{\xi_\rho}{R_g}\right)^2+2\left(\frac{\xi_\rho}{R_g}\right)^4\right)+3d^2R_g^5\left(5-14\left(\frac{\xi_\rho}{R_g}\right)^2-4\sqrt{2}\left(\frac{\xi_\rho}{R_g}\right)^5\right) \\
& -12\sqrt{2}e^{-\frac{2d}{\xi_\rho}}\xi_\rho^7\left(1+\frac{d}{\xi_\rho}\right)^2\Bigg]+\rho^2\pi h_0^2\frac{1}{12(R_g^2-2\xi_\rho^2)^3}\Bigg[40d^3R_g^6+15\sqrt{2}d^2R_g^7 \\
& -24\sqrt{2}d^4R_g^3\xi_\rho^2-144d^3R_g^4\xi_\rho^2+6\sqrt{2}d^4R_g^5\left(2-9\left(\frac{\xi_\rho}{d}\right)^2\right)+ \\
& 12R_g^2\xi_\rho^7\left(4\left(\frac{d}{\xi_\rho}\right)^3-7\left(\frac{d}{\xi_\rho}\right)^2+9\right)-8\xi_\rho^9\left(4\left(\frac{d}{\xi_\rho}\right)^3-9\left(\frac{d}{\xi_\rho}\right)^2+15\right)- \\
& e^{-\frac{2d}{\xi_\rho}}12\xi_\rho^4(d+\xi_\rho)\left(R_g^2(d+3\xi_\rho)(2d+3\xi_\rho)-2\xi_\rho^2(2d^2+5\xi_\rho d+5\xi_\rho^2)\right)\Bigg]\Bigg)\ .
\end{aligned}
\tag{VI.6}
$$

This equation contains quantities that are well defined once the system of interest is selected. For example ρ is the monomer density, R_g is the polymer radius of gyration, N is the degree of polymerization, $g(d)$ is the pair distribution function at contact, $\xi_\rho = R_g/(\sqrt{2}+2\pi R_g^3\rho/N)$ is the density fluctuation correlation length, and h_0 is defined as $h_0 = h(k=0) = -(1-2\xi_\rho^2/R_g^2)/\rho_{ch}$. The only physical quantity that needs to be determined is the hard-sphere diameter, d. This is defined once the Lennard-Jones potential is mapped onto an effective repulsive hard-sphere system as described later in this section of the communication.

In the soft colloidal representation, the friction coefficient is analytically calculated from the definition of the memory function as

$$
\zeta_{\text{soft}} \cong (\beta/3)\ \rho_{ch}\int_0^\infty d\,t\ \int d\mathbf{r}\int d\mathbf{r}' g(r)g(r')F(r)F(r')\,\hat{\mathbf{r}}\cdot\hat{\mathbf{r}}'\int d\mathbf{R}\,S(R;t)S(|\mathbf{r}-\mathbf{r}'+\mathbf{R}|;t)\,, \tag{VI.7}
$$

where $\rho_{ch} = \rho/N$ is the chain density. All the other physical quantities that appear in the integral, for example the pair distribution function, $g(r)$, and the related force, $F(r)$, are the analogous of the one's appearing in the monomer friction definition, but defined here for the soft sphere description. Because the OZ equation is solved analytically in this representation, each quantity is formally defined.[8]

The regime of interest in our calculations is the diffusive limit where $k \ll 1/R_g$ in reciprocal space. Here the dynamic structure factor can be approximated as

$$S(k;t) \approx S(k)\ e^{-Dtk^2} = (1 + \rho_{ch} h^{cc}(k))\ e^{-Dtk^2}\ , \tag{VI.8}$$

with the total correlation function at the center of mass level given in the limit of long chains ($N \geq 30$) by the approximated expression[8]

$$h^{cc}(r) \approx -\frac{39}{16}\sqrt{\frac{3}{\pi}}\frac{\xi_\rho}{R_g}\left(1 + \sqrt{2}\frac{\xi_\rho}{R_g}\right)\left(1 - \frac{9r^2}{26R_g^2}\right)e^{-\frac{3r^2}{4R_g^2}}\ . \tag{VI.9}$$

The resulting expression for soft particle friction is[113]

$$\zeta_{\mathrm{soft}} \cong 4\sqrt{\pi}(D\beta)^{-1}\rho_{ch}R_g\xi_\rho^2\left(1 + \frac{\sqrt{2}\xi_\rho}{R_g}\right)^2\frac{507}{512}\left[\sqrt{\frac{3}{2}} + \frac{1183}{507}\rho_{ch}h_0 + \frac{679\sqrt{3}}{1024}\rho_{ch}^2h_0^2\right]\ , \tag{VI.10}$$

where the value of each physical parameter that enters this equation is defined once the system to simulate is selected. In this way these parameters are identical to the ones that are input to the monomer friction Eq.(VI.6).

When the two equations for the monomer and the soft colloidal friction coefficients are introduced in Eq.(VI.3) the com diffusion coefficient for the chain described as a bead-and-spring is recovered as $D = D^{MS}\zeta_{soft}/(\zeta m R_g\sqrt{3mN/(2k_BT)})$.

The relaxation of the dynamic structure factor in the two CG descriptions for the long-time, large-scale regime is assumed not to depend on the level of coarse-graining. The only parameter that needs to be defined is the value of the effective hard sphere diameter needed to map correctly the properties of the bead-and-spring chain onto a chain of hard-spheres of dimension d. To evaluate the value of d we analyze the dimensionless quantity $D\zeta_m/(k_BT)$, which is identical to N^{-1} if the chain obeys strictly Rouse dynamics in the long-time limit. To fulfill this requirement the chain has to have N smaller than the entanglement degree-of-polymerization N_e and longer than the value of N for which chains start to obey Gaussian statistics, i.e. the central limit theorem applies. Figure VI.1 a) displays the dimensionless friction $D\beta\zeta_m$ from Eq.(VI.6) as a function of hard sphere diameter, d, for PB samples of increasing degree of polymerization. The parameter values (ρ_m, T, N, R_g) are chosen to match those of UA MD simulations in ref.[68]

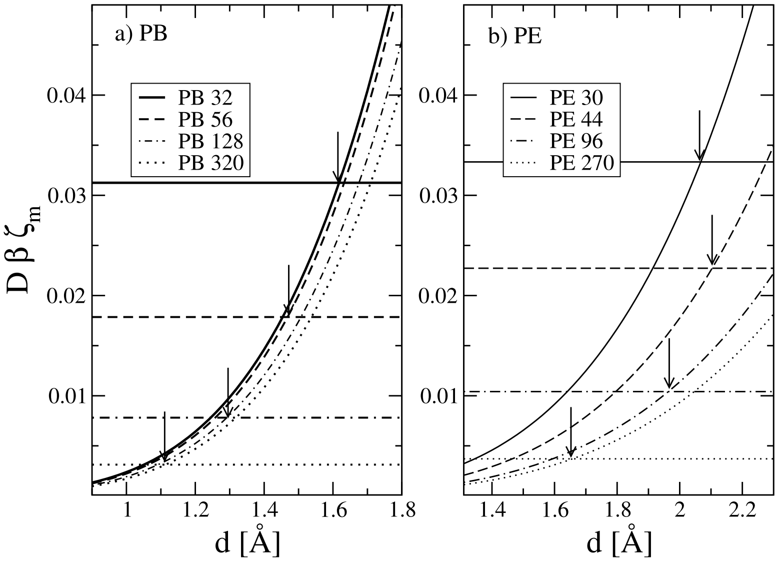

FIGURE VI.1. Dimensionless monomer friction coefficient as a function of hard sphere diameter.

Horizontal lines represent the $1/N$ value for each sample, which is the Rouse value of the physical quantity $D\beta\zeta_m = 1/N$ in the diffusive regime, and reproduces the scaling behavior of the diffusion for unentangled, short-chains. For comparison Figure VI.1 b) displays the analogous plot for the PE samples, which is reproduced from refs.[112] and.[113] It is seen from the Figure VI.1 that d chosen according to the criterion of $D\beta\zeta_m = 1/N$ is decreasing with increasing N. In order to obtain the realistic value of d from condition $D\beta\zeta_m = 1/N$, we need to choose a sample which corresponds to the unentangled state. On the other hand the chain length of the sample should be long enough to obey Gaussian statistics in the monomer distribution, which is one of the basic assumptions used in the theoretical calculations. Under fixed thermodynamic conditions, the value of d should depend only on the local monomer structure, and should be independent of the degree of polymerization. Therefore, once the value of d is chosen for the sample which satisfies the criteria mentioned above, this value is kept fixed for all samples with different molecular weights. In fact the change of d with N observed in Figure VI.1 is a consequence of two different effects: for short chains, end effects are important, while for long chains the crossover to entangled dynamics starts to be important. In this way, it could be argued that in the method described above the actual fitting parameter is not d, but the length of the chosen sample for which d is determined. Clearly when entangled chain are forced to behave according to the Rouse expression the hard sphere diameter needs to be artificially decreased in order to compensate the overlooked increase in the monomer friction, which is associated with entanglement effects growing with increasing N. Whereas the range of lengths in the unentangled region is rather wide, it is always possible to choose the chain length knowing experimentally measured or theoretically estimated value of N_e (for example[119]) and as the low N limit the length of $N = 30$ for which the bead distribution starts following Gaussian statistics. It is important to notice that even if there is some freedom in choosing the reference sample, the deviations of d from the chosen value is not large.

In our previous study of PE melts we fixed the hard sphere diameter following the same procedure and selecting a sample with $N = 44$. The obtained value of $d = 2.1\text{Å}$ (see Figure VI.1b), was larger than the carbon-carbon bond length $l_b = 1.54\text{Å}$, but smaller than the Lennard-Jones parameter $\sigma \simeq 3.9\text{Å}$ typically used in UA MD simulations, which seems to be a reasonable choice of the parameter. Compared to PE, PB chains are more flexible and so they are less entangled. The estimated entanglement degree-of-polymerization, N_e, is calculated from the generalized formula for the plateau value in the shear relaxation modulus,[119] which gives $N_e \simeq 330$ backbone carbon atoms for PB, compared to $N_e \simeq 55$ for PE. Also, as it will be shown later that the onset of the crossover regime to entangled dynamics in the center of mass mean squared displacement occurs at $N \approx 200$ for PB (usually about 120 for PE). Considering the broader range of unentangled PB chains, we select for the calculation of the hard sphere diameter the PB sample with $N = 56$. The obtained value of $d \simeq 1.47\text{Å}$ (which is smaller than the value for PE of 2.1Å given the flexibility of PB) is consistent with the fact that in PB chains half of the carbon bonds are shorter double bond and $l_{db} = 1.34\text{Å}$.

VI.3. Theoretical Predictions of Center-of-Mass Diffusion

The solution of Eq.(VI.3) gives the diffusion coefficient for the center-of-mass of a polymer described at the atomistic level, having as an input the diffusion coefficient calculated from the mesoscale simulation of the CG polymer liquid. The purpose of this procedure is to have ultimately mesoscale simulations that, once properly rescaled, can provide directly the diffusion coefficient, without need of running atomistic simulations. To test our procedure we first run the mesoscale simulations, then we rescale the diffusion coefficient, and finally we compare the theoretical predictions against atomistic simulations and/or experiments. Thermodynamic and molecular parameters entering our equations have to be consistent with the parameters of the system against which we compare our approach.

In this communication we study the dynamics of cis-1,4-Polybutadiene (PB) melts of increasing degree of polymerization and compare our results with the data from the simulations performed by Tsolou et al.[68] The input parameters are displayed in Table VI.1, including the degree-of-polymerization, N, the monomer density ρ, and the mean-square-radius-of-gyration $\left\langle R_g^2 \right\rangle^{UA}$. Note that in the rest of this communication for convenience we will use the term monomer not in its usual meaning but to identify the CH_x group, where $x = 1$, 2 or 3.

The simulations were performed in the NPT ensemble, at the constant pressure, P, and temperature, T, reported in the table. Also reported are the freely rotating chain semi-flexibility parameter, which does not enter the equation, but it is used in calculations reported in the last section of this communication. Note that the values of R_g for systems PB160, PB200, PB240 were corrected from 257 to 275, from 304Å^2 to 340Å^2 and from 401 to 410 correspondingly, after consultation with the authors of ref.[68] The corrections of the typos was motivated by the inconsistency observed when the calculation of R_g is performed using a standard model, such as the Freely-Rotating-Chain, described later on in this communication.

TABLE VI.1. Simulation parameters for 1,4-cis PB chains of increasing lengths.

System	ρ[sites/Å^3]	$\left\langle R_g^2 \right\rangle^{UA}$[Å^2]	g
PB 32	0.0352375	45±5	0.6237
PB 48	0.0363767	70±5	0.6243
PB 56	0.0367159	85±7	0.6339
PB 64	0.0369744	95±10	0.6246
PB 80	0.0373425	125±10	0.6374
PB 96	0.0375921	152±16	0.6394
PB 112	0.0377723	184±15	0.6490
PB 128	0.0379087	215±18	0.6544
PB 140	0.0379910	234±18	0.6523
PB 160	0.0381012	275±25	0.6595
PB 200	0.0382567	340±20	0.6551
PB 240	0.0383610	410±30	0.6557
PB 320	0.0384923	576±30	0.6695
PB 400	0.0385714	678±30	0.6519

T=413K, P=1 atm

In the mesoscale simulations of a polymer melt, each chain is represented as a point particle interacting through a soft-core potential derived from the solution of the Ornstein Zernike equation applying the Hyper Netted Chain closure. MS MD simulations were implemented in the microcanonical (N, V, E) ensemble on a cubic box with periodic boundary conditions. We used reduced units such that all the units of length were scaled by R_g $(r^* = r/R_g)$ and energies were scaled by $k_B T$. More details of our simulation procedure have been reported in previous papers.[17, 112, 120]

Table VI.2 reports the diffusion coefficient directly calculated from the MS MD in the soft sphere representation, $D_{\mathrm{t}}^{\mathrm{MS}}$, and the diffusion coefficient calculated from our rescaling procedure, D. Finally, for comparison the Table shows the diffusion coefficient in the atomistic representation D^{UA}. The diffusion coefficient measured in the mesoscale simulations is several orders of magnitude faster than in the atomistic simulations. However, once it is rescaled the diffusion coefficient becomes very similar to the one obtained directly from the atomistic simulation. It is important to notice that the diffusion coefficient is calculated without any input from the dynamics of the atomistic simulations, so the procedure is predictive. The samples here are relatively short compared to the entanglement degree of polymerization, and these calculations are performed for unentangled and slightly entangled systems. For strongly entangled systems, we proposed a perturbative version of our approach that accounts for the fact that both the tagged chain and the surrounding chains, that provide the entanglements, relax following the same dynamics.

On Figure VI.2 the diffusion coefficient is presented as a function of degree of polymerization N. Filled symbols represent UA MD simulations from ref.[68] and open symbols represent MS MD simulations rescaled as in Eq.(VI.3).

There are three distinct regions on Figure VI.2 in terms of power law dependence of $D \propto N^{-b}$. For $N \lesssim 80$, the faster than Rouse decrease of D with $b > 1$ is attributed in the literature to the free-volume effects due to chain ends which is significant only for very short chains.[121–123] In the intermediate regime for $80 \lesssim N \lesssim 160$ the scaling exponent b is just a little greater than 1 indicating Rouse-like behaviour. For longer chains with $N \gtrsim 200$ the value of $b \approx 2.1$ is typical of the crossover to reptation dynamics.

TABLE VI.2. Diffusion coefficient reconstructed from MS MD simulation compared against UA MD simulations.

N	D_t^{MS}[Å^2/ns]	D[Å^2/ns]	D^{UA}[Å^2/ns]
32	3875	184.5	152.2
48	3400	68.1	69.4
56	3425	51.9	46.4
64	3275	37.3	40.1
80	3174	25.1	24.9
96	3114	18.0	23.2
112	3235	15.1	16.7
128	3283	12.6	15.5
140	3221	10.5	12.0
160	2963	9.1	11.0
200	3245	6.0	6.6
240	3012	4.5	5.4
320	3386	3.2	2.6
400	3016	1.8	1.6

$d = 1.4672$Å(PB56)

The scaling exponents are not clearly defined in this plot because as the degree of polymerization is increasing, the density of the system is changing, as depicted in Figure (VI.3). The different regimes are even less prominent in the MSMD simulations where the transition between regimes is even smoother. In our calculations features like free volume effects due to chain ends (causing faster than Rouse decay of the diffusion coefficient for short chains) enter only indirectly from the interplay of the input parameters, i.e. ρ, R_g, N. The fact that the density is increasing with N density (Figure VI.3) enters our analytical equations through the effective radius of gyration of the polymer, as the compactness of the chain changes with the density (see also Section VI.5 of this communication). Overall the agreement between simulated and reconstructed diffusion coefficients is quite good.

The *cis*-1,4-PB chains are more flexible in comparison to PE chains, therefore we should expect larger entanglement length N_e (for PE $N_e \simeq 130$). Figure VI.2 shows that crossover from Rouse to reptation regime starts at $N = 200$. The largest system shown on Figure VI.2 is for $N = 400$ which is a still very weakly entangled system (1 or 2 entanglements per chain). In general the agreement between our prediction of diffusion coefficient and UA MD simulations is quantitative for all N.

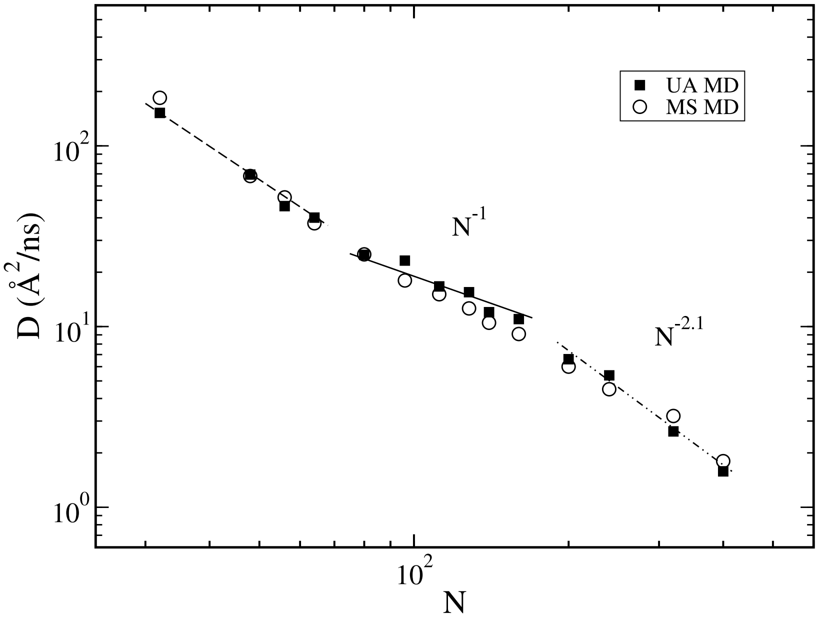

FIGURE VI.2. The center of mass self-diffusion coefficient as a function of degree of polymerization N. The reconstructed from MS MD simulations results (open symbol) are compared against UA MD data (filled symbol) from ref.[68]

VI.4. Internal Dynamics

The coarse-grained model adopted in this communication simplifies the macromolecular structure reducing the description of the molecule to an effective site that is centered on the center-of-mass of the molecule. For this reason, the only dynamics that can be predicted by this CG description, through the rescaling procedure, is the long-time diffusive behavior of the center-of-mass of the molecule. However from the knowledge of the diffusion coefficient the monomer friction coefficient can be obtained, and the latter can be used as an input to the Langevin equation that describes the complete dynamics of the polymer chain at any lenghtscale of interest.

Specifically we follow our approach for the Cooperative Dynamics of a group of macromolecules, or Cooperative Dynamics Generalized Langevin Equation (CDGLE).[124] Conventional theories of polymer dynamics, such as the Rouse theory for unentangled polymer dynamics and the "reptation" model for entangled dynamics, predict diffusive motion at short time following the ballistic regime; this is however in disagreement with simulations and experiments, which show a sub-diffusive regime before the com starts to follow Brownian

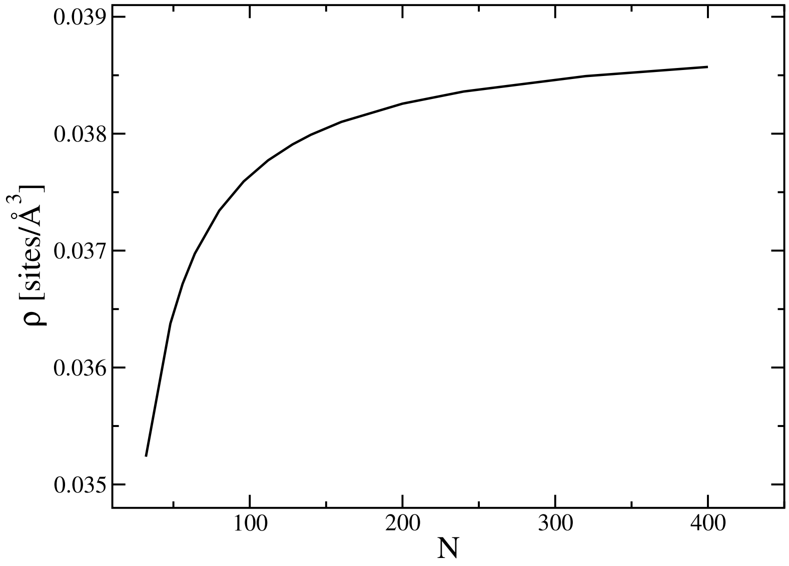

FIGURE VI.3. Density as a function of degree of polymerization N.

motion. Both theories are mean-field approaches of single chain dynamics in an uniform bath.[97] Our approach focuses on the dynamics of a group of polymer chains in a melt and relates the anomalous subdiffusive behavior to the presence of cooperative motion of a group of polymer chains in a dynamically heterogeneous liquid, as observed in simulations data of polymer melts and experiments.[125–128] Theoretical predictions of the com and monomer mean-square displacements are shown to be in quantitative agreement with computer simulations of unentangled[129, 130] and slightly entangled polymer melts,[131] and with scattering experiments of Neutron Spin Echo.[26]

The physical picture underlying the theory builds on the fact that in polymer melts the dynamics appears heterogeneous with the motion of a tagged chain correlated to the dynamics of a group of n chains comprised inside the range of the intermolecular potential. The latter has a range of the order of the correlation hole, i.e. of the radius-of-gyration of the polymer, as it emerges from the solution of the OZ equation. The number of chains comprised in a volume of the order of R_g^3 is given by $n \approx \rho N^{1/2} l^3$ and increases with increasing density, degree of polymerization, and the stiffness of the polymer.

In the Cooperative Dynamic approach the dynamics is described by a set of coupled equations of motion. Each equation is expressed in the space coordinates of the monomer a, belonging to molecule i and positioned at $\mathbf{r}_a^{(i)}(t)$, and it contains a balance of different forces acting on the monomer. These include the viscous force, $\zeta \frac{d\mathbf{r}_a^{(i)}(t)}{dt}$, the intramolecular force $-k_s \sum_{b=1}^{N} \mathbf{A}_{a,b}\mathbf{r}_b^{(i)}(t)$,which contains the structural matrix $\mathbf{A}$, the time-dependent intermolecular mean-field force $\beta^{-1}\frac{\partial}{\partial \mathbf{r}_a^{(i)}(t)} \ln\left[\prod_{k<l}^{n} g(\mathbf{r}^{(l)}(t), \mathbf{r}^{(k)}(t))\right]$, and the random interactions with the surrounding liquid, given by the random force $\mathbf{F}_a^{(i)}(t)$.

$$\zeta_{eff}\frac{d\mathbf{r}_a^{(i)}(t)}{dt} = -k_s \sum_{b=1}^{N} \mathbf{A}_{a,b}\mathbf{r}_b^{(i)}(t) + \frac{1}{\beta}\frac{\partial}{\partial \mathbf{r}_a^{(i)}(t)} \ln\left[\prod_{k<l}^{n} g(\mathbf{r}^{(l)}(t), \mathbf{r}^{(k)}(t))\right] + \mathbf{F}_a^{(i)}(t) \ . \tag{VI.11}$$

Here $\mathbf{A}$ is the matrix of intramolecular connectivity which reduces to the Rouse matrix when infinitely long and completely flexible macromolecules are considered and it is defined as

$$A_{i,j} = \sum_{k,p=2}^{N} M_{k,i} U_{k,p}^{-1} M_{p,j} \ . \tag{VI.12}$$

Here $\mathbf{U}$ is the equilibrium averaged bond correlation matrix

$$U_{k,p} = \frac{< \mathbf{l}_k \cdot \mathbf{l}_p >}{l_k l_p} \ , \tag{VI.13}$$

and $\mathbf{M}$ is a structural matrix, with all the elements equal zero except $M_{1,i} = 1/N$for $i = 1, ..., N$, $M_{i,i} = 1$ with $i = 2, ..., N$, and $M_{i-1,i} = -1$ with $i = 2, ..., N$. The $\mathbf{U}$ matrix is a function of the local semiflexibility parameter $g =< \mathbf{l}_i \cdot \mathbf{l}_{i+1} > /(l_i l_{i+1})$, which is related to the persistence length of the polymer, and for our samples the values of g are reported in Table VI.1.

Through Eq.(VI.13) the eom includes a complete microscopic description of the structure and local flexibility of the specific molecule under investigation, containing all the relevant parameters that define the intramolecular mean-force potential. Equations of motion for different beads belonging to the same chain or to two chains undergoing slow cooperative dynamics are coupled by the presence of intra- and inter-molecular interaction potentials. The intrinsic, chemical dependent semiflexibility of the macromolecule enters explicitly through the description of the $\mathbf{A}$ matrix.

The intermolecular potential is time dependent, as it is a function of the relative position coordinates of the centers-of-mass of a pair of molecules. As the two molecules move with respect to each other the intermolecular force changes. From the initial ensemble of n dynamically correlated chains, molecules diffuse in time and finally they move outside the range of the potential, R_g, in a timescale of $\tau_{decorr} = R_g^2/D$.

The set of coupled equations is solved after transformation into normal modes of motion and numerically using a self-consistent procedure that calculate the effective potential at any given distance. Once n and $\zeta_m = k_B T/(ND)$ are defined, the first from the data and the second from our rescaling procedure, the set of equations has no adjustable parameters.

By applying consideration of symmetry the set of coupled eoms in normal coordinates can be simplified and reduced to two sets of N uncoupled equations in the relative and collective normal-mode coordinates . We assume that the eoms for internal modes ($p > 0$) do not contain intermolecular forces. This approximation is justified on the basis that polymer local dynamics is affected in a similar way by inter- and intra-molecular excluded volume interactions, which in polymer liquids tend to compensate each other. Intermolecular forces, which enter the dynamics through the eom for the first ($p = 0$) normal mode, still perturb the dynamics on the local scale through the linear combination of the normal modes. However, an analysis of the decay in time of the dynamics structure factor for strongly entangled polymer systems, presented in the next section, shows that intermolecular excluded volume interactions at the monomer level become important when strongly entangled polymer systems are considered. In those cases, intermolecular contributions to the local dynamics cannot be discarded.

In the following, we present an overview of some of the quantities analyzed in the original simulations[68] and their comparison with the predictions of the Cooperative Dynamics theory having as an input parameter the rescaled friction coefficient calculated from the soft-sphere simulations and the rescaling procedure as described in the first part of this communication.

Figure VI.4 presents the end-to-end vector, time decorrelation function for the $N = 112$ sample of PB. The Cooperative Dynamic theory with the reconstructed monomer friction coefficient is directly compared against UA MD data. This function represents the rotational relaxation of the chain and cannot be measured from the soft colloid simulation directly. The

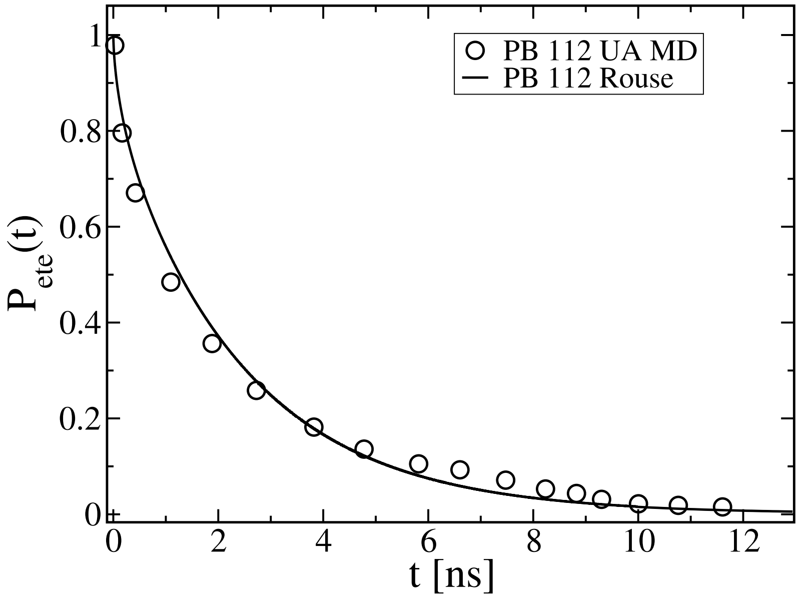

FIGURE VI.4. End-to-end vector time decorrelation function for PB112. UA MD simulation data (symbols) compared against the theory for Cooperative Dynamics with the monomer friction obtained from MS MD simulations after rescaling of the diffusion coefficient.

$N = 112$ sample has chains shorter than the entanglement length and the Cooperative Dynamics theory reproduces the atomistic simulation data rather well.

Figure VI.5 shows the center of mass mean square displacement (com MSD) for three samples of polybutadiene melts with chains of increasing degree of polymerization, $N = 240, 320$ and 400. The long time diffusive dynamics is calculated from the diffusion coefficients obtained from the rescaling procedure. For time shorter than the longest relaxation time, $\tau \approx R_g^2/D$, the mean-square displacement of the com shows a subdiffusive behavior that cannot be reproduced by the conventional theory of unentangled chain dynamics, namely the Rouse approach. In the cooperative dynamics theory the subdiffusive dynamics is a consequence of the cooperative motion of the interpenetrating chains inside the correlation hole region, coupled by the effective intermolecular potential between the coms of the macromolecules. The theory with the monomer friction from rescaled MS MD simulations as an input is compared against the UA MD simulation data. The diffusion coefficient for PB240 is underestimated and for PB320 is slightly overestimated by the theory in comparison with the simulations, which is also can be seen in Table VI.2 and Figure VI.2. The number of correlated chains is optimized in this plot giving

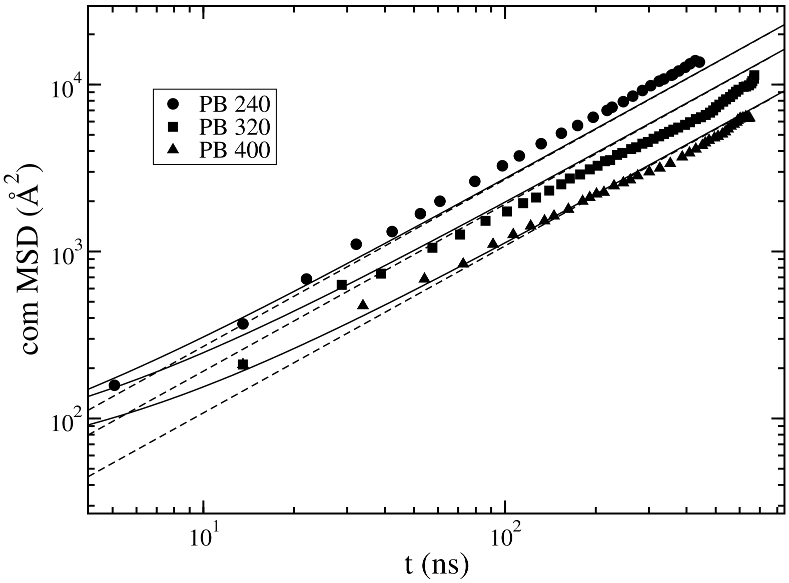

FIGURE VI.5. The center of mass mean square displacement as a function of time for the PB240, PB320 and PB400 samples. Theoretical predictions (solid lines) are compared against the UA MD simulations (symbols). Also shown is the purely diffusive dynamics from the rescaled MS MD simulations(dashed lines).

$n = 10, 10, 12$ for PB240, PB320 and PB400 respectively, giving a trend that qualitatively agree with the predicted scaling behavior.

Starting from the theory of cooperative dynamics, the dynamic structure factor can be calculated as

$$S(\mathbf{q}, t) = \frac{1}{N}\sum_{i,j}^{N} \langle exp[i\mathbf{q} \cdot (\mathbf{r}_i(t) - \mathbf{r}_j(0)]\rangle \approx \frac{1}{N}\sum_{i,j}^{N} exp\left[-\frac{\mathbf{q}^2}{6}\left\langle(\mathbf{r}_i(t) - \mathbf{r}_j(0))^2\right\rangle\right] \ . \tag{VI.14}$$

The average time-dependent distance between two monomers in the tagged chain depends on the presence of the $n - 1$ other chains dynamically correlated, and it is expressed as a function of relative and collective mode coordinates. Once ζ_{eff} and n are determined, the theory predicts the full decay of the dynamic structure factor, at the different experimental wave vectors. Figures VI.6 and VI.7 display the normalized dynamic structure factor obtained from the theory and compared with UA MD simulations for $q = 0.04, 0.1, 0.2, 0.3$Å^{-1}. For unentangled system PB96 shown on Figure VI.6 the agreement is excellent for all values of scattering vector q and time range. The Rouse model (not shown in this figure, see ref.[68]) failed to describe these data

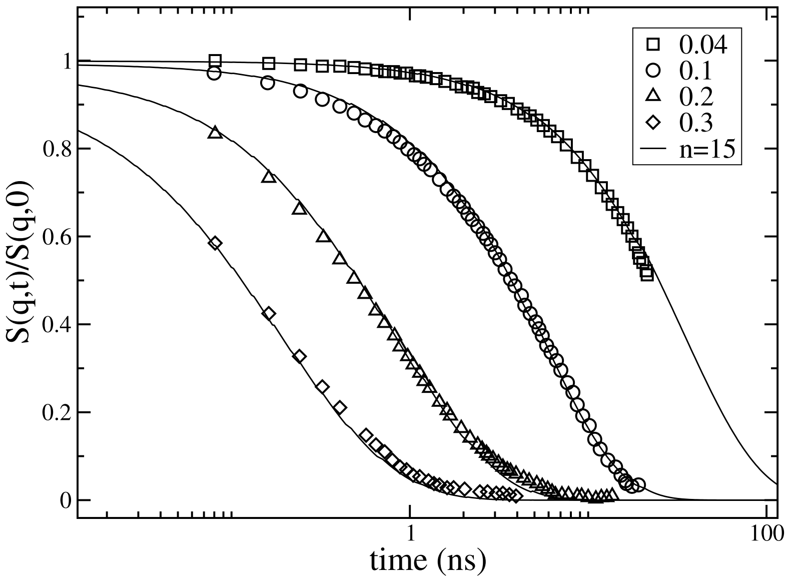

FIGURE VI.6. Normalized dynamic structure factor for PB96 and q=0.04, 0.1, 0.2, 0.3Å^{-1}. The data from UA MS simulations (symbols) are compared against the cooperative dynamics theory where number of correlated chains was set to $n = 15$.

with satisfactory agreement, while the cooperative dynamics theory is found to be in quantitative agreement for samples at different molecular weights, over the whole time range, and for different wave vectors.

On Figure VI.7 the normalized dynamic structure factor is shown for the weakly entangled system PB400. The agreement for the smallest scattering vector which represents global dynamics is quite good at all times, while for intermediate and large values of q the agreement between theory and simulations is good at short times, and less accurate at long time. The theoretical decay, which is faster than simulations at long times, suffers from the lack of properly describing the entanglement effects. A more recent version of the cooperative dynamics theory includes chain uncrossability, i.e. entanglements, and shows the correct slowing down of the relaxation in the long-time regime for entangled samples.

Figure VI.8 displays the monomer mean square displacement for two polybutadiene samples, the first with $N = 112$ and the second with $N = 400$. Theoretical predictions are compared against UA MD data from ref.[68] For PB112 the agreement in both subdiffusive and diffusive regions is very good, while for PB400 the monomer msd from UA MD contains three

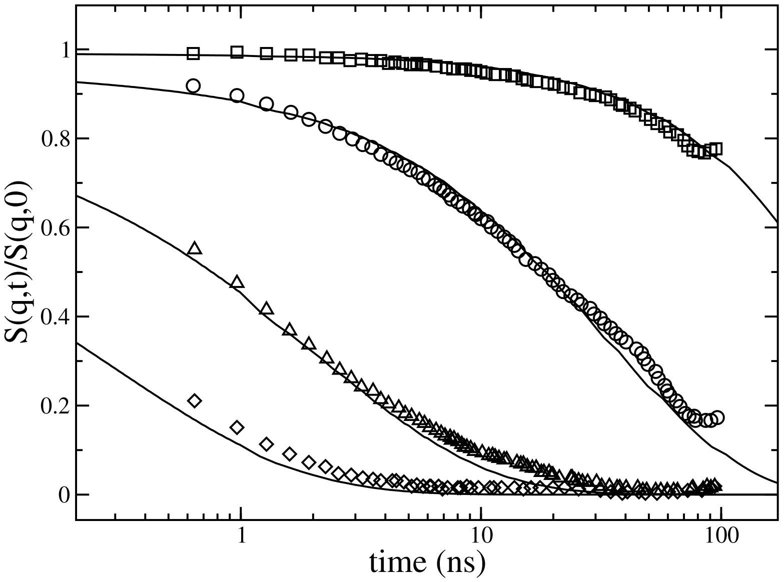

FIGURE VI.7. Normalized dynamic structure factor for PB400 and q=0.04, 0.1, 0.2, 0.3Å^{-1}. The data from UA MS simulations (symbols) are compared against the cooperative dynamics theory where number of correlated chains was set to $n = 12$.

distinct power-law dependencies (shown as dashed lines on Figure VI.8), which is a signature of entangled dynamics. The theoretical curve for PB400 does not recover all the features observed in the simulations for the reason mentioned earlier. The dot-dashed lines represent the long-time diffusive regime, i.e. Brownian motion, for both the PB112 and the PB400 systems.

VI.5. Theoretical Predictions Using the Freely Rotating Chain Model

The purpose of the rescaling procedure is to predict diffusion coefficients when the atomistic simulations or experiments are not available. One key input quantity to the procedure is the molecular radius of gyration. In the previous sections we adopted the values of R_g determined from the atomistic simulations. When there are no data available for the radius of gyration, neither from atomistic simulations nor from experiments, it is convenient to use some simple model, like the freely rotating chain model to provide R_g, as it captures the semiflexibility of the polymer chain. In this section we present a critical discussion of adopting a freely rotating chain model to describe the PB chain, using a constant flexibility parameter g.

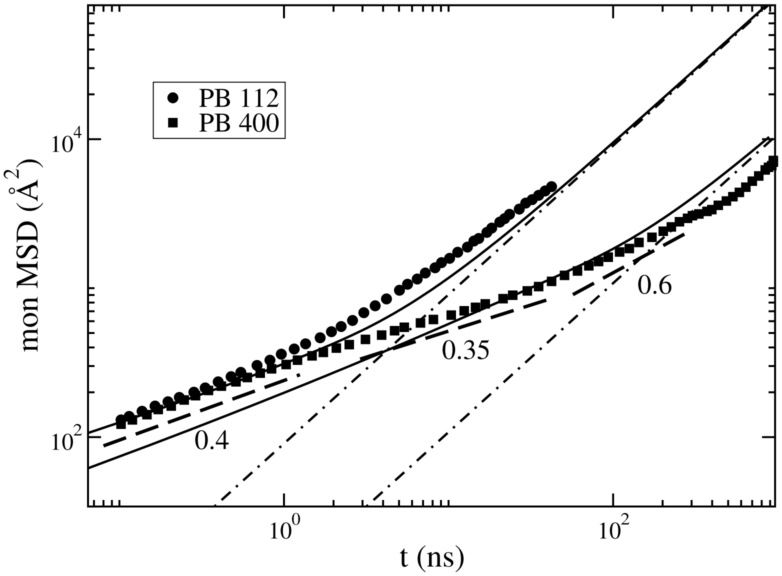

FIGURE VI.8. The innermost chain segments msd as a function of time for PB112 and PB400. The theory predictions (solid lines) are compared against the UA MD simulations (symbols). The predicted from rescaled MS MD simulations diffusion slopes (dot-dashed lines) are shown as well.

For the *cis*-1,4-polybutadiene chain with N carbon atoms along its backbone there are $n_{CH=CH} = N/4$ double bonds with $l_{db} = 1.34$Å, $n_{CH_2-CH_2} = N/4 - 1$ single bonds with $l_b = 1.54$Å and $n_{CH_2-CH} = N/2$ single bonds with $l'_b = 1.5$Å. The average bond length over all $N - 1$ bonds is calculated as

$$l_b^{ave} = \left[l_{db}\frac{N}{4} + l_b\left(\frac{N}{4} - 1\right) + l'_b\frac{N}{2}\right]/(N-1)\,, \tag{VI.15}$$

which in the $N \to \infty$ limit gives the value of $l_b^{ave} = 1.47$Å.

The radius of gyration for a freely rotating chain (FRC) model with semiflexibility parameter g is given as

$$R_g^2 = \frac{N-1}{6}\,(l_b^{ave})^2\left(\frac{1+g}{1-g} - \frac{2g}{(1-g)^2}\frac{1-g^{N-1}}{N-1}\right)\,. \tag{VI.16}$$

Figure VI.9 shows the density dependence of the semiflexibility parameter g in the simulations.

Fitting simultaneously all samples to R_g^{UA} data gives average for all densities $g = 0.6564$. In Figure VI.10 the radius of gyration squared over degree of polymerization R_g^2/N is shown as

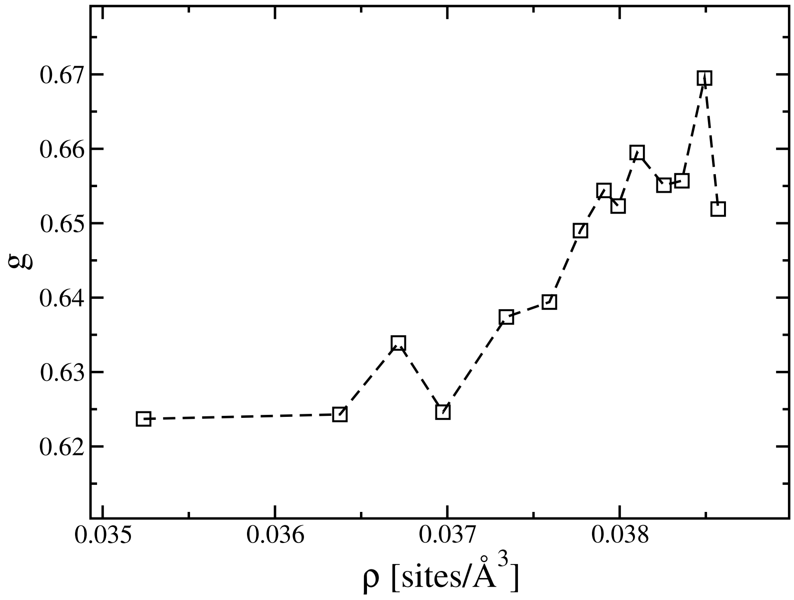

FIGURE VI.9. Density dependence of semiflexibility parameter g calculated from Eq.(VI.16) using UA MD data for radius of gyration R_g.

a function of N. Freely rotating model with averaged g works best for intermediate and large N. The ratio approaches the constant value as $N \to \infty$ where radius of gyration scales as $R_g^2 \propto N$. The deviation of the FRC model compared to UA simulation data in the NPT ensemble, i.e. increasing density, is shown as well. Samples with small N have larger deviation, while the constant flexibility hypothesis works best for the large N samples.

With this in mind, we report in Figure VI.11 the diffusion coefficient calculated from the mesoscale simulations, properly rescaled, where now the input radius-of-gyration is taken from the freely rotating chain model. As it is expected the best agreement between UA simulations and theoretical predicted diffusion is for the samples with larger N. The most relevant conclusion of this part of our study is the fact that it is possible to make predictions for data that are not reported in the UA MD simulations, obtaining information for new systems for which neither simulations nor experiments are available. The disagreement at small N is related to the fact that the density is changing with increasing N in that region of the plot, and the radius of gyration should be properly corrected for this difference. In conclusion, if an exact value of the radius of gyration as a function of thermodynamic conditions and degree of polymerization is known, the

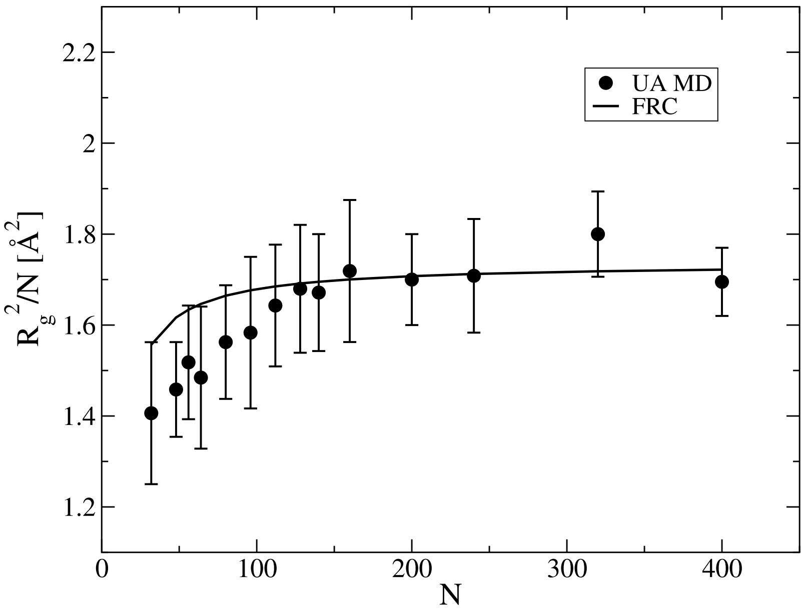

FIGURE VI.10. Radius of gyration squared over degree of polymerization R_g^2/N as a function of N. UA MD data compared against FRC model.

described procedure should be able to provide an accurate estimate of the dynamics starting from the mesoscale simulations of the coarse-grained system, which are computationally very efficient.

VI.6. Conclusion

In a couple of recent papers we have presented an original approach to rescale the dynamics measured in mesoscale simulations of coarse-grained systems and recover the realistic dynamics as measured in atomistic simulations performed in identical thermodynamic conditions. The relevance of this method is in its ability of predicting diffusion coefficient, with good precision, directly from the simulation of a coarse-grained system, without the need of performing an atomistic simulation. Simply put, the method does not need a calibration curve. The previous papers focused on the coarse-grained dynamics of polyethylene samples, while this is the first paper in which the method is applied to a polymer with a different monomeric structure.

In this communication we use an "extreme" level of coarse-graining as the whole chain is represented as a soft colloidal particle. The choice of this representation is motivated by two reasons. The first is that a possible error in the procedure would be clearly made evident in

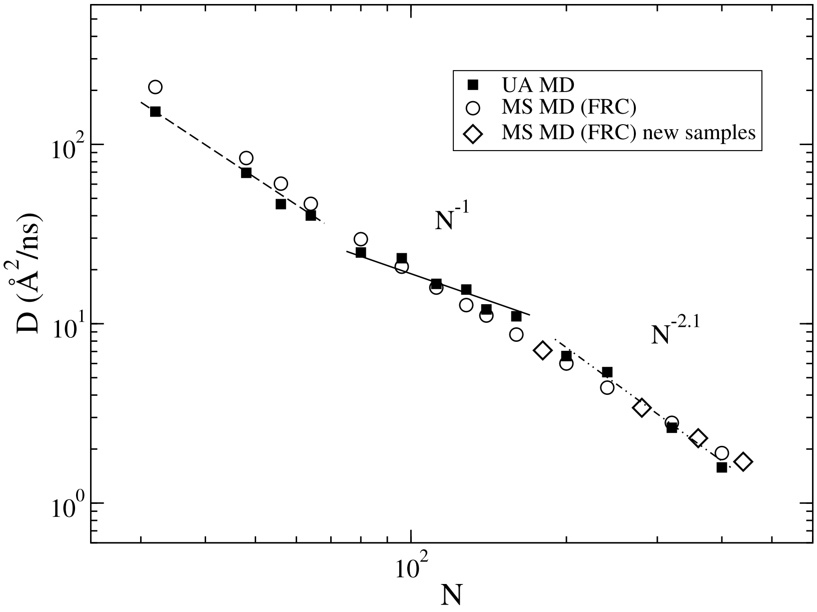

FIGURE VI.11. Diffusion coefficient reconstructed from MS MD simulations with use of FRC model.

this level of coarse-graining, and we believe that the procedure would produce an even better agreement if the macromolecule is coarse-grained at a lower level, e.g. as a collection of soft particles, or blobs;.[75] The second is that for this representation all the physical quantities that enter our approach are analytically solved and the rescaling procedure is formally derived.

The communication presents a comparison between theoretical predictions of coarse-grained simulations properly rescaled following our first-principles procedure, and data from united-atom simulations for *cis*-1,4-Polybutadiene melts. The simulations were performed by Tsolou et al. in a NPT ensemble.[68] The rescaled diffusion coefficient shows good agreement with the diffusion measured in atomistic simulations, which supports the validity of the proposed procedure.

As the coarse-graining model represents the whole polymeric chain as a soft colloidal particle, the only dynamical information that can be collected from the rescaled mesoscale simulation is the diffusion coefficient of the center-of-mass of the polymer. From this, however, the friction coefficient of the monomer is derived. This communication shows how the monomer friction coefficient is used as an input to traditional Langevin equations for the dynamics of polymeric liquids. Specifically we use here the cooperative dynamics model for unentangled chains, given that the samples in the UA simulations are in the regime of unentangled and slightly entangled dynamics. From the theory of cooperative dynamics, which represents the cooperative motion of a group of interacting polymers in a dynamically heterogeneous liquid, all time correlation functions of interest can be calculated. Specifically we present here the comparison with the quantities reported in the original paper by Tsolou et al. and show that the theory, with the rescaled friction coefficient, is able to reproduce quantitatively the dynamics observed in the end-to-end time decorrelation function, and in the dynamic structure factor for unentangled and slightly entangled chains. For entangled chains the local dynamics, represented by the high q regime in the dynamic structure factor and in the monomer mean-square-displacement, shows a slight departure from the theory as the cooperative dynamics approach adopted here does not yet include the effect of entanglements.

CHAPTER VII

CONCLUSION

This dissertation has focused on the reconstruction of polymer liquid structure and dynamics from a heavily coarse-grained description. The main goal was to develop the theoretical framework which allows for the optimization of simulating polymers efficiently. As part of the presented work the original expressions for friction rescaling factors were calculated from the memory function formalism. The advantage of the presented approach is in its analytical character which ensures the transferability to different thermodynamic states. In the following two sections the main results are summarized and a brief overview of the field is given. Future directions of the research are emphasized in the last section.

VII.1. Summary

In this dissertation a theoretical formalism has been developed which allowed us to reconstruct from coarse-grained molecular dynamics simulations correct structural and dynamics information. The formalism was applied and tested for a number of polymer systems including polymer melts of increasing degree of polymerization, different monomeric chemical structure and systems at different thermodynamics states.

To reconstruct the structure of the coarse-grained polymer liquids in this work the monomer total correlation function was calculated. The local information from small united-atom simulations was combined in a multiscale approach with global information provided from coarse-grained at the center-of-mass level simulations of polymer melts. The application of this multiscale procedure became feasible due to ample separation between global and local features of the total correlation function. The resulting monomer total correlation function was compared against the full united-atom simulations and showed quantitative agreement.

The comprehensive theoretical description of two levels of coarse-graining was given in order to formulate the reconstruction formalism for dynamics. For both the monomer level description and center-of-mass level description the Generalized Langevin Equations of motion were derived. Following the reconstruction procedure the free energy due to internal degrees of freedom was reintroduced. With analytically derived expressions for the friction coefficients, the translational diffusion was calculated from mesoscale simulations. Comparison against united atom simulations and experimental data showed a quantitative agreement.

The monomer friction coefficient was subsequently calculated from the reconstructed center-of-mass diffusion coefficient and entered the cooperative dynamics theory as an input parameter. Cooperative dynamics theory which describes the group of neighboring chains through individual and collective modes reproduced anomalous subdiffusive behaviour, rotational diffusion, and dynamic structure factor. Since the monomer friction coefficient was the only required external parameter for cooperative dynamics theory, the reconstruction formalism successfully integrates this piece of information.

VII.2. Field Overview

In this dissertation the underlying conditions which cause the sped up dynamics in coarse-grained simulations were examined from a theoretical point of view. In the effort of systematic and rigorous reconstruction of realistic dynamics the analytical formalism was developed which corrects for missing internal degrees of freedom and change in friction in “a posteriori” fashion. This approach is advantageous to numerical procedures which require computationally expensive algorithms and are state dependent.

In the typical numerical coarse-graining methods the effective pair potential between coarse-grained units is obtained through the Boltzmann inversion procedure. This requires performance of detailed simulations in order to collect enough statistics for coarse-grained units. The effective free energy potentials obtained from distribution functions are then optimized in a self consistent way. Series of coarse-grained simulations are performed reiterating the Boltzmann inversion procedure until the pair distribution function measured in the system will match the one from detailed atomistic simulation. The force field obtained in this scheme not only requires a lot of computational resources and time, but is hard to control and impossible to transfer to a significantly distinct thermodynamic condition.

It has been shown that there is a unique correspondence between the effective pair potential and radial distribution function. Therefore, the criteria of matching radial distributions should give a correct coarse-grained potential. However, the radial distribution function reproduced in coarse-grained simulations is moderately insensitive to changes of the potential especially when the level of coarse-graining is high. This fact gives rise to the situation when significantly different effective pair potentials generate in simulations almost indistinguishable radial distribution functions. Moreover, these numerical potentials usually can reproduce only static properties, whereas thermodynamic properties, such as pressure and free energy of the system remain inconsistent.

Dynamics in numerically coarse-grained systems can be rescaled also only numerically by hand using calibration curves. Construction of calibration curves is necessary for each system and not transferable. The need to perform a detailed atomistic simulation for each calibration can diminish the idea of coarse-graining as a tool of efficiency enhancement for computer simulations.

In the perspective of all the difficulties related to obtaining numerical coarse-graining potentials the development of an analytical formalism, derived from the first principles, is desirable. This work aimed in fulfilling this task starting from the simple idea of determining and applying required corrections and the developed framework contributes with its novelty to the field.

VII.3. Future Research

In this dissertation only two levels of coarse-graining were taken into consideration. The monomer representation describes local properties and chain center-of-mass representation provides the global information. However, the concept of multiscale modeling implies a hierarchy of simulations representing a certain region of interest. The intermediate levels of coarse-graining are of great interest when important physics happens and cannot be described either by bead-and-spring model or by a soft colloidal model. The example of such a system is strongly entangled polymer melts where there is an important intermediate length scale associated with the entanglement length or tube diameter in the reptation model.

The reconstruction method described in this dissertation can be further extended to incorporate intermediate time and length scales. A polymer chain can be analyzed as a multiblock chain and coarse-grained at the intermediate level as a chain of connected soft spheres. The reconstruction of the realistic dynamics in the same manner as the soft sphere simulations necessitates the analytical derivation of the friction coefficient for the block. To demonstrate the potential for future research in this project the derivation of the block friction coefficient is given in Appendix C.

APPENDIX A

INTERNAL ENERGY CALCULATION FOR A FREELY-ROTATING-CHAIN MODEL

The effective mean-force potential for one homopolymer composed of N monomers can be expressed through the structural matrix $\mathbf{A}$ as

$$U = \frac{3k_BT}{2l^2}\sum_{i,j}\mathbf{A}_{i,j}\,\mathbf{r}_i\cdot\mathbf{r}_j = \frac{3k_BT}{2l^2}\sum_{x,y,z}\sum_{i,j}x_i\mathbf{A}_{i,j}x_j = \frac{3k_BT}{2\,l^2}\mathbf{r}^T\mathbf{A}\mathbf{r}\,, \tag{A.1}$$

with the matrix $\mathbf{A}$ being real and symmetric, and diagonalized by the orthonormal matrix of the eigenvectors $\mathbf{Q}^{-1} = \mathbf{Q}^T$, so that

$$\mathbf{r}^T\mathbf{A}\mathbf{r} = \xi^T\mathbf{Q}^{-1}\mathbf{A}\mathbf{Q}\xi = \xi^T\mathbf{\Lambda}\xi\,, \tag{A.2}$$

where $\mathbf{\Lambda}$ is the matrix of the eigenvalues, and ξ is the matrix of the normal modes defined by $\mathbf{r} = \mathbf{Q}\xi$.

In this model, the equilibrium distribution function is

$$\Psi_{eq}(\mathbf{r}) = N_x e^{-\frac{3}{2l^2}x^TAx} N_y e^{-\frac{3}{2l^2}y^TAy} N_z e^{-\frac{3}{2l^2}z^TAz} = N e^{-\frac{3}{2\,l^2}\mathbf{r}^T\mathbf{A}\,\mathbf{r}} = N e^{-\frac{1}{2}\mathbf{r}^T\mathbf{A}'\,\mathbf{r}}\,, \tag{A.3}$$

where for convenience of notation we introduced the matrix $\mathbf{A}' = 3\mathbf{A}/l^2$. Here N_x is the normalization factor, defined by enforcing $\int dx\Psi_x = 1$, as

$$N_x = \left(\frac{3}{2\pi l^2}\right)^{N/2}[det(\mathbf{A})]^{1/2}\ , \tag{A.4}$$

with $N_x = N_y = N_z = N^{1/3}$. The statistically averaged internal energy for one molecule consisting of N monomers simplifies to

$$\left\langle\frac{E}{k_BT}\right\rangle = N\int U e^{-\frac{1}{2}\mathbf{r}^T\mathbf{A}'\mathbf{r}}d\,r = N\int\frac{1}{2}\mathbf{r}^T\mathbf{A}'\mathbf{r}e^{-\frac{1}{2}\mathbf{r}^T\mathbf{A}'\mathbf{r}}\,. \tag{A.5}$$

In one dimension,

$$\left\langle \frac{E}{k_B T} \right\rangle_x \;=\; \frac{3N_x}{2l^2} \int d\mathbf{x}\; \mathbf{x}^T \mathbf{A}\mathbf{x}\, e^{-\frac{3}{2l^2}\mathbf{x}^T\mathbf{A}\mathbf{x}} = N_x \frac{3}{2l^2} \left[\frac{N_x l^2}{3} \prod_{i=1}^{N_x} \sqrt{\frac{2\pi l^2}{3\lambda_i}} \right] = \frac{N}{2} \;, \tag{A.6}$$

which gives, as the final result for the internal energy of one molecule consisting of N monomers,

$$\left\langle \frac{E}{k_B T} \right\rangle = \frac{3N}{2} \;. \tag{A.7}$$

APPENDIX B

THE DYNAMIC MEMORY FUNCTION

We briefly report here the derivation of Eq.(IV.29) starting from Eq.(IV.13). The product of the direct and projected forces is expressed as a function of the density field variables as

$$< \mathbf{F}(0) \cdot \mathbf{F}^{\hat{Q}}(t) > \cong \mathbf{F}(\mathbf{r}) \cdot \mathbf{F}(\mathbf{r}') < \rho_\alpha(\mathbf{r};0)\rho_\gamma(\mathbf{r};t) > \ . \tag{B.1}$$

Because the fluid is uniform and isotropic, the density fields can be replaced by their fluctuation variables, $\Delta\rho_\alpha(\mathbf{r},t) = \rho_\alpha(\mathbf{r},t) - < \rho_\alpha(\mathbf{r}) >$, where the ensemble-averaged density field is approximated by $< \rho_\alpha(\mathbf{r}) > \approx \rho g(r)$. The correlation of the random forces is then expressed as

$$< \mathbf{F}(0) \cdot \mathbf{F}^{\hat{Q}}(t) > \cong \hat{r} \cdot \hat{r}' \rho^2 g(r) g(r') F(r) F(r') \frac{< \Delta\rho_\alpha(\mathbf{r})\Delta\rho_\gamma(\mathbf{r}',t) >}{< \rho_\alpha(r) >< \rho_\gamma(r') >} \ , \tag{B.2}$$

where we adopt a kind of "dynamical" Kirkwood superposition approximation in a weighted average form

$$< \Delta\rho_\alpha(\mathbf{r})\Delta\rho_\gamma(\mathbf{r}',t) > \approx \rho \int d\mathbf{R}\ g(r)g(r')S(R,t)S(|\mathbf{r}-\mathbf{r}'+\mathbf{R}|t) \ . \tag{B.3}$$

Eq.(B.3) describes the multipoint correlation between the density fluctuations at a distance $\mathbf{r}$ from segment α at time zero, and the density fluctuations a distance $\mathbf{r}'$ from segment γ at time t. Because α and γ can be on the same or on different polymer chains, no assumptions are made a priori about the relative importance of intra and intermolecular correlations. In this way, the chain connectivity does not play a dominant role in our description from the very beginning. We then calculate both intra and intermolecular contributions and show that both need to be included in the calculation of the memory function as intramolecular contributions are comparable in size to the intermolecular ones. Substitution of Eq.(B.3) into Eq.(B.2) leads to Eq.(IV.29).

APPENDIX C

EXTENSION OF RECONSTRUCTION METHOD TO THE MULTIBLOCK POLYMER CHAINS REPRESENTED AS THE CONNECTED SOFT SPHERES

The extension of the rescaling method for the dynamics measured in MS MD simulations of soft multiblock chains necessitates the analytical calculation of the friction coefficient for the block. This calculation can be done starting from the same principles in the manner of monomer and soft colloid friction calculations. We start from the expression for block friction coefficient, ζ_b, as the time integral of the memory funcion

$$\zeta_b = \frac{1}{n_b} \sum_{\alpha\gamma} \int_0^\infty dt\, \Gamma_{\alpha\gamma}(t)\,, \tag{C.1}$$

with memory function defined as

$$\Gamma_{\alpha\gamma}(t) \cong \frac{\beta}{3}\rho_b \int d\mathbf{r} \int d\mathbf{r}' g(r)g(r')F(r)F(r')\, \hat{\mathbf{r}} \cdot \hat{\mathbf{r}}' \int d\mathbf{R}\, S_{\alpha\gamma}(R;t) S(|\mathbf{r} - \mathbf{r}' + \mathbf{R}|;t)\,, \tag{C.2}$$

where ρ_b is the number density of the blocks, $g(r) = h(r) + 1$ is the block radial distribution function, and dynamic structure factor includes both inter and intramolecular contributions

$$S(k;t) = \left(\omega_{av}^{bb}(k) + \rho_b h_{av}^{bb}(k)\right) e^{-k^2 D t}\,. \tag{C.3}$$

The polymer chain coarse-grained at block level is represented as a chain of n_b connected soft particles associated with blocks of the macromolecule with N_b monomers contained in each. The characteristic size of each block is its radius of gyration, $R_{gb} = R_g/\sqrt{n_b}$. Assuming that the number of monomers, N_b, per block is large enough to apply Gaussian statistics, the averaged block-block distribution function in reciprocal space as a function of dimensionless wave vector, $\tilde{k} = R_{gb}k$, can be expressed as the double sum[75]

$$\omega_{av}^{bb}(\tilde{k}) = \frac{1}{n_b^2} \sum_{\alpha=1}^{n_b} \sum_{\beta=1}^{n_b} e^{\tilde{k}^2|\alpha-\beta|} Q_{\alpha\beta}(\tilde{k})\,, \tag{C.4}$$

where $Q_{\alpha\beta}(\tilde{k}) = e^{-\frac{2}{3}\tilde{k}^2}$ for all $\alpha \neq \beta$ and $Q_{\alpha\beta}(\tilde{k}) = 1$ for $\alpha = \beta$. Using more compact notation for double summation in Eq.(C.4)

$$\omega_{av}^{bb}(\tilde{k}) = 1 + \frac{2}{n_b^2} \sum_{\alpha > \beta} e^{\tilde{k}^2(\alpha - \beta + \frac{2}{3})} \, . \tag{C.5}$$

where summation is performed for all α and β excluding terms when $\alpha = \beta$. The double summation can be taken and the expression transforms to

$$\omega_{av}^{bb}(\tilde{k}) = \frac{1}{n_b} + \frac{2\left(e^{\tilde{k}^2} - n_b e^{-\tilde{k}^2} + (n_b - 1)\right)}{n_b^2 (e^{-\tilde{k}^2} - 1)^2} e^{-\frac{2}{3}\tilde{k}^2} \, . \tag{C.6}$$

The averaged total correlation function for the block centers of mass can be expressed using the Ornstein-Zernike relation

$$h_{av}^{bb}(k) = \frac{c_0 \left(\omega_{av}^{bm}(k)\right)^2}{1 - N\rho_m c_0 \, \omega^{mm}(k)} \, , \tag{C.7}$$

where c_0 is the monomer direct correlation function at $k = 0$. The intramolecular monomer distribution function about the block center of mass is[75]

$$\omega_{av}^{bm} = \frac{N}{n_b} e^{-\frac{1}{6}\tilde{k}^2} + \frac{2N}{n_b} \left[\frac{e^{-n_b \tilde{k}^2} - n_b e^{-\tilde{k}^2} + (n_b - 1)}{n_b^2 \tilde{k}^2 (e^{-\tilde{k}^2} - 1)} \right] e^{-\tilde{k}^2/3} \, . \tag{C.8}$$

The intramolecular monomer distribution is a Debye function

$$\omega^{mm}(\tilde{k}) = \frac{2}{\tilde{k}^4} \left(\tilde{k}^2 - 1 + e^{-\tilde{k}^2} \right) \, . \tag{C.9}$$

Substituting Eqs.(C.8) and (C.9) into Eq.(C.7) and performing a Taylor expansion with respect to the wave vectors relevant for the considered level of coarse graining, $k \ll 1/R_{gb}$, the averaged total correlation function for blocks becomes

$$h_{av}^{bb}(k) = \left(A_1 + A_2 \, \tilde{k}^2 + \ldots \right) e^{-\frac{\tilde{k}^2}{3}} \, , \tag{C.10}$$

where both A_1 and A_2 depend on four parameters n_b, c_0, N, ρ_m as

$$A_1 = \frac{c_0}{n_b^4 (1 - c_0 N \rho_m)} \, , \tag{C.11}$$

$$A_2 = -c_0 \frac{2(1-n_b) + c_0 N \rho_m (2n_b - 1)}{3n_b^3 (c_0 N \rho_m - 1)^2} \, . \tag{C.12}$$

The Fourier transform from reciprocal to real space of Eq.(C.10) gives the expression

$$h_{av}^{bb}(\tilde{r}) = \left(B_1 + B_2\,\tilde{r}^2\right) e^{-\frac{3}{4}\tilde{r}^2} \, , \tag{C.13}$$

where $\tilde{r} = r/R_{gb}$ is the reduced spatial variable and B_1, B_2 depend on the same set of parameters as A_1, A_2

$$B_1 = \frac{3}{32}\sqrt{\frac{3}{\pi}} \frac{c_0 N^2}{n_b^4 (c_0 N \rho_m - 1)^2} \left[4 + 12 n_b (n_b - 1) - 4 c_0 N \rho_m - 6 c_0 N \rho_m n_b (2n_b - 1)\right] \, , \tag{C.14}$$

$$B_2 = -\frac{3}{32}\sqrt{\frac{3}{\pi}} \frac{c_0 N^2}{n_b^4 (c_0 N \rho_m - 1)^2} \left[6 n_b (n_b - 1) - 3 c_0 N \rho_m n_b (2n_b - 1)\right] \, . \tag{C.15}$$

The simplified approximations for the averaged intra and intermolecular distributions of the blocks allow the analytical solution of the memory function integral Eq.(C.2). The expression for the calculated friction coefficient for the block, taking into account only the repulsive contribution of $h_{av}^{bb}(r)$ is

$$\begin{aligned}
\zeta_b \;=\; & \frac{2}{3}\beta^{-1} D^{-1} \rho_b \frac{8\pi}{27} R_{gb}^3 B_1^2 \Bigg[\frac{3}{8}\sqrt{\frac{3\pi}{2}} + \frac{3\sqrt{3\pi}}{n_b^2} \sum_{\alpha>\beta} (4 + 3(\alpha - \beta))^{-3/2} + \\
& \frac{\sqrt{\pi}}{n_b^4} \sum_{\alpha>\beta} \sum_{\gamma>\delta} (2 + \alpha - \beta + \gamma - \delta)^{-3/2} + 2\rho_b \Bigg(A_1 \frac{\sqrt{\pi}}{4} + A_2 \frac{3\sqrt{\pi}}{8} + \\
& A_1 \frac{3\sqrt{3\pi}}{2n_b^2} \sum_{\alpha>\beta} (5 + 3(\alpha - \beta))^{-3/2} + A_2 \frac{27\sqrt{3\pi}}{4n_b^2} \sum_{\alpha>\beta} (5 + 3(\alpha - \beta))^{-5/2} \Bigg) + \\
& \rho_b^2 \Bigg(A_1^2 \frac{3\sqrt{3\pi}}{32} + 2A_1 A_2 \frac{27\sqrt{3\pi}}{256} + A_2^2 \frac{405\sqrt{3\pi}}{2048} \Bigg) \Bigg] \, .
\end{aligned} \tag{C.16}$$

REFERENCES CITED

[1] M. Gell-Mann and J. B. Hartle, Phys. Rev. A **76**, 022104 (2007).

[2] D. Frenkel and B. Smith, *Understanding Molecular Simulation. From Algorithms to Applications* (Academic Press, London, 2002).

[3] A. Uhlherr, M. Doxastakis, V. G. Mavrantzas, D. N. Theodorou, S. J. Leak, N. E. Adam and P. E. Nyberg, Europhys. Lett. **57**, 506 (2002).

[4] M. Kröger and S. Hess, Phys. Rev. Lett. **85**, 1128 (2000).

[5] S. K. Sukumaran and A. E. Likhtman, Macromolecules **42**, 4300 (2009).

[6] J. T. Padding, and W. J. Briels, J. Chem. Phys. **117**, 925 (2002).

[7] H. C. Öttinger *Beyond Equilibrium Thermodynamics* (Wiley, Hoboken, N.J.2005).

[8] G. Yatsenko, E. J. Sambriski, M. A. Nemirovskaya and M. Guenza, Phys. Rev. Lett. **93**, 257803 (2004).

[9] M. Karttunen, I. Vattulainen, and A. Lukkarinen (eds.), *Novel Methods in Soft Matter Simulations*; Lect. Notes Phys. **640** (Spinger-Verlag Berlin Heidelberg 2004).

[10] T. A. Knotts IV, N. Rathore, D. C. Schwartz and J. J. de Pablo, J. Chem. Phys. **126**, 084901 (2007).

[11] M. L. Klein and W. Shinoda, Science **321**, 798 (2008).

[12] G. Milano and F. Müller-Plathe, J. PHys. Chme. B **109**, 18609 (2005).

[13] S. O. Nielsen, C. F. Lopez, G. Srinivas and M. L. Klein J. Phys.: Condens. Matter **16**, R481 (2004).

[14] V. A. Harmandaris and K. Kremer, Macromolecules **42**, 791 (2009).

[15] M. Mondello and G. S. Grest, J. Chem. Phys. **106**, 9327 (1997).

[16] J. McCarty, I. Y. Lyubimov and M. G. Guenza, Macromolecules **43**, 3964 (2010).

[17] J. McCarty, I. Y. Lyubimov and M. G. Guenza, J. Phys. Chem. B **113**, 11876 (2009).

[18] V. Krakoviack, J.-P. Hansen and A. A. Louis, Europhys. Lett. **58**, 53 (2002).

[19] K. S. Schweizer and J. G. Curro, Adv. Chem. Phys. **98**, 1 (1997).

[20] McQuarrie, D. A. *Statistical Mechanics*; University Science Books: Sausalito, C. A., 2000 (see discussion in Section 13-9).

[21] E. J. Sambriski, G. Yatsenko, M. A. Nemiroskaya and M. G. Guenza, J. Chem. Phys. **125**, 234902 (2006).

[22] A. A. Louis, P. G. Bolhuis, J. P. Hansen and E. J. Meijer, Phys. Rev. Lett. **85**, 2522 (2000).

[23] J.-P. Hansen and I. R. McDonald, *Theory of Simple Liquids* (Academic Press, London, 1991).

[24] M. G. Guenza, J. Phys.: Condens. Matter **20**, 033101 (2008), and references therein.

[25] M. Guenza Phys. Rev. Lett. **88**, 25901 (2002).

[26] M. Zamponi, A. Wischnewski, M. Monkenbusch, L. Willner, D. Richter, P. Falus, B. Farago and M. G. Guenza J. Phys. Chem. **112**, 16220 (2008), and references therein.

[27] E. J. Sambriski, G. Yatsenko, M. A. Nemiroskaya and M. G. Guenza J. Phys.: Cond. Matt. **19**, 205115 (2007).

[28] E. Caballero-Manrique, J. K. Brey, W. A. Deutschman, F. W. Dahlquist and M. G. Guenza Biophys. J. **93**, 4128 (2007).

[29] B. Dünweg, A. J. C. Ladd, Adv. Polym. Sci. **89**, 221, (2008).

[30] P.-G. de Gennes, *Scaling Concepts in Polymer Physics* (Cornell University Press, Ithaca, NY, 1979).

[31] J.P. Wittmer, P. Beckrich, H. Meyer, A. Cavallo, A. Johner, J. Baschnagel, Phys. Rev. E **76**, 011803, (2007); H. Meyer, J. P. Wittmer, T. Kreer, P. Beckrich, J. Farago, J. Baschnagel, Eur. Phys. J. E **26**, 25, (2008).

[32] P. J. Flory, *Statistical Mechanics of Chain Molecules* (Hanser Publishers, Cincinnati, OH, 1989).

[33] F. Tombolato, A. Ferrarini, J. H. Freed, J. Phys. Chem. B **110**, 26248, (2006).

[34] T. Sauer, C. Grebogi, J. A. Yorke, Phys. Rev. Lett. **79**, 59,(1997); S. Dawson, C. Grebogi, T. Sauer, J. A. Yorke, Phys. Rev. Lett. **73**, 1927,(1994).

[35] M. P. Allen, D. J. Tildesley, *Computer Simulation of Liquids* (Oxford Science Publications, Oxford, 1992).

[36] I. Y. Lyubimov, J. McCarty, A. Clark, and M. G. Guenza, J. Chem. Phys. **132**, 224903 (2010).

[37] J. Baschnagel, F. Varnik, J. Phys.: Condens. Matter **17**, R851,(2005).

[38] W. Shinoda, R. Devane, M. L. Klein, Mol. Sim. **33**, 27,(2007); S. O. Nielsen, C. F. Lopez, G. Srinivas, M. L. Klein, J. Phys.: Condens. Matter **16**, R481,(2004).

[39] S. Izvekov, G. A. Voth, J. Chem. Phys. **125**, 151101, (2006).

[40] D. A. McQuarrie, *Statistical Mechanics* (University Science Books, Sunsalito, CA, 2000).

[41] G. S. Grest, K. Kremer, Phys. Rev. A **33**, 3628, (1986).

[42] W. Paul, D. Y. Yoon, G. D. Smith, J. Chem. Phys. **103**, 1702, (1995).

[43] K. Binder, Ed. *Monte Carlo and Molecular Dynamics Simulations in Polymer Science* (Oxford University Press, New York, 1995).

[44] K. Binder, Comp. Phys. Comm. **147**, 22, (2002).

[45] A. Uhlherr, M. Doxastakis, V. G. Mavrantzas, D. N. Theodorou, S. J. Leak, N. E. Adam, P. E. Nyberg, Europhys. Lett. **57**, 506, (2002).

[46] G. Yatsenko, E. J. Sambriski, M. G. Guenza, J. Chem. Phys. **122**, 054907, (2005).

[47] E. J. Sambriski, G. Yatsenko, M. A. Nemirovskaya, M. G. Guenza, J. Chem. Phys. **125**, 234902, (2006).

[48] E. J. Sambriski, M. G. Guenza, Phys. Rev. E **76**, 051801, (2007).

[49] E. J. Sambriski, G. Yatsenko, M. Nemirovskaya, M. G. Guenza, J. Phys.: Condens. Matter **19**, 205115, (2007).

[50] P. J. Flory, W. R. Krigbaum, J. Chem. Phys. **18**, 1086, (1950).

[51] P. G. Bolhuis, A. A. Louis, J.-P. Hansen, E. J. Meijer, J. Chem. Phys. **114**, 4296, (2001) and references therein.

[52] J. Dautenhahn, C. Hall, Macromol. **27**, 5399, (1994).

[53] M. Murat, K. Kremer, J. Chem. Phys. **108**, 4340, (1998).

[54] K. S. Schweizer, J. G. Curro, Chemical Physics **149**, 105, (1990).

[55] K. S. Schweizer, J. G. Curro, Adv. Chem. Phys. **98**, 1, (1997).

[56] A. B. Bhatia, D. E. Thornton, Phys. Rev. B **2**, 3004, (1970).

[57] E. Jaramillo, D. T. Wu, G. S. Grest, J. G. Curro, J. Chem. Phys. **120**, 8883, (2004).

[58] D. Heine, D. T. Wu, J. G. Curro, G. S. Grest, J. Chem. Phys. **118**, 914, (2003).

[59] G. Santangelo, A. Di Matteo, F. Müller-Plathe, and G. Milano J. Phys. Chem. B **111**, 2765 (2007).

[60] S. O. Nielsen, C. F. Lopez, G. Srinivas, M. L. Klein J. Phys.: Condens. Matter **16** R481 (2004).

[61] K. Binder Ed. *Monte Carlo and Molecular Dynamic Simulations in Polymer Science* (Oxford University Press, New York, 1995).

[62] J. McCarty, I. Y. Lyubimov, and M. G. Guenza Macromol. **43**, 3964 (2010).

[63] J-X. Hou, C. Svaneborg, R. Everaers, G. S. Grest Phys. Rev. Lett. **105**, 068301 (2010).

[64] R. D. Groot, and P. B. Warren **107**, 4423 (1997).

[65] N. Ch. Karayiannis, V. G. Mavrantzas, and D. N. Theodorou, Phys. Rev. Lett. **88**, 105503 (2002).

[66] V. A. Harmandaris, V. G. Mavrantzas, D. N. THeodorou, M. Kröger, J. Ramirez, H. C. Öttinger, and D. Vlassopoulos, Macromol. **36**, 1376 (2003).

[67] M. Pütz, K. Kremer, and G. S. Grest, Europhys. Lett. **49**, 735 (2000).

[68] G. Tsolou, V. G. Mavrantzas, D. Theodorou Macromol. **38**, 1478 (2005).

[69] P. Carbone, F. Negri, and F. Müller-Plathe Macromol. **40**, 7044 (2007).

[70] P. Ilg, H. C. Öttinger, and M. Kröger Phys. Rev. E **79**, 011802 (2009).

[71] E. J. Sambriski, G. Yatsenko, M. A. Nemirovskaya, and M. Guenza, J. Chem. Phys. **125**, 234902 (2006).

[72] E. J. Sambriski, G. Yatsenko, M. A. Nemiroskaya, and M. G. Guenza J. Phys.: Cond. Matt. **19**, 205115 (2007).

[73] G. Yatsenko, E. J. Sambriski, and M. Guenza, J. Chem. Phys. **122**, 054907 (2005).

[74] E. J. Sambriski, and M. G. Guenza, Phys. Rev. E **76**, 051801 (2007).

[75] A. J. Clark, and M. G. Guenza, J. Chem. Phys. **132**, 044902 (2010).

[76] J. McCarty, and M. G. Guenza J. Chem. Phys. **133**, 094904 (2010).

[77] V. A. Harmandaris and K. Kremer, Macromol. **42**, 791 (2009); V. A. Harmandaris and K. Kremer, Soft Matter **5**, 3920 (2009).

[78] Q. Wang, D. J. Keffer, D. M. Nicholson, and J. B. Thomas Phys. Rev. E **81**, 061204 (2010).

[79] J. T. Padding and W. J. Briels J. Chem. Phys. **117**, 925 (2002).

[80] R. L. C. Akkermans and W. J. Briels J. Chem. Phys. **113**, 6409 (2000).

[81] M. G. Guenza, J. Phys.: Condens. Matter **20**, 033101 (2008).

[82] M. Dolgushev, A. Blumen J. Chem. Phys. **132**, 124905 (2010).

[83] E. Caballero-Manrique, J. K. Brey, W. A. Deutschman, F. W. Dahlquist, and M. G. Guenza Biophys. J. **93**, 4128 (2007).

[84] V. Krakoviack, J. -P. Hansen, and A. A. Louis, Europhys. Lett. **58**, 53 (2002).

[85] C. N. Likos, H. Löwen, M. Watzlawek, B. Abbas, O. Jucknischke, J. Allgaier, D. Richter Phys. Rev. Lett. **80** 4450 (1998).

[86] J. von Seggern, S. Klotz and H. -J. Cantow, Macromol. **24** 3300 (1991).

[87] D. S. Pearson, G. Ver Strate, E. von Meerwall and F. C. Schilling, Macromol. **20** 1133 (1987).

[88] D. S. Pearson, L. J. Fetters, W. W. Graessley, G. Ver Strate and E. von Meerwall, Macromol. **27** 711 (1994).

[89] D. Richter, L. Willner, A. Zirkel, B. Farago, L. J. Fetters and J. S. Huang, Phys. Rev. Lett. **71** 4158 (1993).

[90] A. Z. Akcasu, and J. J. Duderstadt, Phys. Rev. **188**, 479 (1969).

[91] P. Mazur, and I. Oppenheim Physics **50**, 241 (1970).

[92] M. Guenza J. Chem. Phys. **110**, 7574 (1999).

[93] K. S. Schweizer J. Chem. Phys. **91**, 5802 (1989).

[94] S.-H. Chong, M. Aichele, H. Meyer, M. Fuchs, and J. Baschnagel Phys. Rev. E, **76**, 051806 (2007); M. Bernabei, A. J. Moreno, and J. Colmenero J. Chem. Phys. **131**, 204502 (2009).

[95] M. Guenza, Phys. Rev. Lett. **88**, 025901 (2001).

[96] M. Guenza, Macromol. **35**, 2714 (2002).

[97] M. Doi, and S. F. Edwards, *The Theory of Polymer Dynamics* (Oxford University, Oxford, 1986).

[98] R. Zwanzig *Nonequilibrium Statistical Mechanics* (Oxford University Press, New York, 2001).

[99] M. Bixon, and R. Zwanzig J. Chem. Phys. **69**, 1896 (1978).

[100] H. Yamakawa, *Modern Theory of Polymer Solutions* (Harper and Row, New York, 1971).

[101] E. Helfand, and S. A. Rice J. Chem. Phys. **32**, 1642 (1960).

[102] D. A. McQuarrie *Statistical Mechanics* (University Science Books, Sunsalito, CA, 2000).

[103] Y. Song, E. A. Mason, R. M. Stratt J. Phys. Chem. **93**, 6916 (1989).

[104] W. Paul, and G. D. Smith Rep. Prog. Phys. **67** 1117 (2004).

[105] W. Paul, D. Y. Yoon, and G. D. Smith J. Chem. Phys. **103** 1702 (1995).

[106] M. Pütz, K. Kremer, G. S. Grest Europhys. Lett. **49**, 735 (2000); L. J. Fetters, D. J. Lohse, and D. J. Lohse J. Pol. Sci. B: Pol. Phys. **37**, 1023 (1999); D. Richter, L. Willner, A. Zirkel, B. Farago, L. J. Fetters, and J. S. Huang Phys. Rev. Lett. **71**, 4158 (1993); P. Schleger, B. Farago, C. Lartigue, A. Kollmar, and D.Richter, Phys. Rev. Lett. **81**, 124 (1998).

[107] W. Hess Macromol. **21**, 2620 (1988); W. Hess and R. Klein, Adv. Phys. **32**, 173 (1983).

[108] S. Plimpton J. Comput. Phys. **117**, 1 (1995).

[109] C. Catlett, et. al. *HPC and Grids in Action; Advances in Parallel Computing Series* L. Grandinetti Ed. (IOS Press: Amsterdam, 2007).

[110] D. P. Fletcher, J. Klein Polym. Commun. **26**, 2, 6476 (1985).

[111] T. P. Lodge Phys. Rev. Lett. **83**, 3218 (1999).

[112] I. Y. Lyubimov, J. McCarty, A. Clark, and M. G. Guenza, J. Chem. Phys. **132**, 224903 (2010).

[113] I. Y. Lyubimov, M.G. Guenza Phys. Rev. E **84**, 031801 (2011).

[114] G. Tsolou, V. G. Mavrantzas, D. Theodorou Macromol. **38**, 1478 (2005).

[115] G. Tsolou, V.A. Harmandaris, V.G. Mavrantzas Macromol. Theory Simul. **15**, 381 (2006).

[116] P.S. Stephanou, C. Baig, G. Tsolou, V.G. Mavrantzas, and M. Kroger J.Chem.Phys **132**, 124904 (2010).

[117] M. Doi and S. F. Edwards, *The Theory of Polymer Dynamics* (Clarendon Press, Oxford, 1986).

[118] K. S. Schweizer, J. Chem. Phys. **91**, 5802 (1989).

[119] L.J. Fetters, D.J. Lohse, C.A. Garcia-Franco, P. Brant, and D. Richter Macromol. **35**, 10096 (2002).

[120] J. McCarty, I. Y. Lyubimov, and M. G. Guenza Macromol. **43**, 3964 (2010).

[121] F. Bueche, Physical Properties of Polymers (Interscience, New York, 1962).

[122] V.A. Harmandaris, M. Doxastakis, V.G. Mavrantzas, D.N. Theodorou J.Chem. Phys. **116**, 436 (2002).

[123] E. von Meerwall, S. Beckman, J. Jang, and W.L. Mattice J.Chem. Phys. **108**, 4299 (1998).

[124] Marina Guenza, J. Chem. Phys. **110**,7574 (1999).

[125] B. Frick, G. Dasseh, A. Cailliaux and C. Alba-Simionesco, Chem. Phys. **292**, 311 (2003).

[126] A. Arbe, J. Colmenero, B. Farago, M. Monkenbusch, U. Buchenau and D. Richter, Chem. Phys. **292**, 295 (2003).

[127] J. Colmenero, F. Alvarez and A. Arbe, Phys. Rev. E **65**, 041804 (2002).

[128] G. Tsolou, V. A. Harmandaris and V. Mavrantzas, J. Non-Newtonian Fluid Mech. **152**, 184 (2008).

[129] Marina Guenza, Phys. Rev. Lett. **88**, 025901 (2002).

[130] Marina Guenza, Macromol. **35**, 2714 (2002).

[131] P. Debnath and M. G. Guenza, Phil. Mag. **88**, 33 (2008).